FRACTURE AND ADHESION OF SOFT MATERIALS: A REVIEW

Costantino Creton[1,2], Matteo Ciccotti[1,2]

1   Sciences et Ingénierie de la Matière Molle, CNRS UMR 7615, École Supérieure de Physique et de Chimie Industrielles de la Ville de Paris (ESPCI), ParisTech, PSL Research University, 10 rue Vauquelin, F-75231 Paris cedex 05, France

2   SIMM, UPMC Univ Paris 06, Sorbonne-Universités, 10 rue Vauquelin, F-75231 Paris cedex 05, France

Costantino.Creton@espci.fr; Matteo.Ciccotti@espci.fr

Abstract

Soft Materials are materials with a low shear modulus relative to their bulk modulus and where elastic restoring forces are mainly of entropic origin. A sparse population of strong bonds connects molecules together and prevents macroscopic flow. In this review we discuss the current state of the art on how these soft materials break and detach from solid surfaces. We focus on how stresses and strains are localized near the fracture plane and how elastic energy can flow from the bulk of the material to the crack tip. Adhesion of pressure-sensitive-adhesives, fracture of gels and rubbers are specifically addressed and the key concepts are pointed out. We define the important length scales in the problem and in particular the elasto-adhesive length Γ/E where Γ is the fracture energy and E is the elastic modulus, and how the ratio between sample size and Γ/E controls the fracture mechanisms. Theoretical concepts bridging solid mechanics and polymer physics are rationalized and illustrated by micromechanical experiments and mechanisms of fracture are described in detail. Open question and emerging concepts are discussed at the end of the review.

List of symbols

α reciprocal of the attenuation length of the normal stress in Kaelble's model of peeling

β reciprocal of the attenuation length of the shear stress in Kaelble's model of peeling

γ thermodynamic surface energy

Γ fracture energy

Γ_0 threshold fracture energy

Γ_{app} apparent fracture energy

δ indentation depth

δ_D critical crack opening displacement according to Dugdale model

ε strain, nominal strain in a probe tack test

$\dot{\varepsilon}$ strain rate

ε_H true strain or Hencky strain = $\ln \lambda$

ε_{max} maximum nominal strain at failure or debonding

η viscosity

η^+ extensional viscosity at onset of flow

θ peel angle

λ stretch = l/l_0

$\lambda_1, \lambda_2, \lambda_3$ the three principal stretches

λ_c critical stretch at fracture in the cohesive failure of a peeled adhesive layer

λ_{hard} critical stretch where $f^*(\lambda)$ reaches its minimum value in a uniaxial tensile test

λ_{max} maximum extensibility of the 2nd network in a Double Network Gel

μ shear modulus

$\mu'(\omega)$ dynamic shear storage modulus

$\mu''(\omega)$ dynamic shear loss modulus

μ_e plateau modulus due to entanglements

μ_x shear modulus due to permanent crosslinks

ν Poisson's ratio

ν_e volume density of entanglements in a network

ν_x volume density of crosslinks in a network

ρ crack tip radius, mass of monomer per unit volume of material

ρ_0 mass of monomer per unit volume of unswollen network

ρ^* crack tip radius at propagation

σ stress

σ_c maximum normal stress at failure or debonding

σ_f molecular fracture stress in a fibril

σ_{max} maximum stress at the tip of an elliptical crack, maximum tensile stress measured in a probe tack test

σ_N nominal stress

σ_p plateau stress in a probe test

σ_T true stress

σ_Y yield stress

Σ areal density of chains crossing the interface

τ_c maximum shear stress at debonding

$\phi(a_T v)$ dissipative factor in peel or fracture tests

ϕ_p polymer volume fraction

χ Flory interaction parameter

ω pulsation (rad/s)

a radius of the contact area in a probe test, size of the monomer

a_i width of the interface between two polymers

a_T shift factors of time-temperature superposition

A area of the crack

A_{max} maximum contact area in a probe tack test

b width of a peeled strip, size of half the small axis of an elliptical crack

c crack length, size of half the large axis of an elliptical crack

$C_{hard}(\dot\lambda)$ minimum of $f^*(\lambda)$ as a function of $1/\lambda$. Represents the permanent component of the shear modulus at the stretch rate $\dot\lambda$

$C_{soft}(\dot\lambda)$ $\mu - C_{hard}(\dot\lambda)$. Represents the relaxing component of the shear modulus at the stretch rate $\dot\lambda$

$\frac{dc}{dn}$ crack growth per cycle in a fatigue test

DIC   digital image correlation

D diffusion coefficient

E Young's modulus

E^* threshold Young's modulus for spontaneous adhesion on a rough surface

E_B Young's modulus of the backing of an adhesive tape

E_{eff} effective Young's modulus of the material in the damaged zone

F force

ΔF_{exc} excess free energy

$f^*(\lambda)$ reduced stress or Mooney stress = $\sigma_N/(\lambda - 1/\lambda^2)$

$\mathcal{G}$ energy release rate

$\mathcal{G}_{max}$ maximum applied energy release rate in a cyclic fatigue test

g_{local} local energy release rate near the crack tip

h thickness of adhesive layer

h_0 undeformed thickness of an adhesive layer or sample

h_B thickness of the backing of a tape

h_c height of a penny-shaped interfacial defect (figure 20)

Δh increase in thickness of the adhesive layer during debonding in a probe test

H_0 undeformed thickness of the yielded zone near the crack tip

I_1 first invariant of the Cauchy-Green tensor

J J-integral of Rice

J_m maximum value of $I_1 - 3$ in the Gent model

k_B Boltzmann's constant

k_{local} local stress intensity factor in a damaged zone near the crack tip

K stress intensity factor, dimensionless parameter in Kaelble's model

K_c critical stress intensity factor

l, l_0 deformed and undeformed length of tensile sample

l_{fib} fibril diameter

ℓ_D Dugdale length : size of the plastic region at the crack tip at crack propagation

ℓ_{EA} elasto-adhesive length $= \Gamma/E$

ℓ_{EAD} length scale of elasto-adhesive dissipation $= \Gamma_{app}/E$

L length over which energy is dissipated in the Lake-Thomas model

L_0 Characteristic length over which energy is dissipated by linear viscoelasticity at the crack tip

M_0 Molar mass of the monomer

n power law exponent in the fracture dissipation function

N_x number of monomers between crosslinks

p tensile hydrostatic stress on a cavity or interfacial crack

P peel force

P_c critical cavitation stress, contact pressure during the bond formation in probe tack tests

PSA pressure-sensitive-adhesive

r distance in radial coordinates from the crack tip

r_0 initial size of a spherical defect in a cavitation experiment

R radius of the crack related dissipation zone, radius of spheres, cylinders or asperities in contact mechanics models

R_0 radius of the local damage zone

R_c radius of curvature of a penny-shaped defect at the interface (figure 20)

R_d radius of a penny-shaped defect at the interface (figure 20)

SSY   small scale yielding

t time

t_C contact time during the bond formation in the probe tack test, characteristic loading time in the Kaelble's model

$\tan\delta(\omega)$ viscoelastic loss factor = $\mu''(\omega)/\mu'(\omega)$

T temperature

T_0 reference temperature, threshold tearing energy (c.f. Γ_0)

T_g glass transition temperature

$\tan\delta(\omega)$ loss factor = $\mu''(\omega)/\mu'(\omega)$

u displacement

u_{11} displacement in the direction normal to the crack propagation direction

U_b bond energy

U_w external work

U_{el} stored elastic energy

v crack or peel front velocity

V, V_{deb} velocity of the probe in a probe tack test

w thermodynamic (reversible) energy cost per unit fracture area

$W(\lambda)$ strain energy density as a function of stretch

W_{2nd} strain energy density of the second network in a double network gel

W_c strain energy density at debonding in Kaelble's model

W_{deb} work of debonding in a probe test (in J/m^2)

1. INTRODUCTION

For most people, soft materials are materials where the deformation can be felt by hand or seen with the naked eye without applying an excessive force. In this category are clearly many synthetic, polymer made materials, such as rubbers, gels and self-adhesive materials, but also many more materials made from naturally occurring molecules such as food or living tissues. In particular because of the need to replace sick or damaged living tissue with artificial counterparts, the biomedical field is an avid user of soft materials. The materials described above remain solids, in the sense that they can sustain static loads and store elastic energy in the long term, but their elastic modulus can vary from typically 10^3 to 10^7 Pascals. A sparse population of percolating strong bonds inside the material prevents flow at the macroscopic scale without preventing (some) molecular motion at the microscopic scale. Soft materials are used in real life for their ability to accommodate large deformations without or with little permanent damage. This makes them attractive for seals and joints but also for adhesives, for tires and implants inside the body. Adhesion and fracture, which imply either the failure of interfacial bonds or of primary bonds, are particularly complex due to this dual nature of interactions inside the material. Understanding the failure of soft materials requires knowledge of mechanics at large strain, and viscoelasticity, but also polymer physics, statistical physics and thermodynamics.

There are several important general aspects that should be pointed out at the onset. First, soft dense polymer materials present a large difference between bulk modulus (usually around 10^9 Pa) and shear modulus. This implies that they can be generally modeled as incompressible and that failure mechanisms are very sensitive to the presence of hydrostatic stress. Second, the importance of large deformations requires the use of finite strain mechanics to model the process. Third, deformations in soft materials are related to the molecular structure and elastic restoring forces are mostly of entropic origin.

As a result, a description of the deformation, adhesion and fracture of soft materials requires a discussion of relevant length scales (molecular, microscopic mechanisms, sample size), characteristic time scales (due to viscoelastic behavior) and evaluation of the amounts of dissipated or stored energy.

Theory and experiments will be addressed, but rather than presenting an exhaustive list of experimental or theoretical investigations we have favored a more detailed presentation of selected studies chosen for their insight.

Section 2 reviews the basic concepts of Linear Elastic Fracture Mechanics and discusses differences between conventional (hard) materials and soft materials. Section 3 describes the main experimental methods used for the characterization of adhesion and fracture of soft materials, which are presented as materials in section 4. Sections 5 and 6 discuss more specifically the debonding mechanisms and fracture mechanisms of soft materials in light of the concepts presented before. Section 7 discusses emerging materials, designed to better control or enhance fracture resistance. Finally, section 8 presents the sketch of a unified picture for the fracture and adhesion of soft materials and section 9 discusses some open questions.

2. PHYSICAL CONCEPTS AND SCALES IN THE FRACTURE OF SOFT MATERIALS

2.1 BASICS OF LINEAR ELASTIC FRACTURE MECHANICS

In order to understand the paradigms and pitfalls induced (separately or jointly) by both the soft nature of materials and their viscoelasticity, it is worth opening this review with some scaling concepts in fracture mechanics. We will deliberately start with linear elastic fracture mechanics (LEFM) concepts in order to bridge this review with the most widely established knowledge base of materials scientists. Although most of these tools will be inadequate for soft materials, they remain a useful guide. We will omit all numerical prefactors in this introduction and limit ourselves to scaling laws and order of magnitude estimations (indicated by the $\sim$ symbol instead of =).

LEFM is established on the hypothesis that the bulk material behavior remains linearly elastic everywhere except in a very small region around the crack tip that is schematically collapsed into a linear crack front spanning an interface. The original argument by Griffith(Griffith, 1920) associated the creation of a new crack to the conversion of mechanical energy (external work U_w and variations of the elastic energy U_{el}) into a thermodynamic (reversible) energy cost per unit area $\Gamma = w = 2\gamma$ to create new surfaces, named

the Dupré work of adhesion, according to the equilibrium relation:

$$\mathcal{G} = \frac{\partial U_w}{\partial A} - \frac{\partial U_{el}}{\partial A} = \Gamma \qquad \textbf{1}$$

where $\mathcal{G}$ is called the strain energy release rate, with unit J/m², and it represents the relevant part of the loading condition and structural response of the sample for the purpose of crack propagation. The stable nature of this equilibrium condition is determined by the positive sign of the derivative of $\mathcal{G}$ upon the crack area A, which is a property of the studied structure (sample). We deliberately neglect all dynamic effects, since this review is mainly devoted to quasi-static debonding.

An equivalent description of LEFM can be expressed in terms of a singular stress field in the neighborhood of the crack tip in the form of an inverse square root dependence of the stress on the distance r from the crack tip:

$$\sigma(r) \sim \frac{K}{\sqrt{r}} \qquad \textbf{2}$$

The equilibrium/propagation condition can thus be expressed as $K \geq K_C$, where the loading parameter $K \sim \sqrt{E\mathcal{G}}$ is called the stress intensity factor (SIF). $K_C \sim \sqrt{E\Gamma}$ is called the fracture toughness and is a material property (with unit Pa·m$^{1/2}$), E being the elastic modulus of the material.

The elastic displacement field $u(r)$ close to the crack tip can be derived as:

$$\varepsilon(r) \sim \frac{\sigma}{E} \sim \frac{K}{E\sqrt{r}}$$
$$u(r) \sim \int \epsilon \, dr \sim \frac{K\sqrt{r}}{E} \qquad \textbf{3}$$

The elastic crack opening profile $u(x)$ of an initially sharp slit can be shown to have locally a parabolic shape with radius of curvature ρ given by:

$$u(x) \sim \frac{K\sqrt{x}}{E}$$
$$\rho \sim 1/\frac{\partial^2 x}{\partial u^2} \sim \frac{K^2}{E^2} \sim \frac{\mathcal{G}}{E} \qquad \textbf{4}$$

Since K and $\mathcal{G}$ assume a maximum value at (quasistatic) stable crack propagation, we observe here the emergence of a first physical length scale of fracture which is the crack tip radius at propagation ρ^*:

$$\rho^* \sim \frac{K_C^2}{E^2} \sim \frac{\Gamma}{E} \qquad \textbf{5}$$

We remark that ρ^* is a material property, and that it can be related to a more general physical length scale $\ell_{EA} = \Gamma/E$, that we can name the elasto-adhesive length[1], naturally emerging from the units of the related constitutive material properties. ℓ_{EA} represents the length scale where the cost of creating new surfaces and the bulk elastic energy density for a large deformation have a comparable value, and thus where they can couple. Saying it differently, ℓ_{EA} is the scale below which surface energy effects become dominant and where they can cause bulk deformations larger than $\varepsilon = 1$ (100%).

We remark that when limiting to orders of magnitude, all these arguments are equally valid for interfacial fracture, taking care to use the Dupré interfacial work of adhesion $w = \gamma_1 + \gamma_2 - \gamma_{12}$ (which reduces to 2γ for cohesive fracture), and considering the substrate as infinitely stiff for simplicity.

In order to conclude this introduction on LEFM, we should comment further on the conditions of validity of this theory and formalism. LEFM is valid provided that all inelastic or nonlinear processes are limited to a small size (generally known as Small Scale Yield condition, SSY(Williams, 1984)). If this condition is met, the present formalism can be extended to more general materials constitutive laws, such as plasticity, viscoelasticity, and nonlinear elasticity of soft materials. However, we should never forget that the validity of the SSY approximation should be checked for all the sources of inelasticity and non-linearity by considering the comparison with both the geometrical dimensions of the sample (in particular the smallest distance between the crack tip and one of the boundaries), and the length c of the crack (even if we are referring to a model defect microcrack). Moreover, the plane strain condition should be verified. Under these circumstances, all the LEFM formalism can be extended by simply substituting the (reversible) thermodynamic fracture energy w with an irreversible *fracture energy* Γ, intended as an effective surface energy, which can possibly

---

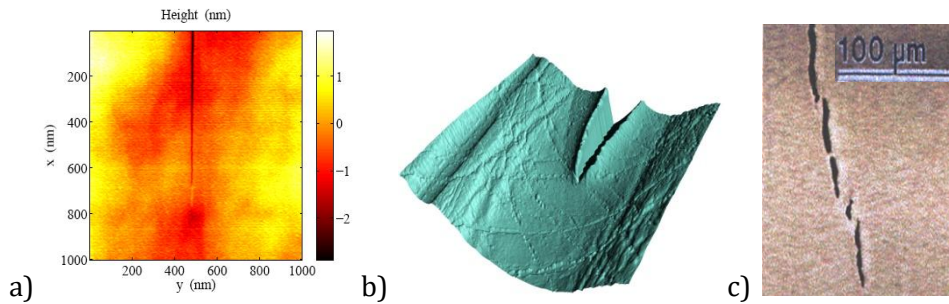[1] For simplicity this term will be used for both adhesion and fracture

depend on crack propagation velocity $\Gamma(v)$. We remark that in any case we should have $\Gamma(v) > w$ since the thermodynamic surface energy is the minimum required energy cost for propagating a crack, and in polymers Γ can indeed become several orders of magnitude larger than w under appropriate temperature and crack velocity combinations.

A classical well established example is the case of hard elasto-plastic materials, which under small deformations can be simply characterized by adding to the elastic modulus a second material parameter that is the yield stress σ_Y. By comparing the yield stress with the singular stress field in eq. 2 we can directly identify a physical length scale, named after Dugdale(Dugdale, 1960):

$$\ell_D = \frac{K_C^2}{\sigma_y^2} \sim \frac{E\Gamma}{\sigma_y^2} \qquad \mathbf{6}$$

which defines the size of the plastic region at the crack tip at crack propagation, and which is also the region where all energy is dissipated under SSY conditions. A second physical length scale can be obtained by substituting ℓ_D into equation 4 and thus obtaining the critical crack opening displacement:

$$\delta_D = \frac{K_C^2}{E\sigma_Y} \sim \frac{\Gamma}{\sigma_Y} \qquad \mathbf{7}$$

The fracture energy can be written as $\Gamma = \sigma_Y \delta_D$, i.e. the plastic work done at stress σ_Y to separate the crack lips up to a critical distance δ_D. We remark that the surface energy w is neglected here because it is small relative the dissipated plastic work. However Γ still characterizes properly the energy to propagate a crack into a specific material. As a few examples, silicate glasses have typical values of $E \sim 70$ GPa, $\sigma_Y \sim 10$ GPa and $\Gamma \sim 10$ J/m^2, so that $\ell_D \sim 7$ nm and $\delta_D \sim 1$ nm; glassy polymers, such as PMMA, have typical values of $E \sim 3$ GPa, $\sigma_Y \sim 100$ MPa and $\Gamma = 300$ J/m^2, so that $\ell_D \sim 10$ µm and $\delta_D \sim 1$ µm; metals, such as steel, have typical values of $E \sim 210$ GPa, $\sigma_Y \sim 1$ GPa and $\Gamma = 40$ kJ/m^2, so that $\ell_D \sim 8$ mm and $\delta_D \sim 40$ µm (c.f. Figure 1 for the appearance of crack tips in these materials). The first conclusion is that LEFM can easily be applied to standard cm size test samples in glasses and glassy polymers, but metals require either huge samples or more advanced non linear methods(Rice, 1968). The second conclusion is that the propagation of a typical micrometer size flaw in the material can be treated with LEFM on glasses, and tentatively on glassy polymers, but not on metals, where the plastic zone will be larger than the defect size, resulting in a plastic blunting of the defect instead of unstable propagation. This is the core of the brittle or ductile nature of these materials under the application of a uniform stress such as in tensile testing.

Figure 1: Images of crack tips in elasto-plastic materials a) AFM image of the crack tip in an inorganic glass (size = 1 µm), image from (Han et al., 2010) b) AFM image of a crack in a glassy polymer (size = 40 µm) image from (Nziakou, 2015); c) crack tip in a metal alloy (titanium aluminium) (size = 200 µm), image from (Bouchaud and Paun, 1999).

2.2 CONSIDERATIONS ON THE FRACTURE OF SOFT ELASTIC MATERIALS

While we commonly refer to soft materials as having a low value of the Young's modulus, between 1 kPa and 10 MPa, for fracture problems, the definition should be based on the competition between the elastic energy and the (effective) surface energy Γ (we initially assume that all dissipation only occurs in a very small molecular region, so that Γ can be treated as w). A material can thus be qualified as "soft" at length scales comparable or smaller than the elasto-adhesive length $\ell_{EA} = \Gamma/E$.

When considering again equations 3 and 5, we remark that the elastic radius of curvature at crack propagation $\rho*$ is also the distance from the crack tip below which any material would experience large strain (the transformation from a sharp crack to a round tip implies infinite local deformation). LEFM is thus intrinsically limited by this length scale, but remains essentially valid at larger scales (if the sample is large enough to see them), independently of the value of E. ℓ_{EA} can thus be seen as the elastic blunting size, due to both dimensional arguments and to the fact that the singular field in eq. 2 is preserved at larger scales.

This argument would also apply to nominally stiff solids. However, for most stiff enthalpic solids ℓ_{EA} is smaller than molecular dimensions, and is therefore masked by plastic deformation occurring at larger scales. The relevant scale for SSY plastic deformation in stiff solids is given by the Dugdale length ($\ell_D \sim K_C^2/\sigma_y^2 \sim E\Gamma/\sigma_y^2$) which is significantly larger than the molecular size (see previous section). For soft materials on the other hand, with a lower estimate for the fracture energy provided by Van der Waals interactions at $w \sim$ 40 mJ/m^2, we obtain a lower estimate for ℓ_{EA} which ranges from 40 μm to 4 nm depending on the value of E, and this value can increase significantly when dissipation comes into play by increasing Γ by several orders of magnitude. Figure 2 presents the images of crack tips in two soft materials such as a rubber or a hydrogel, to be compared with the images in Figure 1 for stiff elastoplastic materials.

a)

b)

b)
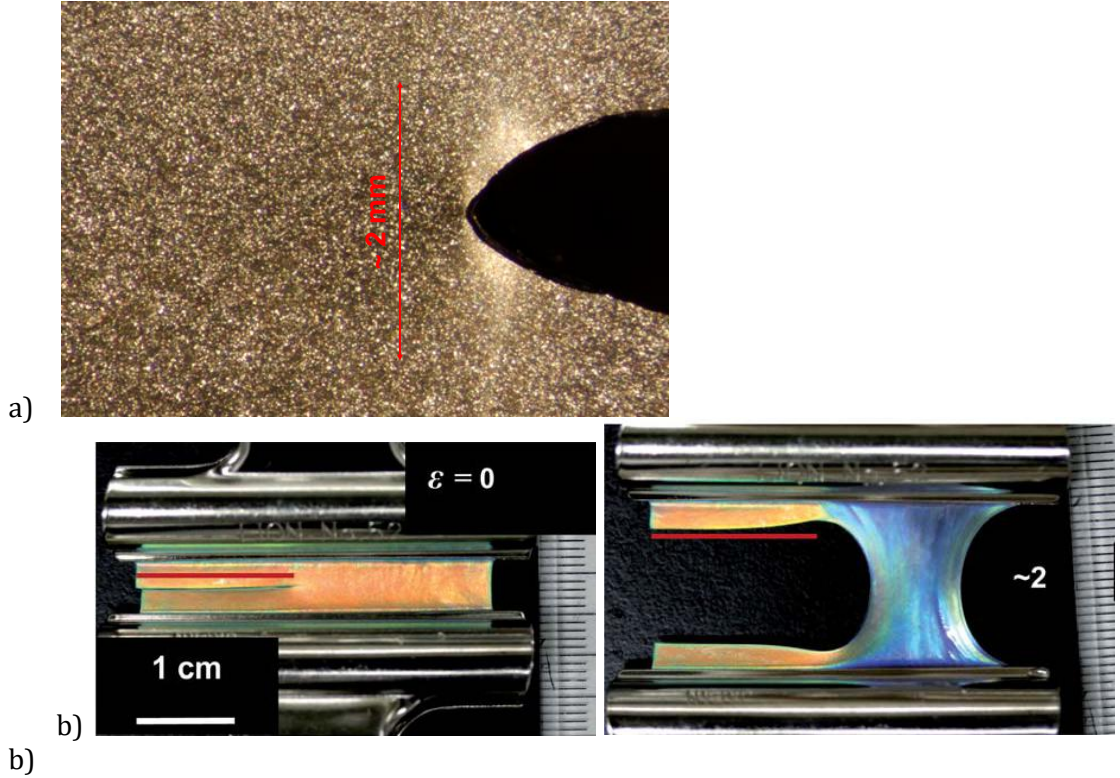
Figure 2: Images of crack tips in soft materials a) a typical rubber (size = 2 mm), data from (Mzabi et al., 2011) b) a soft hydrogel at λ = 1 and λ = 3 (size = 1 cm), images from (Haque et al., 2012).

When considering the fracture or adhesive debonding of a soft layer, the crack tip stress singularity of LEFM is no longer applicable when the thickness h of the layer becomes comparable to the elasto-adhesive length ℓ_{EA} and the square root stress singularity is progressively modified and suppressed for even thinner layers. For the same reason, if we consider an inner (or interfacial) small and sharp penny crack of radius $c < \ell_{EA}$, LEFM can no longer be applied at the crack front and the crack will grow in a 'soft' manner, i.e. by developing into a round cavity and expanding in the bulk of the soft material (Shull and Creton, 2004, Shull, 2006, Lin and Hui, 2004). We remark that while in these conditions it is no longer possible to define a stress intensity factor K, and a related value of the toughness K_c, the energy based Griffith formalism described by equation 1 remains valid as long as the bulk

deformation remains elastic, or if the region where energy is dissipated close to the crack tip remains smaller than ℓ_{EA} and than any geometrical feature such as h and c. The validity of these energetic arguments in soft materials have been very clearly demonstrated experimentally by the seminal work of Rivlin and Thomas (Rivlin and Thomas, 1953), and have subsequently been the focus of important theoretical developments to determine the J integral for nonlinear elastic materials (Rice, 1968).

As discussed in the introduction, an important property of soft dense materials, such as polymers and hydrogels, is to be virtually incompressible, meaning that their Poisson ratio is close to 0.5, or equivalently, that their elastic compression modulus ($\sim 10^9$ Pa) is several orders of magnitude larger than the shear modulus. This implies that the elastic strain fields are essentially constituted by a (deviatoric) shear strain tensor. On the other hand, the stress tensor field can be separated into a shear field and an additional hydrostatic stress field that plays a major role in the overall deformation. This becomes particularly important when a soft material is geometrically confined between rigid interfaces, as in the case of most adhesives, and it results in the build-up of very strong hydrostatic tensile stresses that play a major role on the growth of cavities from small defects (and on the inelastic response of the materials).

2.3 CONSIDERATIONS ON THE FRACTURE OF SOFT DISSIPATIVE MATERIALS

When the energy dissipation in a soft (or hard) material can no longer be considered as limited to a very small region close to the crack tip, most of the theoretical foundations of fracture mechanics (even non-linear) are lost, and even the existence of a well defined fracture energy becomes questionable, where we mean a material (or interfacial) quantity that can be separated from the structural response. Unfortunately, this is the case in most realistic soft materials, where the large deformations taking place in extended regions of the samples quite invariably cause energy dissipation at virtually all scales. Under these circumstances, it becomes very complex and subtle to separate the energy that is dissipated due to fracture propagation from the energy that is dissipated due to the macroscopic sample deformation. The energy required to propagate a crack thus becomes intimately related to the specific mechanical configuration of the structure, and

each structure must be analyzed individually. When using samples with convenient translational invariance, this can still result in an *apparent fracture energy $\Gamma_{app}(v)$*, and we can still define a length scale of elastoadhesive dissipation $\ell_{EAD}(v) = \Gamma_{app}(v)/E$. For example in the peeling of an adhesive strip ℓ_{EAD} is typically larger than the thickness of the adhesive layer and is not an intrinsic property of a fracture surface or interface, but rather an *effective work of debonding* of a given structure/joint. Such a value of $\Gamma_{app}(v)$ will generally change when changing some geometrical characteristic of the structure such as the thickness of the adhesive layer. In this review we will generally use the symbol $\Gamma(v)$ to characterize the intrinsic fracture energy , i.e. that part of the energy dissipation that can unambiguously be associated to crack propagation and separated from any other source of bulk dissipation occurring at larger scales which should rather be attributed to the loading history of the sample seen as a structure.

This field is a very active subject of research, and many efforts have been made to identify some special conditions where fracture mechanics can still be applied in a sound way, and where the measured $\Gamma(v)$ can still be associated with an effective surface/interface process. We will limit our introductory discussion here to viscoelastic materials, having in mind mainly polymer based materials, and consider a hypothetic condition where either the material is stiff enough, or the (effective) surface energy is low enough, that the elasto-adhesive length $\ell_{EA} = \Gamma/E$ is small in front of all other structural (and defect) length, so that linear viscoelasticity applies over all of the sample at length scales $> \ell_{EA}$. Under these circumstances all the bulk material's response is defined by a stress relaxation function (or any other complete linear rheological characterization), and the structural response of the sample can be derived by applying the Boltzmann superposition principle on each element of the structure.

In the particular case where the structure is a fracture test sample with a well defined precrack of constant length c (non propagating, or with a very slow crack propagation velocity non appreciable on a macroscopic scale), the response of the material to any loading history can be obtained by applying the Boltzmann superposition principle to the elastic solution of the structure (this is called the correspondence principle and it is the base of interpretation of all DMA measurements). The strain energy release rate is thus simply derivable by applying the same

materials relaxation functions to the elastic strain energy release rate. For example, after loading the sample to some fixed displacement, the energy release rate will decrease in the same way as the relaxation of the measured applied load, and if the fracture propagation is well described by a fracture energy $\Gamma(v)$, the crack propagation velocity will be observed to progressively slow down in time.

A second notable case is when the material relaxation is fast enough that a relaxed soft elastic condition is reached over all of the scales of the sample, except for some small scales around the slowly moving crack tip, where the crack propagation induces a continuous evolution of the local boundary condition and thus determines the continuous setup of a new viscoelastic relaxation that persists over some time after the crack has passed by some point. Or equivalently over some limited distance from the crack tip, if we use the steady state crack propagation velocity to map time into traveled distance. This assumption is the foundation of the de Gennes trumpet scaling arguments for the energy dissipated by a moving crack into a linearly viscoelastic material(de Gennes, 1988, de Gennes, 1989, de Gennes, 1996), and has been the core of virtually all other important works in this domain(Schapery, 1975b, Schapery, 1975a, Schapery, 1975c, Hui et al., 1992b, Xu et al., 1992, Barthel and Fretigny, 2009, Haiat et al., 2002, Persson et al., 2005).

According to these theories it is possible to relate the fracture energy $\Gamma(v)$ to the linear viscoelastic properties of the material (Saulnier et al., 2004) (defined for example by the knowledge of $\mu'(\omega)$ and $\mu''(\omega)$ over a very broad frequency range). However, most attempts to check these predictions experimentally on a sound quantitative base for rubbers have up to now invariably failed to the best of our knowledge (Barthel and Fretigny, 2009, Cristiano et al., 2011, Gent, 1996a). Even a very important protagonist of this domain such as Gent, has pointed out the intrinsic failure of these theories to describe the real data(Gent, 1996a), and called for an extension of these models to cope with more realistic conditions occurring during fracture propagation in soft materials.

The main factors that should be taken into account are clearly the non-linear finite deformations of soft materials and the non trivial modifications of the viscoelastic dissipation under finite deformations. Moreover, the effects of geometric confinement on both the material response and deformation mechanisms should be adequately taken into account. More subtle problems require the distinction between (non-linear) viscoelastic dissipation and damage mechanisms occurring in the polymer networks under large strains. At last, the thermomechanical energy balance should also be carefully taken into account, because the strong energy dissipation affecting these materials can cause significant changes in the local temperature field, and the mechanical response of these materials is particularly sensitive to even weak changes in temperature due to changes in both the molecular mobility and the entropic nature of elasticity. Some of these issues have been tackled by more recent models(Persson et al., 2005, Persson and Brener, 2005), but the large strain zone close to the crack tip has still been treated as a black box. This approach gives reasonable predictions if the energy dissipation is dominated by viscoelastic dissipation far from the crack tip(Plazek et al., 1983, Plazek et al., 1988), but typically fails for more elastic materials and low strain rates(Cristiano et al., 2011).

All these issues will be a major focus of our present review, where well defined experiments will be selected to clarify at least some of these points up to the present level of knowledge.

3. Experimental methods

We describe here the main experimental tests that are generally used to characterize the failure of soft materials and discuss their advantages and limitations. Typical tests based on linear elastic fracture mechanics are not adapted to these highly deformable non-linear elastic and often viscoelastic materials. The calculation of detailed stress fields is very difficult and global energetic approaches are usually preferred for nearly elastic materials. However, such energetic approaches are not yet clearly established for markedly viscoelastic materials.

3.1 Adhesion tests: peeling, tack tests

Soft adhesives, also called pressure-sensitive-adhesives (PSA), are soft polymer layers that are used to bond two stiffer structures together(Creton, 2003) . Since the lateral dimension of the adhesive joints are generally much larger than the thickness h of the polymer layer, the geometrical confinement is quite strong and deeply affects the mechanics. The

debonding of the adhesive from the substrate can occur by different mechanisms, implying either the propagation of a crack along one of the two interfaces and/or extensive deformation in the bulk of the adhesive layer. Even when failure is localized at a specific interface, it can involve or not strong dissipative mechanisms acting in the whole PSA layer.

Most experimental methods for testing an adhesive joint, such as the peel test or the probe tack test, are based on the measurement of the structural response of the whole joint during debonding and they provide a global result (a peel force or debonding energy) that does not reveal anything about the detailed mechanisms

of debonding. In this section we will review the basics of these techniques as applied to a generic joint, while the interpretation of these measurements in light of the specific mechanisms occurring in soft polymer adhesives will be presented in section 5 after the materials have been introduced in more detail in section 4.

The case of weak adhesion of elastic soft materials (where Γ/E is small related to all geometric dimensions of the polymer layer) has been extensively studied and reviewed(Shull, 2002) and is typically based on the analysis of the contact between a sphere and a flat or two crossed cylinders (Figure 3).
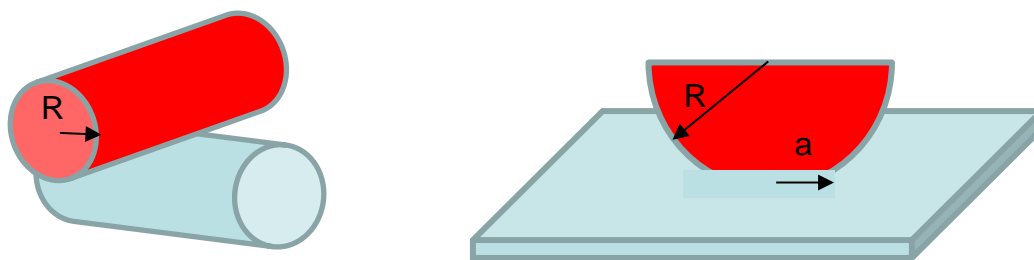

Figure 3: Simple contact geometries used in contact mechanics. Crossed cylinders and sphere on flat.

Because in this type of analysis the elastically deformed volume in the bulk can be clearly separated from the typical length scale of dissipative interfacial processes, the problem can be treated as a classic interfacial fracture propagation problem according to the so called JKR analysis (Maugis and Barquins, 1978a). Such experiments typically yield curves where the energy release rate is imposed and the crack velocity v is measured and it is found that a unique effective adhesion energy curve Γ (v) can be obtained from a set of measurements done in different loading conditions and it constitutes a good characterization of the adhesive properties of the interface between the two solids (Maugis and Barquins, 1978a, Deruelle et al., 1998, Ahn and Shull, 1998b).

However, if the adhesion is stronger or if the material is more viscoelastic in the bulk during the time scales of the test, then the strain energy release rate G becomes dependent on loading history and the adhesion energy is no longer easily separable from the energy dissipated in the bulk. In extreme cases, the elastic energy released by the deformed material may not be

sufficient to propagate a crack and external work must be continuously applied. Under these circumstances the JKR geometry is not well suited and the two tests that have been used most extensively to investigate adhesion of soft viscoelastic material are the probe test, where a cylindrical, flat or hemispherical-ended probe is pulled at constant speed from an adhesive layer, and the peel test, where a thin adhesive strip backed with a stiff layer, is peeled at a constant velocity from the surface of a usually rigid substrate. Both tests are schematically described in Figure 4. The probe test imposes a well-defined geometry of loading on the adhesive layer but does not provide information on steady-state propagation. On the contrary the peel test is ideal to study steady-state propagation but loads the adhesive film in a variable and more complex geometry. Fixed load peel tests at a zero angle of peel (called shear tests in the PSA community) are also typically carried out to study the long term adhesion at low stress levels. However the details of the catastrophic failure remain poorly understood, so we will not focus on that type of test in this review.
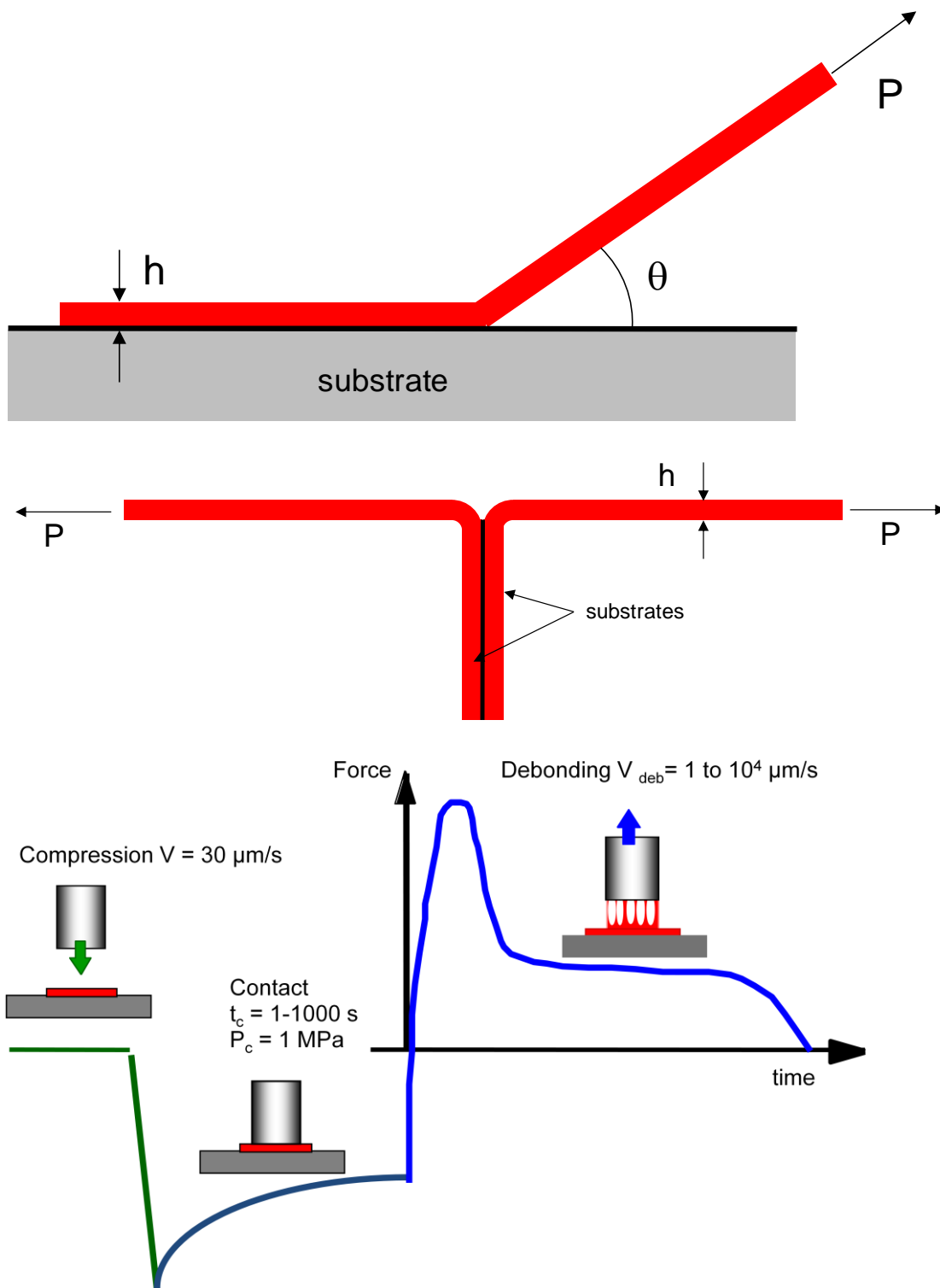
Figure 4: Schematic of a peel test and of a probe test used to test adhesion of soft materials

The peel test is typically used to test the adhesion of tapes and the peel force (per unit width of tape) is used as a measure of the adherence energy. The experiment is normally carried out at a constant peel angle and by applying either a constant peel velocity (a standard test in industry) or a constant load. Although the effect of the peel angle has been the object of several studies(Kaelble, 1960, Gent and Kaang, 1987, Williams, 1993, Williams and Kauzlarich, 2005), most materials are tested at a peel angle of 90° or 180°(PSTC, 2000). Despite its apparent simplicity, the peel test applies a rather complex strain field in the region of the debonding front, resulting from a coupling between the bending stiffness of the backing and

the mechanical properties of the deformable adhesive itself. It has however the advantage to focus on the steady-state propagation of a crack rather than on its nucleation. Typically in peel tests the soft adhesive material is reinforced with a backing that is much stiffer in tension than the adhesive, avoiding therefore to account for the tensile deformation of the arm. If the peel angle is not too small (a few degrees) the strain energy release rate $\mathcal{G}$ is given by:

$$\mathcal{G} = \frac{F}{b}(1 - cos\theta) \qquad \textbf{8}$$

where b is the width of the peeled strip. This reduces to $\mathcal{G} = 2F/b$ for a T-peel test (see Figure 4), that is conveniently carried out in tensile testers. The typical outcome of a peel test is the steady-state peel force as a function of peel velocity, which under quasistatic steady state peeling can be directly translated into an apparent fracture energy $\Gamma_{app}(v)$ by normalizing the peel force by the width of the peeled strip[2]. However, in the absence of a detailed knowledge and modeling of the deformation and failure mechanisms occurring in the debonding of the soft polymer, such a single parameter, although useful for comparative purposes, does not provide a well defined property of the interface and it is generally strongly dependent on the thickness of the adhesive layer and peel angle(Villey et al., 2015, Gardon, 1963a).

The probe test, schematically shown on Figure 4, provides very different and complementary information on the adhesive properties of soft materials. In this test an adhesive layer is first compressed between a flat ended cylindrical probe of radius a and a hard substrate. After a set contact time, the probe is removed from the surface at a constant velocity V_{deb} and the load F is measured as a function of time or distance, as illustrated in Figure 4. The advantage of the probe test is the application of a well defined displacement field to the deformable adhesive, since all parts of the measuring instrument have a negligible bending stiffness. Moreover, a well defined strain history can be applied to the adhesive before debonding, although the effect of the compression/decompression stage is ignored in most experimental investigations on soft adhesives(Shull and Creton, 2004).

---

[2] The Work done by the force is the Force multiplied by the peeled length x. The Adherence energy is then this work divided by the peeled area xb, hence $\Gamma_{app}(v)=F(v)/b.$
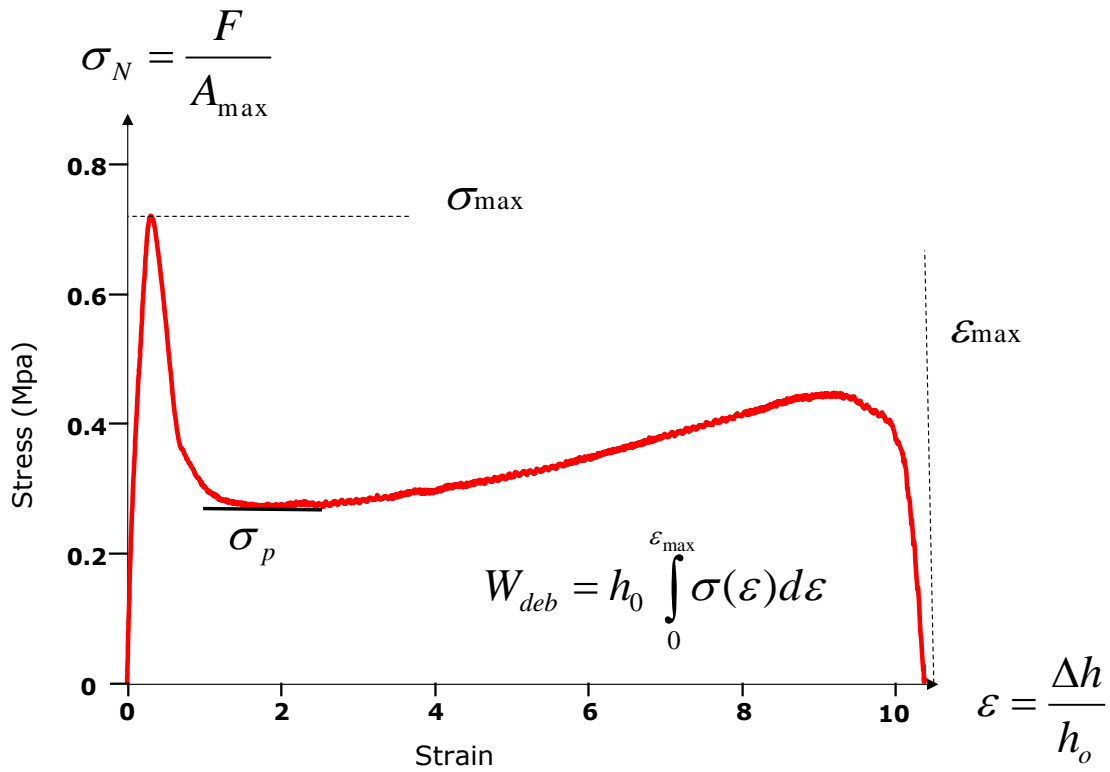
Figure 5: Normalized force displacement curve typically obtained for a probe test and definition of the main parameters that can be extracted from it.

The results of a probe test are a force vs. displacement curve. This curve is usually transformed into a nominal stress vs. nominal strain curve (
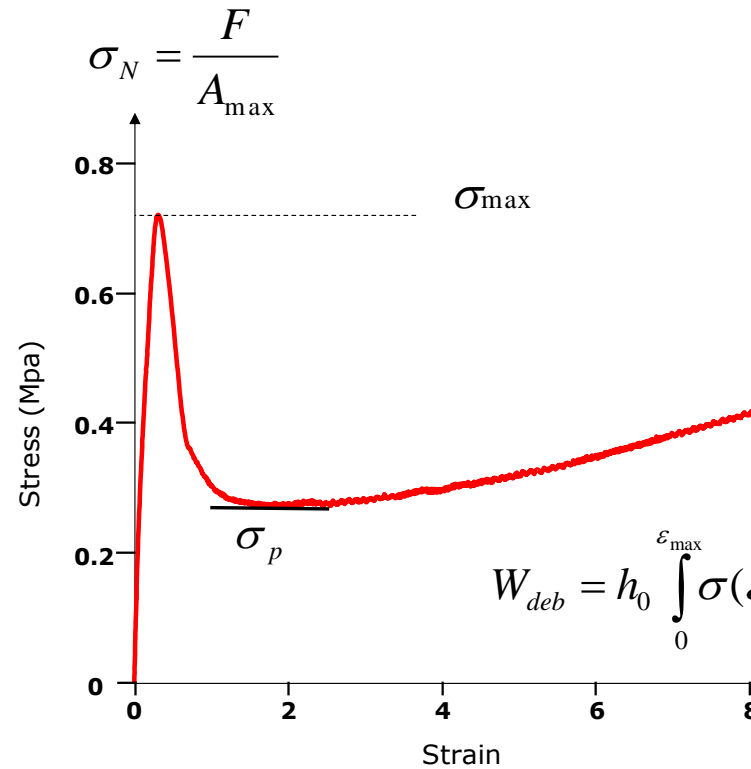
Figure 5), which is obtained by normalizing the force by the maximal area of contact A_{max} during the compression stage (related to the probe radius a_0) and the displacement Δh by the initial layer thickness h_0 :

$$\sigma_N = \frac{F}{A_{max}}, \varepsilon = \frac{h-h_0}{h_0} \qquad \qquad 9$$

Because the debonding mechanism of a soft confined adhesive layer is usually complex and is not a simple propagation of an axisymmetric crack from the edge toward the center, data from probe tests cannot be easily compared in a quantitative way to a model or to a simulation. However, the shape of the stress-strain curve reveals details about the deformation mechanisms. In particular, four main parameters can be extracted from the curve: the peak stress σ_{max}, the maximum extension ε_{max}, the plateau stress σ_p and the work of debonding W_{deb} (i.e. the area under the loading curve multiplied by h_0). The nominal stress-strain curve obtained from the test can be compared for different materials and different test conditions providing significantly more information than the simple value of the peel force. However, once again, in order to derive some sound physical interpretation from these measurements, a separate investigation of the deformation and failure mechanisms during the debonding should be performed, and will be discussed in more detail in section 5.

Probe tests can be carried out both in a sphere on flat geometry or in a flat punch geometry. The sphere on flat geometry is widespread for adhesion of non fibrillating elastic rubbers where ℓ_{EAD} << a, due to two key advantages relative to a flat punch method: firstly, its insensitivity to small misalignments between sample and probe and secondly, the well-defined crack propagation geometry that the hemispherical probe introduces. However, for highly viscoelastic and soft adhesives where ℓ_{EAD} is comparable or larger than the radius of the probe a, these two key advantages are offset by the more complex stress field imposed by the spherical probe and by the increased difficulty of modifying chemically a curved surface (Crosby and Shull, 1999b, Crosby and Shull, 1999a). As a result the flat-ended probe has been used extensively for soft viscoelastic adhesives since the mid 1980's (Zosel, 1985, Zosel, 1989, Zosel, 1992, Lakrout et al., 1999, Creton and Fabre, 2002, Shull and Creton, 2004, Poivet et al., 2003, Teisseire et al., 2007). Initial studies focused on the adhesion energy alone (Zosel, 1997, Zosel, 1992, Zosel, 1985, Zosel, 1989), and then the combined analysis of the complete stress-strain curve and of the synchronized images obtained from a properly positioned video camera led to a

much more detailed interpretation and understanding of the micromechanisms (Lakrout et al., 1999, Creton et al., 2001, Brown et al., 2002, Chiche et al., 2005a, Tanguy et al., 2014). An example of the schematic setup built in the ESPCI laboratory and of the images obtained is shown on Figure 6. It is based on a stiff sample holder, a set of three screws to adjust alignment and a 45° mirror to observe the debonding through the transparent glass substrate supporting the adhesive film.
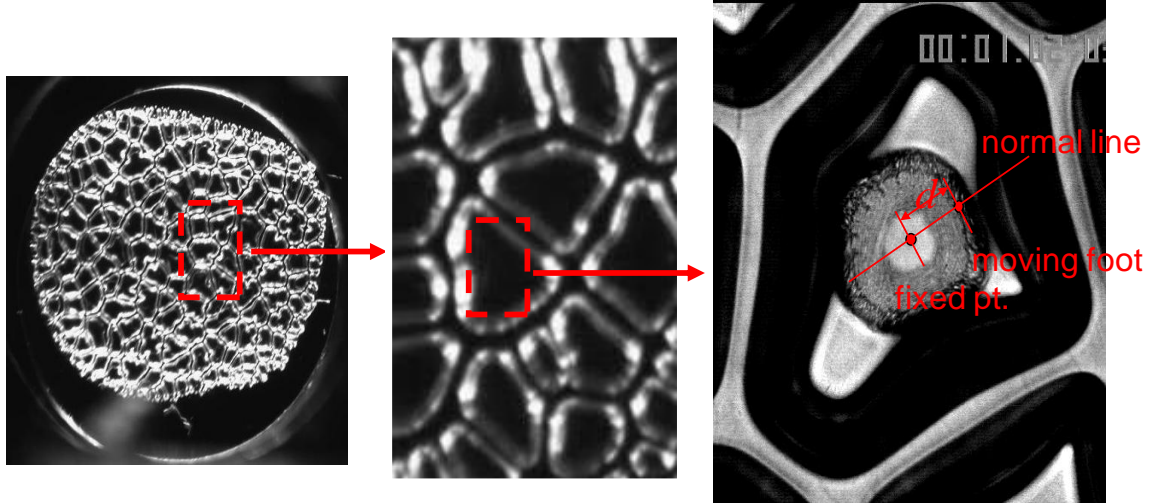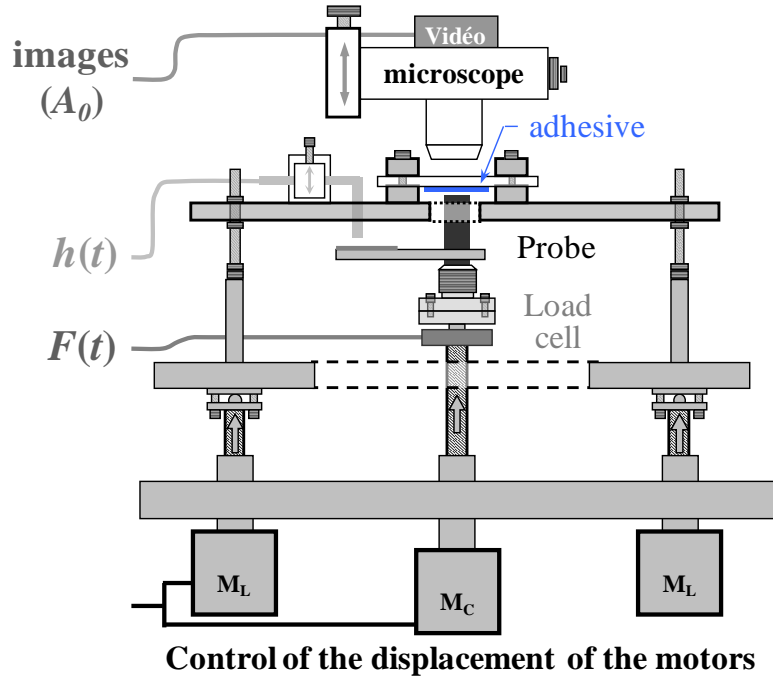
Figure 6: Schematic of an instrumented probe tack test and typical images obtained during debonding at different magnifications. The instrumentend probe test is based on a stiff sample holder, a set of three screws to adjust alignment and a 45° mirror to observe the debonding through the transparent glass substrate supporting the adhesive film.

3.2 FRACTURE MECHANICS FOR RUBBERS: TEARING, PURE SHEAR DOUBLE EDGE NOTCH

As opposed to adhesion tests where the adhesive layer is confined between two stiffer surfaces, fracture tests are usually carried out on unconfined samples (films, sheets or thick samples) with materials much less viscoelastic than soft adhesives and a value of $\ell_{EAD} << c$ and

the dimensions of the sample. However fracture can occur in plane stress conditions (for thin samples) or plane strain conditions (for thick samples) giving different results for $\Gamma(v)$. Furthermore adhesion experiments involve the presence of an interface, which is typically mechanically weaker than the bulk material and constitute therefore a preferential path for the crack. Such preferential path does not exist for

17

bulk fracture and leads sometimes to crack deviations even when the loading is in pure mode I(De and Gent, 1996).

Typical test geometries that are suited for studying fracture propagation in soft viscoelastic materials such as rubber are shown in Figure 7. The choice of a particular geometry for a fracture test usually depends on practical considerations. The so-called trousers test, which creates a weak propagation plane by decreasing the thickness of the sample along a side groove, is well adapted to very tough materials, but typically includes significant dissipative processes that are not related to the fracture process itself, i.e, it measures a total work of fracture $\Gamma_{app}(v)$ rather than a fracture energy $\Gamma(v)$. Two easier tests to analyze are the pure shear test and the simple or double edge notch test. The pure shear test geometry shown in Figure 7 has the distinct advantage to apply an energy release rate $\mathcal{G}$ that is independent of crack length c if the material is elastic in the bulk and $c > h_0/2$ where h_0 is the height of the undeformed sample. For a purely elastic material the energy release rate can be written as:

$$\mathcal{G} = W(\lambda)h_0 \qquad \textbf{10}$$

where $W(\lambda)$ is the strain energy per unit volume well ahead of the crack tip under the given fixed stretch λ. This geometry is well suited for both steady-state crack propagation and for fatigue crack propagation, i.e. crack propagation under cyclic load. It requires however a specific sample geometry and a careful grip. This is easily doable in an industrial setting where samples can be molded, but is more difficult to do in the lab with small samples and has only been rarely used for hydrogels (Seitz et al., 2009, Baumberger et al., 2006a, Sun et al., 2012). Hence, many academic fracture studies have been published using the single or double edge notch test or the trousers test instead (Tanaka et al., 2005, Lin et al., 2010, Cristiano et al., 2011, Greensmith, 1963, Bhowmick et al., 1983, Gent et al., 1994). In the single or double edge notch test, also shown on Figure 7, a prenotched strip of material is stretched in tension. For elastomers (which typically display Neo-Hookean elasticity for moderate stretch) an empirical expression was proposed by Greensmith (Greensmith, 1963) based on experiments on single edge notch geometry with different crack lengths $c \ll a$, where a is the sample thickness as indicated in Figure 7:

$$\mathcal{G} = \frac{6W(\lambda)c}{\sqrt{\overline{\lambda}}} \qquad \textbf{11}$$

where $W(\lambda)$ is the strain energy per unit volume and is typically obtained from the stress-strain curve of an unnotched sample of identical dimensions. It should be noted that in this geometry the energy release rate increases with crack length, i.e. $d\mathcal{G}/dc$ is positive so that the crack will accelerate once it starts to move and spontaneous uncontrolled propagation will occur.
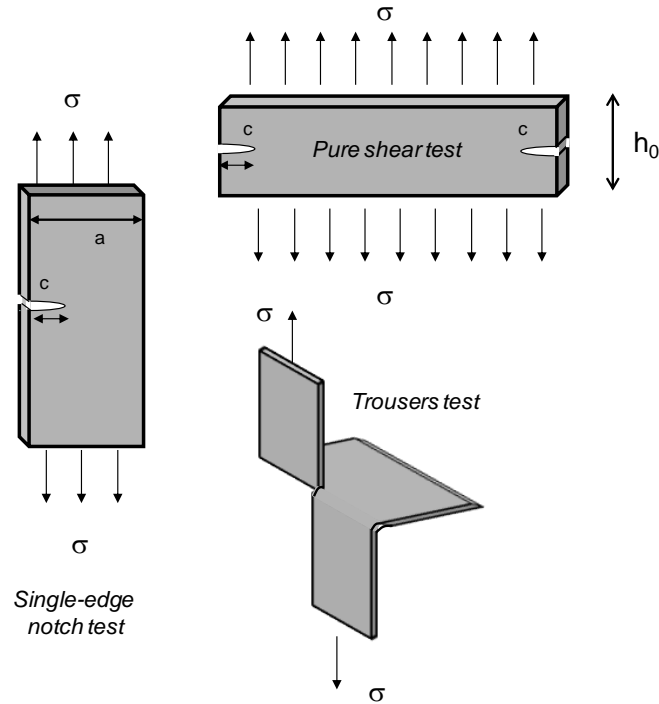
Figure 7: Schematic of the most common geometries used for fracture of rubbers: single-edge notch test (SEN), trousers tests also called tear test and pure shear test (PS).

4. SOFT POLYMER MATERIALS:
STRUCTURE AND DEFORMATION

Soft materials are typically defined as deformable materials with a low elastic modulus. Yet in this review we will have to make some further restrictions in terms of structure. The most important one is that we will focus on soft materials made predominantly with flexible polymers above their glass transition temperature. This definition includes three important categories of soft materials of practical and technological importance: elastomers, pressure-sensitive-adhesives and swollen gels. All three (depicted schematically in Figure 8) have in common to be networks of connected polymer chains and to have an elastic behavior mostly due to a change in entropy rather than internal energy. Their Young's modulus ranges between 1 kPa and 10 MPa.

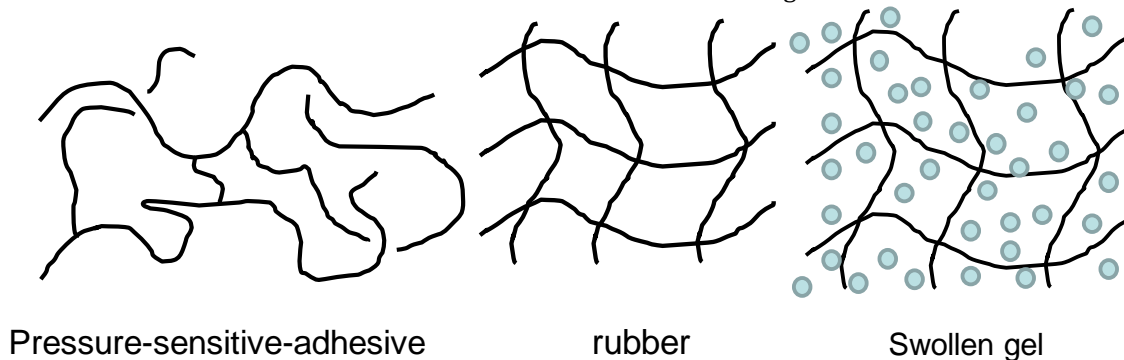**Figure 8: Schematic of a weakly crosslinked and entangled pressure-sensitive-adhesive, a crosslinked rubber and a swollen gel.**

The linear viscoelastic properties of soft polymer based materials have been the focus of many studies. However, the overwhelming majority of these studies have focused on two extreme cases where the physics is better known: the ideal rubber (Figure 8) where all polymer chains are

attached at both ends by covalent bonds (Treloar, 1973) and the case of entangled but uncrosslinked polymers, which are actually viscoelastic fluids above their T_g (Doi and Edwards, 1986, de Gennes, 1979, Rubinstein and Colby, 2003). Briefly, the shear elastic modulus μ_x of a crosslinked but unentangled rubber can be described by the sum of the free energy of its chains, i.e.

$$\mu_x = \nu_x k_B T \qquad\qquad 12$$

where ν_x is the number of elastic chains between crosslinks, per unit volume. If the rubbery material is not chemically crosslinked but simply entangled, another important physical quantity is the plateau modulus generally called by rheologists G_N^0. In this case the modulus can be described as the sum of the free energy of the elastic chains between entanglements. For coherence of notation we will call it here μ_e defined as:

$$\mu_e = \nu_e k_B T \qquad\qquad 13$$

where ν_e is the number of elastic chains between entanglements, per unit volume. These two contributions to the modulus are additive so that when both crosslinks and entanglements are present, the elastic modulus is $\mu \sim \mu_x + \mu_e$. Soft materials can be roughly divided in two categories. When $\mu_x > \mu_e$ the soft material is typically a rubber or a swollen gel. The case of $\mu_e > \mu_x$ is more relevant for soft adhesives. It should be noted that μ_e is a characteristic of the flexibility and monomer composition of the polymer chain and does not depend on molecular weight or degree of chemical crosslinking. In the melt state, i.e. in the absence of solvent, μ_e typically ranges between 10^5 and 10^6 Pa.

To decrease further the modulus and make the material softer there are two options. The first is to reduce the concentration of elastic chains by swelling the polymer with a solvent. This situation corresponds to decreasing ν_x, and hydrogels, where the solvent is water, are a good example. Their modulus generally varies from 1 to 100 kPa depending on polymer concentration and level of crosslinking in the gel. The second option is to both reduce the level of chemical crosslinking and to broaden the molecular weight distribution to include shorter chains. In this case the elastic modulus becomes markedly frequency dependent and the material is highly viscoelastic. This case is representative of soft adhesives. The storage component of the elastic modulus μ' as a function of frequency for these different materials is shown schematically in Figure 9.
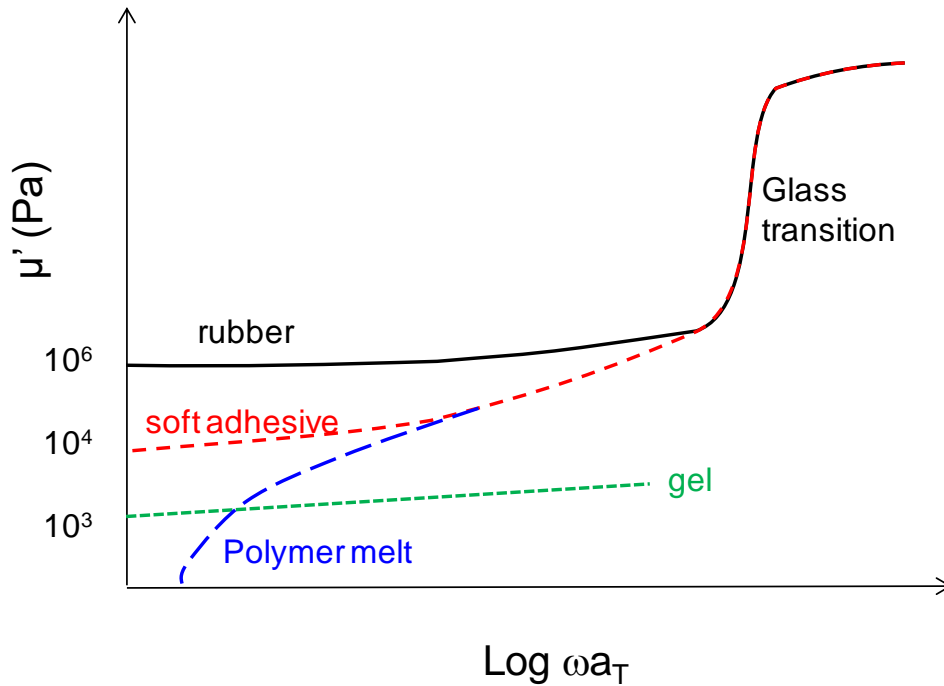

Figure 9: Schematic of the storage component of the elastic modulus $\mu'(\omega)$ at a fixed temperature T as a function of reduced frequency for representative soft materials. The a_T are the frequency-temperature shift factors according to the time-temperature superposition principle(Williams et al., 1955).

While the density of entanglements and crosslinks as well as the characteristic times related to chain dynamics can be extracted from the linear viscoelastic properties of polymer networks by using suitable molecular models(Rubinstein and Colby, 2003), the large strain behavior, in particular under uniaxial extension; cannot be quantitatively predicted from linear viscoelaticity. In this regime the presence of entanglements, hydrogen bonds and crosslinks couples and introduces a marked non-linearity in the behavior.

The simplest way to characterize the non-linear behavior of soft materials is in simple extension at a fixed strain rate until failure. Conventional shear rheometers can be used as well to probe large strain behavior in a cyclic test (the so-called Large Amplitude Oscillatory Shear, LAOS(Hyun et al., 2011)) but require the material to have a steady-state behavior in a cyclic test,(i.e; no damage mechanism but only non-linear viscoelasticity) and are therefore more adapted to complex fluids than complex solids.

Uniaxial extension tests can be carried out essentially in two main ways: at a constant strain rate with an extensional rheometer or at a constant crosshead velocity with a tensile tester. Until recently the first method (in principle adapted to polymer melts) was very difficult to implement (Münstedt and Laun, 1979). However, the development of the counter-rotating cylinders geometry (also called Sentmanat Extensional Rheology after (Sentmanat et al., 2005)) to measure the extensional viscosity of polymer melts has made this method much more readily available (Wang et al., 2007) and it turns out that its experimental design makes the measurement ideally adapted to soft and sticky solids. The constant crosshead velocity extensional test is more suitable for rubbers or gels and it gives a more accurate measurement of the initial modulus and of the extension ratio, which is typically measured locally with an optical extensometer. However, a conventional tensile test carried out in a machine by moving the crosshead at a constant velocity does not deform the sample at a constant true strain rate. Schematics of both experimental setups are shown on Figure 10.
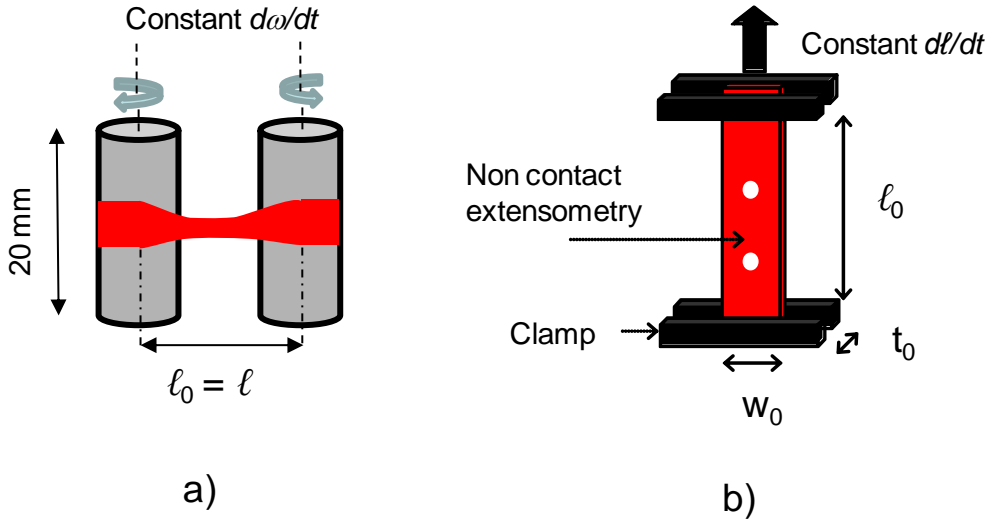
Figure 10: Schematic of: a) the extensional rheology setup (SER version) where two cylinders counter-rotating at a constant angular velocity, stretch the sample at a constant strain rate, since the gauge length is fixed and imposed by the distance between the cylinders. b) the tensile test setup where the sample is stretched at a fixed crosshead velocity and the strain rate $d\ell/\ell$ decreases with time.

Whether tested at constant strain rate or at constant crosshead velocity, the typical stress-strain curve of a soft material does not change qualitatively its main features but only its strain rate history. When representing a uniaxial tensile test, rheologists like to represent the extensional viscosity η^+ as a function of time in which is defined as.

$$\eta^+ = \frac{\sigma_T}{\dot{\epsilon}_H} \qquad 14$$

where σ_T is the true stress and $\varepsilon_H = ln\ \lambda$ is the Hencky strain and the stretch $\lambda = l/l_0$, where l is the deformed length and l_0 is the undeformed length. Materials scientists on the other hand prefer to represent the nominal stress σ_N as a

function of λ. The two quantities are of course connected by:

$$\eta^+ = \frac{\sigma_T}{\dot{\epsilon}_H} = \frac{\sigma_N \lambda^2}{\dot{\lambda}} \qquad 15$$

For entangled and crosslinked soft materials, the large strain behavior is dominated by rubber elasticity. The simplest way to represent the strain energy density W of a crosslinked material

$$W = \frac{\nu_x k_B T}{2}\left(\lambda_1^2 + \lambda_2^2 + \lambda_3^2 - 3\right) = \frac{\nu_x k_B T}{2}(I_1 - 3)$$

where $I_1 = \lambda_1^2 + \lambda_2^2 + \lambda_3^2$ is the first invariant of the left or right Cauchy-Green tensor. For incompressible materials we must have $\lambda_1 \lambda_2 \lambda_3 = 1$. When considering an uniaxial extension test, the value of the nominal stress σ_N in uniaxial extension can be predicted by deriving this strain energy density function relative to the uniaxial stretch $\lambda = \lambda_1$ (with $\lambda_2 = \lambda_3 = 1/\sqrt{\lambda}$):

$$\sigma_N = \nu_x k_B T \left(\lambda - \frac{1}{\lambda^2}\right) \qquad 17$$

This prediction works well for crosslinked rubbers and hydrogels ($\mu_x \geq \mu_e$) at moderate strains. At large strains the main assumption of

(neglecting both entanglements and strain hardening) is the so-called neo-Hookean model(Treloar, 1958). According to this model, which is based on the sum of the entropic elasticity of the elastic chains, W can be represented as a function of the three principal stretches as:

$$\qquad 16$$

the affine network model, i.e. Gaussian elasticity of the polymer chains, does not hold anymore. In particular, the chains approach their finite extensibility limit and stiffen markedly. Several models have been used to account for that stiffening, but while the stiffening of an individual chain is well described by the Langevin function (Treloar, 1958), the stiffening of an elastic material cannot be easily predicted simply from the density of crosslinks ν_x or entanglements ν_e. Hence, an additional finite extensibility parameter is used in empirical models. One of the simplest of such models is that proposed by Gent in 1996 (Gent, 1996b), where W and σ_N in uniaxial extension are written as:

$$\qquad 18$$

$$W = -\frac{\nu_x k_B T}{2} J_m ln\left(1 - \frac{(I_1 - 3)}{J_m}\right)$$

$$\qquad 19$$

$$\sigma_N = \nu_x k_B T \left(\lambda - \frac{1}{\lambda^2}\right) \Big/ 1 - \left(\frac{(I_1 - 3)}{J_m}\right)$$

where J_m is the maximum allowable value of $I_1 - 3$ and has the meaning of the square of the maximum extensibility in uniaxial tension.

If $\mu_e \ll \mu_x$ does not hold, it is important to include in the model the effect of the topological entanglements. If the material remains elastic, meaning here non dissipative and with stresses that only depend on W, the combined presence of crosslinks and entanglements is well captured by molecularly based models combining the Doi-

Edwards tube model and the affine network model. One of the most complete molecular models has been proposed by Rubinstein and Panyukov in 2002 (Rubinstein and Panyukov, 2002).

The prediction of the model in uniaxial extension is a slight softening both with positive stresses (in tension) and with negative stresses (in compression). The engineering stress σ_N is then given by:

$$\qquad 20$$

$$\sigma_N = \nu_x k_B T \left(\lambda - \frac{1}{\lambda^2}\right) + \nu_e k_B T \left(\lambda - \frac{1}{\lambda^2}\right) \Big/ (0.74\lambda + 0.61\lambda^{-0.5} - 0.35)$$

More complex molecularly based models have been proposed and in particular taking into account the combined effect of entanglements
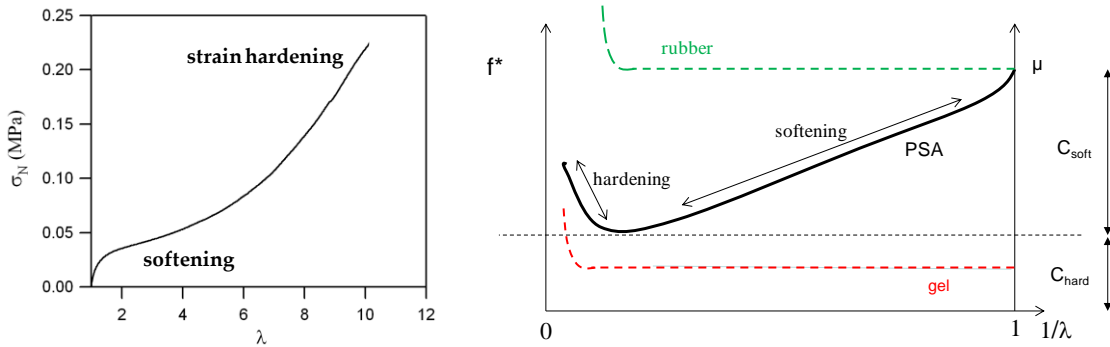
and finite extensibility (Edwards and Vilgis, 1988), but this was done at the expense of the physical interpretability of the parameters.

A convenient way to characterize experimentally the deviation from the affine network model is to represent the reduced stress also called Mooney stress defined as:

$$f^*(\lambda) = \frac{\sigma_N}{\left(\lambda - \frac{1}{\lambda^2}\right)} \qquad \mathbf{21}$$

For the affine network model of rubber elasticity, f^* is a constant independent of λ so that any dependence on λ can be interpreted either as the signature of the presence of entanglements, or of the onset of the finite extensibility of the chains, or of viscoelastic relaxation (discussed in more detail in section 6.2 within the context of fracture). Chain orientation between entanglements(reversible) and viscoelastic relaxation (irreversible) reduce the value of f^* with increasing strain, while the finite extensibility of the chains increases f^* at large strains.

Such a representation can in principle be used for any material with a mechanical behavior dominated by entropic elasticity. In strain-crystallizing rubbers, as for example natural rubber, and in rubbers of technological interest, which are filled with nanoparticles such as carbon black or silica, f^* varies a lot with λ due to changes of structure, and filler/polymer interactions taking place during deformation so that the unambiguous interpretation of $f^*(\lambda)$ for such complex materials is very difficult and yields limited insight. However, for unfilled rubbers, gels and soft adhesives $f^*(\lambda)$ is more directly related to the changes in stored entropic elasticity in the chains of the network and can be used for molecular insight. The analysis of $f^*(\lambda)$ is particularly useful for soft adhesives where the non linearity is marked and both softening and hardening are present. Figure 11a shows a typical stress-strain curve in uniaxial extension of a PSA and Figure 11b shows f^* as a function of $1/\lambda$ for the same adhesive and for a typical elastic gel and elastic rubber in comparison.

Figure 11: a) Typical nominal stress vs. uniaxial stretch plot for a PSA and b) Mooney representation of the same data as a function of $1/\lambda$ and comparison with an elastic gel and an elastic rubber.

The amplitude of non-linear softening of the stress at intermediate values of λ translates into a steady decrease in $f^*(\lambda)$ from its initial shear modulus μ (at $\lambda = 1$) to a minimum value corresponding to the onset of strain hardening. The shear modulus μ can then be conveniently separated into a relaxing component C_{soft} and a permanent component C_{hard}. The interpretation of these two quantities will be further discussed in section 5.3.3 on fibril growth in soft adhesives.

To conclude this overview of the large deformation of soft materials, we should point out that for viscoelastic fluids an equally active community has focused on characterizing strain hardening as a deviation from linear viscoelasticity(Zülle et al., 1987). This type of strain hardening, well captured by non-linear models for viscoelastic fluids(Bird et al., 1987, Giesekus, 1982, Phan-Thien, 1978), is identified in the extensional viscosity η^+ vs. time curve as a

deviation from the linear viscoelastic prediction. The two types of strain hardening are rather different. For a viscoelastic fluid strain hardening means that the relaxation of the stress does occur less rapidly with time than the linear relaxation would predict. On the other hand, for a viscoelastic solid strain hardening means that the stress increases faster with strain than Gaussian elasticity would predict.

This concludes the brief overview of the structure and deformation of the soft polymer materials of interest for our review. We have introduced the notion of crosslinks, entanglements, viscoelasticity and large strain behavior. We will now focus on two specific cases where large deformations occur over significant volumes and where considerations on the polymer structure become particularly important: we will address first the physics of stickyness, i.e. the adhesion of soft viscoelastic

and confined layers to rigid surfaces, and then the fracture of soft materials, i.e. the case a crack tip propagates in the bulk along with a

5. BONDING AND DEBONDING MECHANISMS OF SOFT ADHESIVE LAYERS

Soft adhesives are essentially thin soft and viscoelastic polymer layers that are applied between two more rigid bodies in order to hold them together. They are commonly found in a large variety of applications around us, where the adhesive bond does not need to sustain very high stresses or where reversible adhesion is required. This includes of course adhesive labels and packaging tapes, but nowadays encompasses also a lot of more technical fastening applications such as in microelectronics, automotive or biomedical where the use of a solventless solid adhesive is very attractive (Creton, 2003).

Before we discuss in more detail the current understanding of the adhesion mechanisms, it is worthwhile to present a short historical prospective. Early studies on the mechanisms of adhesion are based on the peel test, which mainly provides a peel force as a function of velocity of steady state debonding, and they pointed out immediately the crucial role played by rheology and large deformation. The seminal series of papers of Dave Kaelble from 3M on the physics of peeling(Kaelble, 1959, Kaelble, 1960, Kaelble, 1964, Kaelble, 1965, Kaelble, 1969) laid the foundations of the current understanding of the mechanisms already in the 60's. He first pointed out that the rheological properties of the soft adhesives were (with a few exceptions) more important than the surface properties of the adherend (Kaelble, 1969), that peel adhesion master curves could be constructed by using time-temperature shift factors (Kaelble, 1964) and that cavitation had to occur ahead of peel

significant region of large deformations and dissipation

fronts (Kaelble, 1965). Several much better cited studies followed focusing on the interplay between rheological properties, surface interactions and the apparent fracture energy $\Gamma_{app}(v)$(Gent and Petrich, 1969, Andrews and Kinloch, 1973a, Andrews and Kinloch, 1973b, Gent and Schultz, 1972) and confirmed indeed that the work to debond a soft viscoelastic adhesive was dependent on both the interfacial interactions and the rheological properties of the adhesives, although the details of the deformation mechanisms were undoubtedly complex and these studies did not address the effect of adhesive thickness.

The details of the deformation mechanisms were in parallel addressed by experiments using a probe method, described in section 2, which provides a more homogeneous and controlled loading condition, during both bond formation and debonding. The earliest such study to our knowledge is that of Erb and Hanson (Erb and Hanson, 1960) who used a high speed camera to observe fibril formation from the side on a series of liquids and speculated that these fibrils were initiated by cavities. Cavitation itself was studied also in rubbers with poker-chip tests (Gent and Lindley, 1959, Gent and Tompkins, 1969), in simple liquids (Briggs, 1950, Briggs, 1951) and in viscoelastic liquids (Kaelble, 1971), but experimental evidence was indirect or post-mortem. The first direct evidence of the nucleation and growth of cavities *during* debonding of a soft adhesive from a probe was carried out by Lakrout et al. (Lakrout et al., 1999) with a camera positioned under a transparent glass substrate and the debonding scenario that they proposed shown in Figure 12, remains a good microscopic description of the debonding mechanism.
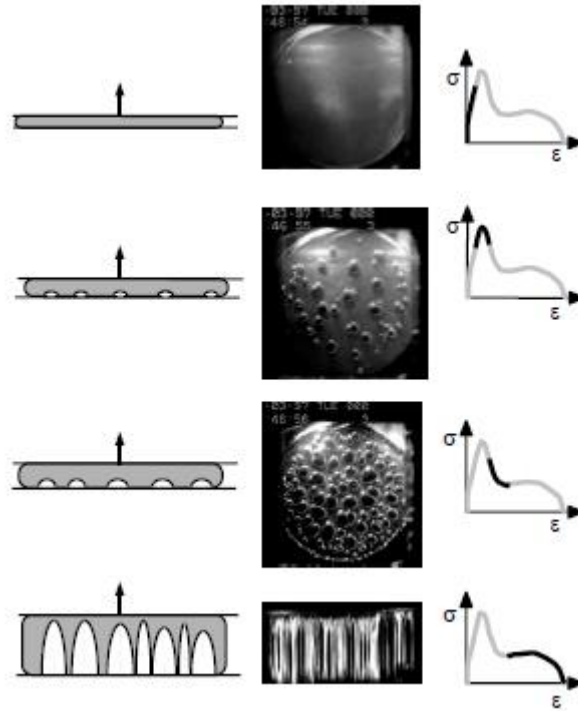
Figure 12: Schematic of the debonding mechanism of a soft adhesive from a rigid surface in a probe tack test. Reprinted from (Lakrout et al., 1999).

The first stage is the contact formation where the soft material makes an intimate contact with the surface. If that surface is rough, the extent of real contact and the air pockets remaining trapped at the interface depend on the interplay between the viscoelastic properties of the PSA, the strength of adhesive interactions at the interface and the topography of the surface(Persson et al., 2004, Hui et al., 2000, Creton and Leibler, 1996, Fuller and Tabor, 1975). After the contact has been established, the probe is normally maintained in contact for a set dwell time, and subsequently removed at a constant velocity. During this stage the force first returns to zero and then becomes tensile as shown schematically on the interface and then can grow normal to the interface and form the fibrillar structure previously observed from the side. The details of such a scenario depend strongly on the material properties of the adhesive and on the surface chemistry and topography.

It is now the purpose of the next sections to discuss the details of the bonding and debonding mechanisms. It should be noted here that the peel test is an inherently steady state test where a well defined crack front propagates involving an apparent fracture energy $\Gamma_{app}(v)$, while probe tests are transient tests that separate the microscopic details of the contact formation from the debonding as a function of time (or position of the probe) while providing the measurement of a total work of debonding per unit area W_{deb}. It is therefore logical to begin with a description of the general common features involved in the bond formation. We then turn to the most interesting and complex physics occurring during debonding, where we will first address the experimentally simpler peel test that describes the more common way of debonding and then move on to the probe test for a more detailed investigation of the microscopic mechanisms of debonding.

5.1 BOND FORMATION: SPONTANEOUS CONTACT ON ROUGH SURFACES

A crucial requirement for a PSA to stick to a surface is to form at least van der Waals bonds with the largest proportion of the macroscopic surface as possible. This process of contact formation is often described in the trade literature as "wetting the surface". However, most soft adhesives cannot flow and are best seen and described as soft viscoelastic solids.

Therefore it is best to start with elastic solids and to subsequently introduce viscoelasticity. For an elastic solid, the minimum criterion for the formation of an intimate contact on a rough surface is that the elastic strain energy stored in

25

the adhesive per unit area of contact should not exceed the Dupré work of adhesion w, i.e. the energy gain in forming an interface. This simple idea can be seen already qualitatively by examining the contact of radius a between a single hemispherical rigid asperity of radius R and a soft planar surface of modulus E. The excess free energy of the contact of a single asperity is given by:

$$\Delta F_{exc} \sim - wR\delta + E \left(\frac{\delta}{a}\right)^2 a^3 \qquad \textbf{22}$$

where δ/a is the elastic deformation that takes place over a volume of the order a^3, and δ is the indentation. If one uses the approximate geometric relation $a \sim \sqrt{R\delta}$ and minimizes ΔF_{exc} with respect to δ, one obtains an expression between the modulus of the material and the indentation depth δ for an asperity of radius R in order to maintain an equilibrium contact area or radius a in the absence of any applied force other than van der Waals interactions at the interface.

$$E^* (P = 0) \sim w \left(\frac{R^{\frac{1}{2}}}{\delta^{\frac{3}{2}}}\right) \qquad \textbf{23}$$

For a single asperity, the steeper the asperity (small R, large δ) the softer must the material be to create the same surface of contact a. For a fully indented asperity of 2 μm in height and a radius of 100 μm, and a work of adhesion w = 50 mJ/m^2, one finds a value of E* = 0.2 MPa, which is very close to what is the practical limit for good contact.

Of course real surfaces are rough and have a random distribution of asperities. Two modeling strategies have been mainly used for random surfaces: a strategy modeling a population of uncorrelated asperities with identical radii, but a distribution of heights (Fuller and Tabor, 1975, Greenwood and Williamson, 1966, Creton and Leibler, 1996, Hui et al., 2000) and a second strategy where the roughness is described by a power spectrum, which emphasizes wavelength and correlation between asperities more than height of individual asperities (Persson and Tosatti, 2001, Persson, 2002, Persson et al., 2004). The first strategy works well for a low level of contact, in other words when only the tip of the asperities come into contact. The second strategy typically calculates, as a function of wavelength, the strain energy necessary to force the contact of the soft material on a rigid rough surface. By comparing the strain energy per unit area of contact, to the work of adhesion this second approach determines the range of wavelengths where contact is energetically favorable, and from the power spectrum of the surface, it determines the fractional area in contact. This results in a wavelength dependent adhesion, because very small wavelength roughness entails significant deformation costs and will lose contact for lower elastic moduli than the long wavelength roughness.

Both types of models predict qualitatively the increase in true contact area with decreasing elastic modulus and decreasing roughness amplitude or aspect ratio. However, quantitative comparisons with experimental data are rare (Lorenz and Persson, 2009, Lorenz et al., 2013) because random rough surfaces are difficult to obtain and to characterize. Moreover extracting a truly relevant parameter from a random distribution of asperities is not straightforward despite recent progress in particular with simulations. (Pastewka and Robbins, 2014).

The key physical aspect in these models is the notion that the interfacial area that is truly in molecular contact is generally incomplete. The elastic energy stored in the adhesive near the interface during the contact formation is a driving force to *spontaneously* detach the adhesive from the surface even without any macroscopic tensile force (Greenwood and Williamson, 1966, Fuller and Tabor, 1975, Persson et al., 2002). In the absence of viscoelastic dissipation the contact is fully reversible and the applied pressure during the compression stage does not influence the detachment process (i.e. the tensile part of the curve). This prediction can only hold for very weakly adhesive rubbers and is counterintuitive to any person who has used soft adhesives. Yet it is the basis of equation 23 that predicts the existence a threshold modulus at long times E* above which the soft material will not spontaneously adhere to the surface under zero applied load.

While the picture presented above is true for elastic materials, pressure-sensitive adhesives are highly viscoelastic. This introduces two important differences: 1) the whole history of contact formation matters for debonding, so that the energy dissipated during debonding depends on the applied contact pressure and the contact time. This is well addressed in single asperity contacts (Barthel and Haiat, 2002, Haiat et al., 2002, Lin et al., 1999), but is usually ignored in multi asperity contact theories (Hui et al., 2000, Maugis, 1996).

Technologists use an empirical criterion called the Dahlquist's criterion (Dahlquist, 1969), which specifies a maximum value of 0.1 MPa for the storage modulus μ' at 1 Hz and hence assumes that most of the contact formation occurs over a typical time of the order of 1s. If

after a one second contact and removal of the compressive force the leftover elastic stored energy per unit area near the interface exceeds the work of adhesion w, the contact will spontaneously break even under zero applied force.

5.2 MACROSCOPIC ANALYSIS OF THE STEADY STATE DEBONDING BY THE PEELING TEST

The peel tests constitute the easiest method to test a soft adhesive, yet the interpretation of the measured peeling energy as a function of the mechanical properties of the adhesive itself remains challenging. Due to the very soft nature of the adhesive films, it is generally bonded to a flexible but weakly extensible backing and the two are peeled together from a rigid flat substrate at an angle θ as shown in Figure 4. For non-vanishing peeling angles, the strain energy release rate $\mathcal{G}$ can be easily evaluated from the measured peel force by equation 8 and under

steady-state propagation $\mathcal{G}$ corresponds to an apparent fracture energy $\Gamma_{app}(v)$ as in Figure 13. $\Gamma_{app}(v)$ typically increases with velocity up to a peak that is followed by stick-slip dynamics(Barquins and Maugis, 1988, Villey et al., 2015, Ciccotti et al., 2004) and which is out of the scope of the present review. If we limit ourselves to the steady-state propagation (slow branch with positive slope on Figure 13) the apparent fracture energy $\Gamma_{app}(v)$ is related to the three main ingredients of the adhesive joint: 1) the rheology of the soft adhesive, 2) the intensity of the surface interactions (discussed in section 5.3) and 3) the geometry of the adhesive layer (thickness h) and loading (peeling angle θ).
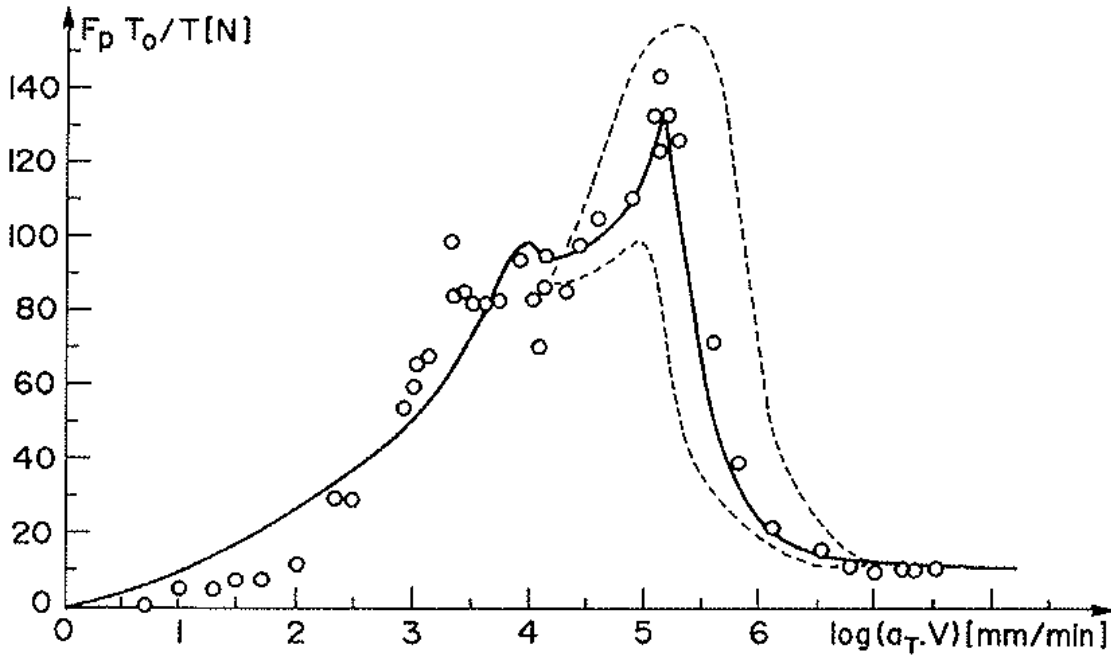
Figure 13: Peel force as a function of peel rate for a typical uncrosslinked viscoelastic polymer (Figure from (Derail et al., 1998))

While the applied strain energy release rate $\mathcal{G}$ (given by equation 8) is independent of the nature of the adhesive, the measured fracture energy $\Gamma_{app}(v)$ is dominated by the energy dissipated during the deformation of the thin adhesive layer during debonding. A quantitative prediction of $\Gamma_{app}(v)$ from the properties of the adhesive requires an adequate knowledge of the

strain field in the adhesive during peeling, which turns out to be very complex due to both the elevated confinement of the adhesive and the complex deformation mechanisms that can occur at micrometer scales, such as cavitation and fibrillation(Urahama, 1989, Ito et al., 2014, Chiche et al., 2005b, Villey et al., 2015).

The essential point to understand when describing the peeling of a thin adhesive layer is that, due to the extremely soft nature of the adhesive used, the stress singularity at the crack tip cannot be developed within the bulk of the adhesive layer and the extremely blunt crack front can only act as a moderate local stress concentrator to some finite stress value. If we consider for example a typical viscoelastic adhesive layer of modulus E debonded from the substrate with an apparent fracture energy $\Gamma_{app}(v)$, according to equation 5 the typical stress singularity of LEFM given by equation 2 can only set up at scales larger than $\Gamma_{app}(v)/E$. Both the apparent fracture energy $\Gamma_{app}(v)$ and the effective storage modulus E are increasing functions of the crack velocity, and their ratio can be estimated as larger than 1 mm for most steady state peeling conditions, which is larger than the typical thickness of the adhesive layers(Villey et al., 2015). The stress and strain fields in the peeled adhesive can thus be assumed to be uniform through the thickness of the adhesive and to be a scalar function of the position along the tape, thus constituting a sort of cohesive zone between the backing and the substrate. This treatment assumes the adhesive to act as a series of independent strands, and it is mathematically represented by an elastic or viscoelastic foundation which is the basis of the theories for the peeling of thin adhesive layers that are described in the rest of this section.

The first such theory of peeling of soft adhesives was proposed by a 3M scientist, David H. Kaelble (Kaelble, 1964, Kaelble, 1960, Kaelble, 1965). The theory only aims at modeling the steady state peeling, where a coherent constant energy balance can be established through the different scales of the problem. The backing is treated as a flexible and extensible elastica, i.e. a thin linear elastic strip of typical Young's modulus $E_B \sim$ GPa and thickness h_B (comparable to the thickness h of the adhesive), submitted to en external force F applied at an angle θ. The stress distribution in the adhesive constitutes all the remaining boundary condition for the solution of the elastic profile of the backing. The effect of confinement on the mechanical response of the adhesive is neglected and its constitutive behavior is considered as linearly viscoelastic, or more precisely as linear elastic with frequency dependent elastic moduli E and $\mu = E/3$ that depend on the peeling velocity through a local time scale t_c defined later. In a first version of the model (Kaelble, 1960) cavitation is neglected and the crack front is still treated as a simple triple line (between substrate, adhesive and air). Under these assumptions the following analytical solution can be derived to express the stress distribution in the bonded part of the adhesive as a function of the distance x from the crack front:

$$\tau(x) = \tau_0 \exp(\alpha x) \qquad \alpha = \left[\frac{\mu}{2E_B h_B h}\right]^{\frac{1}{2}}$$

$$\sigma(x) = \sigma_0(\cos\beta x + K\sin\beta x)\exp(\beta x) \qquad \beta = \left[\frac{3E}{8E_B h_B^3 h}\right]^{\frac{1}{4}}$$

where K is a dimensionless constant depending on the peeling angle θ. This model can be interpreted as follows. Due to the linearity of the analysis, the shear and normal stress distributions can be treated as independent. Both shear and normal stress distributions present a stress concentration at the crack front and an exponential decay as a function of the distance inside the bond (as in Figure 14). The attenuation lengths (or stress concentration lengths) are given respectively by $1/\alpha$ and $1/\beta$, which scale with the adhesive thickness h (close to h_B) and are strongly dependent on the ratio of the elastic moduli of the backing and adhesive.

For a typical adhesive thickness of 20 μm the attenuation lengths are of the order of 1 mm for shear stress and 100 μm for normal stress and are independent of the loading condition (F, θ). Moreover, the traction part presents an additional oscillation with a wavelength identical to the attenuation length (i.e. a critically damped oscillation). The two stress distributions are found to depend on the peeling angle θ through the dimensionless constant K (ranging between 0 and 1 for non vanishing angles), which depends on the ratio between shear and normal stress.
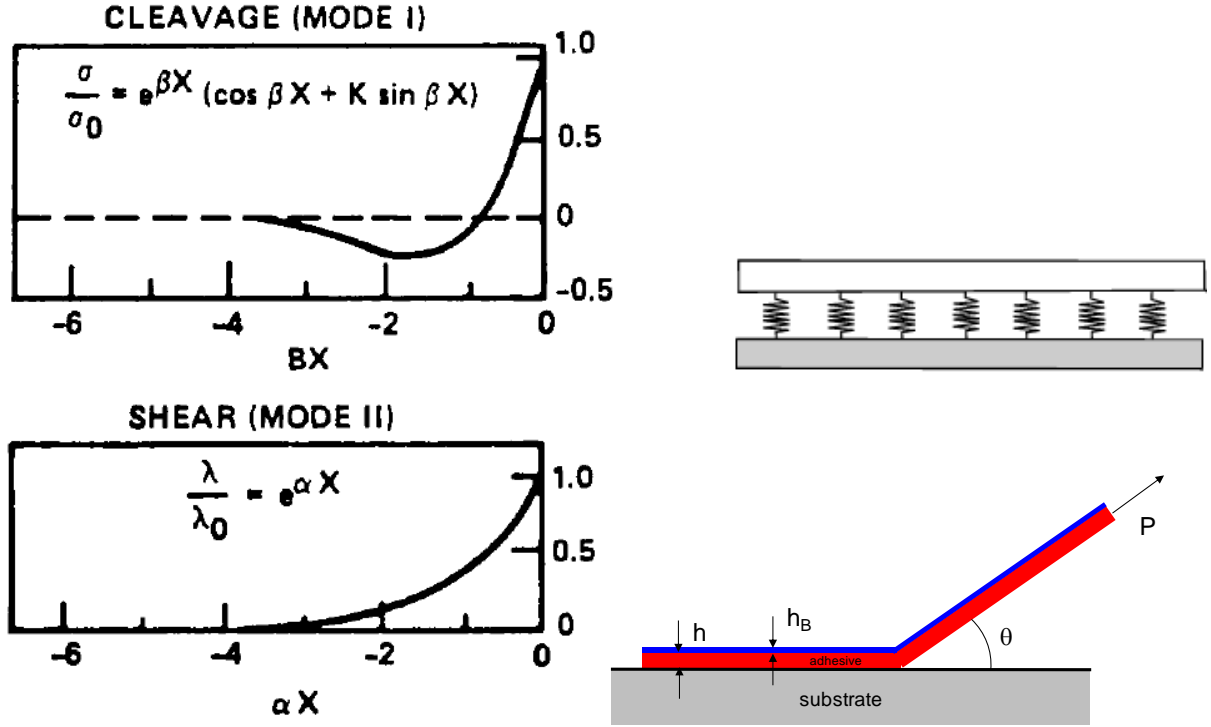
Figure 14: Left: Representation of the normal (cleavage) and shear stress distributions in the Kaelble's model for the peeling of a flexible elastic backing on an elastic foundation of independent springs. Right: mechanical schemes from (Kaelble, 1992).

The maximum values of the stresses are related to the peel force *F* through:

$$\tau_0 = \frac{\alpha}{b} F \cos \theta \qquad \sigma_0 = \frac{2\beta}{b(1-K)} F \sin \theta \qquad\qquad 25$$

which simply means that each force component is balanced by a stress concentrated on a length $1/\alpha$ or $1/\beta$ respectively. By imposing a debonding criterion based on a maximum traction stress σ_c for the debonding at the crack front (which is reasonable for non vanishing peeling angles), the apparent fracture energy can be derived as:

$$\Gamma_{app}(v, \theta) = hK^2 W_c(v) \qquad\qquad 26$$

where W_c is the maximum density of stored elastic energy given by σ_c^2/E according to the linear character of the model. Kaelble gave a more complete description of the contribution of shear to the fracture energy, but this can be neglected for most non-vanishing peeling angles and is not discussed here. The most important prediction of equation 26 is that $\Gamma_{app}(v)$ should be proportional to the thickness *h* of the adhesive layer and is not explicitly related to the Dupré work of adhesion *w*, although the intensity of the molecular interactions comes into play through the value of the maximum

stress σ_c. Although the linear dependence of $\Gamma_{app}(v)$ on *h* is rarely observed experimentally, for practical adhesive layer thicknesses (10-300 μm) $\Gamma_{app}(v)$ clearly increases with *h*(Kaelble, 1992, Gardon, 1963b). This makes it clear that such apparent fracture energy should not be confused with a fundamental fracture property of the interface between the adhesive and the substrate, but it is rather the result of the deformation of the whole adhesive layer. The role of the rheology of the adhesive on $\Gamma_{app}(v)$ was investigated by Kaelble (Kaelble, 1964) and others(Derail et al., 1997, Derail et al., 1998, Gent and Petrich, 1969, Yarusso, 1999) who presented extensive measurements at different peel rates and temperatures. The data of the peeling force as a function of velocity and temperature were shown to be generally collapsed into a single master curve by the same type of time-temperature equivalence used for the linear viscoelastic properties of the bulk polymer. This is strong evidence of the viscoelastic origin of the dissipation in peeling of soft adhesives, yet it does not carry exact information on the nature of the mechanisms of

29

deformation that are involved. Kaelble's model introduces the effect of viscoelasticity by using in equations 24 the real part of the complex viscoelastic modulus associated to the characteristic local loading time t_c that is obtained by dividing the attenuation (oscillation) length of the traction stress function in 24 by the constant peeling velocity v. Since σ_c is assumed to follow the same time-temperature scaling as the elastic moduli, equation 26 justifies that also the peeling force F or the apparent fracture energy Γ_{app} follow the same scaling.

Kaelble (Kaelble, 1964) presents extensive data covering a wide range of peeling velocities and temperatures, and also the effect of using eight different substrates. The data are claimed to globally support his model for the link with rheology. However, some critical (and questionable) assumptions have been made in order to fit the data. As discussed before, the critical density of elastic energy W_c in equation 26 is given by σ_c^2/E, according to linear elasticity, but the associated strain σ_c/E is well beyond the regime where linear elasticity holds. Secondly, the estimate of the velocity dependence of σ_c remains unsatisfactory. Kaelble (Kaelble, 1964) simply decided to use the well established data from Smith(Smith, 1958) on the true stress at break for a crosslinked elastomer as a function of temperature and strain rate. However, this is not the same physical quantity as the maximum stress sustainable at an interface before detachment, and the final experimental validation of the model is thus unsatisfactory
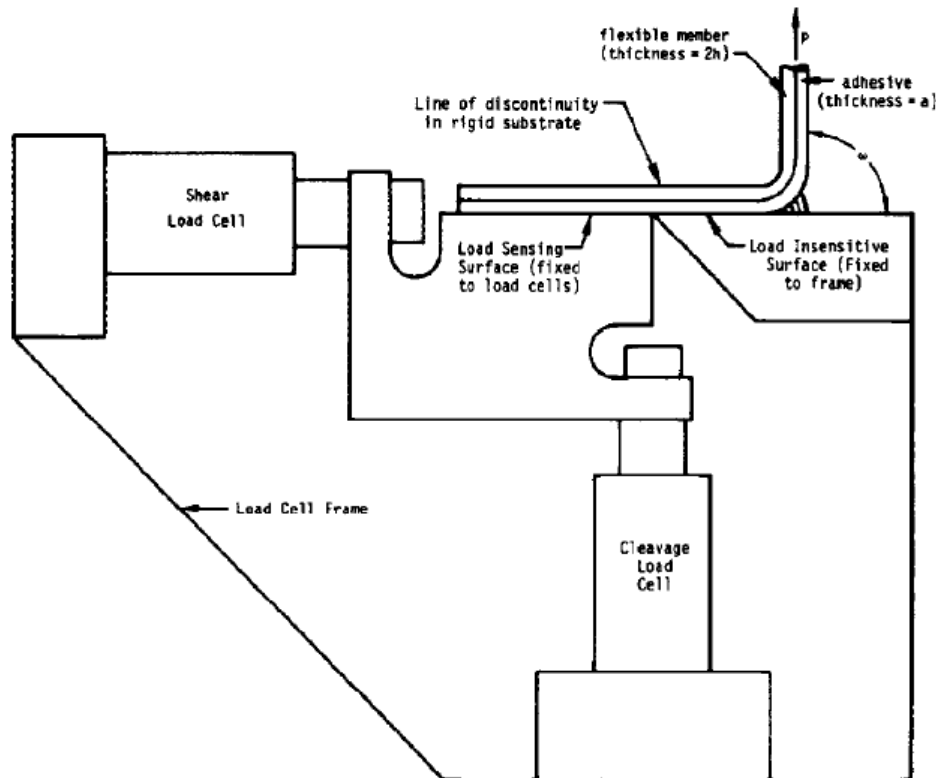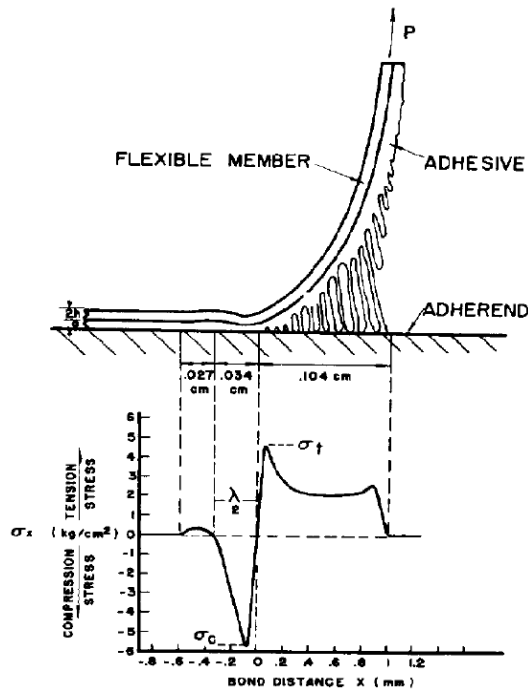

Figure 15: Schematic of the peeling device from (Kaelble and Ho, 1974) where the left half of the substrate beam is connected with two shear and traction load cells.

As a parallel path to validate his model, Kaelble (Kaelble and Ho, 1974, Kaelble, 1964, Kaelble, 1960, Kaelble, 1969) developed a custom peeling device based on two Split Beam Transducers (SBT). The device is represented schematically in Figure 15 and through clever mechanical design it can measure both the shear and the normal components of the force as a function of the position of the peeling point under steady state propagation. The data can then be used to reconstruct the spatial distribution of shear and normal stresses in the bond as shown in Figure 16. The validity of the overall predictions on the shear and normal distributions have been verified on the intact part of the bond (left of the maximum tensile

stress). But there is evidence of a significantly more extended region of tensile stress on the right of the peak, instead of the expected abrupt stress drop. Kaelble (Kaelble, 1965) correctly attributed this extended debonding region to the occurrence of a region of cavitation and fibrillation. He also investigated the physics and conditions for cavitation in soft viscoelastic media (Kaelble, 1971). However, he could not reach a sound modeling of the effective stress applied to the peeled backing by the fully fibrillated region, and he could not integrate this important element into his elaborate model for the cohesive zone and for the link with rheology. He chose instead to apply his model to the uncavitated bonded region on the left of the stress peak. While the modeling seems consistent with experiments, much of the physical interpretation becomes less clear.

However, the very important picture that he proposed in (Kaelble, 1965) of the debonding mechanisms (cf. Figure 16) provides the first qualitative sound explanation of the link between the fibrillated region and the stress distribution in the bond region and of the non trivial effect of changing the peel angle on the debonding energy as demonstrated recently(Villey et al., 2015). The shape of the tensile stress profile in the cohesive region is strongly reminiscent of the traction curves of the probe tests that were extensively studied in the 80's, 90's and 2000(Zosel, 1985, Zosel, 1989, Shull and Creton, 2004) (cf. Figure 16) in order to better understand the details of the debonding mechanisms of cavitation and fibrillation and will be presented in detail in section 5.3.

Figure 16: Schematic of the debonding mechanism of a soft adhesive from a rigid surface in a probe tack test along with the measured traction stress profile (after(Kaelble, 1965)).

A very interesting complementary investigation was presented by Gent and Petrich (Gent and Petrich, 1969) who tested a set of model adhesives, mostly uncrosslinked, designed to catch the importance of the non linear behavior of the adhesive under large stretch. The experiment consists in a T peel test (cf. Figure 4) carried out at different peel rates and temperatures. The peeling force data $F(v)$ were then reduced into master curves, which are in good agreement with the WLF time-temperature equivalence. The link between peel

mechanics and rheology of the adhesive is made by using a simplified model based on similar assumptions as Kaelble's model. However, the bond stress distribution was completely neglected and only the deformation of individual fibrils up to debonding was considered. The adherence energy $\Gamma_{app}(v)$ was thus estimated as the work of debonding at a constant strain rate related to the peeling velocity by: $\dot{\epsilon} = v/a$ in an analog way to equation 26 from Kaelble:

$$\Gamma_{app}(v) = \frac{F(v)}{b} = h \int_0^{\sigma_c} \sigma(\epsilon)d\epsilon \qquad \textbf{27}$$

where σ_c is again the maximum stress attained in each strand and b is the strip width. However, σ_c was assumed to be limited by two possible failure criteria: cohesive rupture of the adhesive when the tensile strength of the polymer is attained first, or detachment from the substrate when the maximum tensile stress that the interface can withstand is reached first.

The $F(v)$ curves are similar to those of Figure 13, but they present two major peaks. The peak at lower velocity was attributed to the transition from cohesive to adhesive debonding, since the transition strain rate was in agreement with the terminal relaxation time (reptation time) of the polymer, which marks the onset of viscous flow. Additionally this peak was shown to disappear upon crosslinking the adhesives and suppressing therefore the possibility of viscous flow and cohesive debonding. The second peak at higher velocity was associated to a combined effect of the glass transition and of the specific T-peel test geometry, on the mechanisms of adhesive debonding. Unlike Kaelble, Gent ant Petrich

assumed a constant value of the maximum tensile stress σ_c (which is the only adjustable parameter of the theory), but they took into account the influence of large strain non-linear rheology of the adhesive in uniaxial extension (Gent and Petrich, 1969). They pointed out that two adhesives with very similar linear viscoelastic properties, can result in different

peeling curves $\Gamma_{app}(v)$ when they differ significantly in their large strain behavior. This prediction was recently demonstrated by (Villey et al., 2015). Moreover, the increase of the strength of the interfacial interactions results in a comparatively stronger effect of the differences in non linear properties on the peel force as shown in Figure 17

.
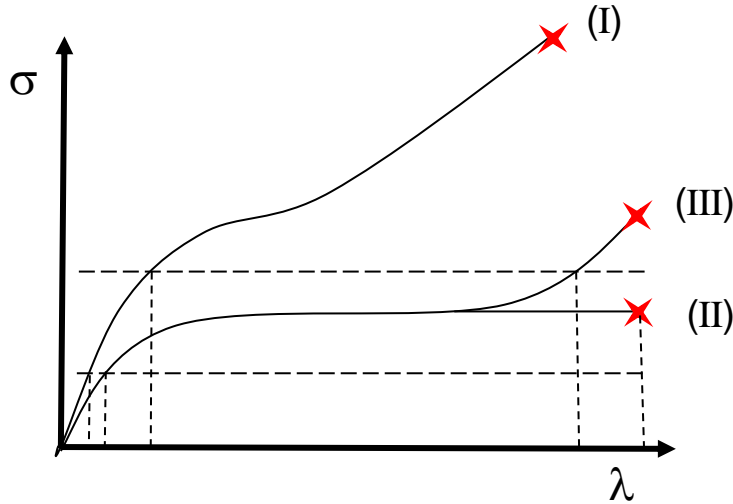
Figure 17: Schematic stress-strain relations for rubbery (1), liquid-like (II) and strain hardening (III) materials. The horizontal dashed lines denote possible levels of the maximum interfacial bond stress σ_c. The vertical dotted lines denote the limiting extensions attainable in each case.. Inspired by the original scheme in (Gent and Petrich, 1969).

Another important contribution to the modeling of the peel curve $F(v)$ was proposed by Derail et al. in a series of papers focusing on peeling of uncrosslinked polybutadiene model polymers(Derail et al., 1998, Derail et al., 1997) and of several kinds of hot melts PSA adhesives(Marin and Derail, 2006, Derail et al., 2004, Gibert et al., 2003, Gibert et al., 1999). Similarly to the previously cited models, the prediction of the peel force was obtained by combining the analysis of the bending of the elastic backing (with some complications from plasticity here) with the modeling of the cohesive force applied from the soft viscoelastic adhesive. For the sake of simplicity the flexural profile of the backing was considered as a circular region connected to two straight regions (bonded and unbonded). The cohesive stress of the adhesive was treated again as the uniaxial extension of independent strands. While the confinement effects were neglected, the large strain extension was modeled with a viscoelastic fluid model using parameters extracted from linear rheology and adhesive composition. The

peeling curves were reduced to a general master curve using a time-temperature equivalence for a given adhesive and a Deborah number defined as the experimental time divided by the terminal relaxation time of the polymer measured in linear rheology. The same scaling was applied to all peeling regimes (cohesive, slow interfacial, stick-slip, fast interfacial).

The critical point of the analysis is the choice of the criterion for propagation. In the cohesive regime (Derail et al., 1997) a critical stretch $\lambda_c = 4.5$ was reasonably chosen as a fracture criterion, in agreement with experimental measurements of the fracture strain of the same adhesives under variable uniaxial strain rates. In the adhesive regime, a much more questionable fracture criterion was chosen. Derail et al. proposed that the fibrils detach when the total work done on the fibril attains a critical value $\sigma_c(\lambda_c - 1) h_0 = $ cst, where λ_c is the stretch in the fibril at the debonding point. This fracture criterion is however poorly justified theoretically and the important parameters are

not accessible experimentally. Nevertheless, this set of articles provides very interesting measurements on the relation between the structure of the adhesive and their peeling properties. The data set can also be completed by the work of Gower and Shanks on several families of acrylic based PSA adhesives(Gower and Shanks, 2006, Gower and Shanks, 2005, Gower and Shanks, 2004b, Gower and Shanks, 2004a) and by that of Benyahia et al. on soft block copolymer adhesives for medical applications(Verdier et al., 1998, Benyahia et al., 1997). We remark that while the link with rheology in Kaelble's model is related to the loading rate of the zone of stress concentration in the bonded adhesive, this zone is absent in the model of Derail, where the only dynamic length is the radius of curvature of the bent part of the backing and the dissipation seems more related to the finite extension of the adhesive in a cohesive zone (associated to a fibrillated zone) where stretch can be significant.

In the late '90, the peeling investigation at 3M was taken over by another scientist, Dave Yarusso, who published an interesting investigation in 1999 concerning the modeling of the 180° peeling of natural rubber based PSA(Yarusso, 1999). The deformation of the adhesive was still modeled as the uniaxial extension of individual independent strands. The constitutive law of the adhesive was taken as a linear viscoelastic fluid (the generalized Maxwell model), the parameters of which were fitted on linear rheological measurements. The measured peeling master curves were shown to be consistent with a different fracture criterion based on a critical value of the stored elastic energy (it is indeed a criterion for the failure of each individual strand), but it should be reminded that Yarusso's investigation was limited to uncrosslinked adhesives that can flow and that estimating the stored elastic energy at large strains in soft viscoelastic solids is more complex.

We remark, to conclude, that all the presented descriptions of the peeling of thin soft adhesive layers share the representation of the adhesive deformation as that of a parallel array of independent strands. This description is of course reminiscent of the fibrillar structure often observed in the cohesive zone close to the crack front(Ito et al., 2014, Urahama, 1989, Verdier et al., 1998, Chiche et al., 2005b, Villey et al., 2015). However, the complexity of the local inhomogeneous deformation in the peel test has always hampered the quantitative investigation of these microscale mechanisms, which could only be approached by the probe test investigations described in the following section.

5.3 MICROSCOPIC ANALYSIS OF THE DEBONDING MECHANISMS BY THE PROBE TACK TEST

5.3.1 Transition from interfacial debonding to bulk deformation

As discussed in section 5.1, the contact against an imperfect surface (as most surfaces are) leaves small pockets of air in valleys that are not in contact. These pockets can be the seed of a localized deformation when a tensile stress is applied to the adhesive layer, leading to either the propagation of interfacial cracks or to the growth of cavities in the bulk that eventually lead to a complex fibrillar structure. This key result was demonstrated experimentally(Lakrout et al., 1999, Lakrout, 1998, Zosel, 1998) and described theoretically(Chikina and Gay, 2000, Gay, 2002, Gay and Leibler.L., 1999) in the late 90's.

Probe tests, and in particular those carried out with flat-ended probes and visualization tools, provide information on the transient stages of debonding under a more homogeneous and controlled loading, while providing the full stress vs. strain curve characteristic of the debonding mechanism and will be addressed here in detail(Shull and Creton, 2004). As the probe is lifted from the surface, the average nominal stress σ_N increases. If the material is incompressible, the tensile stress on a highly confined layer ($a >> h_0$, where a is the radius of the contact area and h_0 is the layer thickness) has a parabolic profile and the maximum tensile stress occurs under the center of the probe (Gent, 1994, Ganghoffer and Gent, 1995, Creton and Lakrout, 2000). Above a certain critical value of local stress, the air pockets trapped at the interface between the surface and the adhesive expand in volume and become optically visible. This expansion process in a soft elastic material has been studied theoretically both at the level of the individual cavity(Lin and Hui, 2004, Dollhofer et al., 2004, Williams and Schapery, 1965, Gent and Wang, 1991) and at the more collective level of the whole probe(Chikina and Gay, 2000, Yamaguchi and Doi, 2006, Yamaguchi et al., 2006).
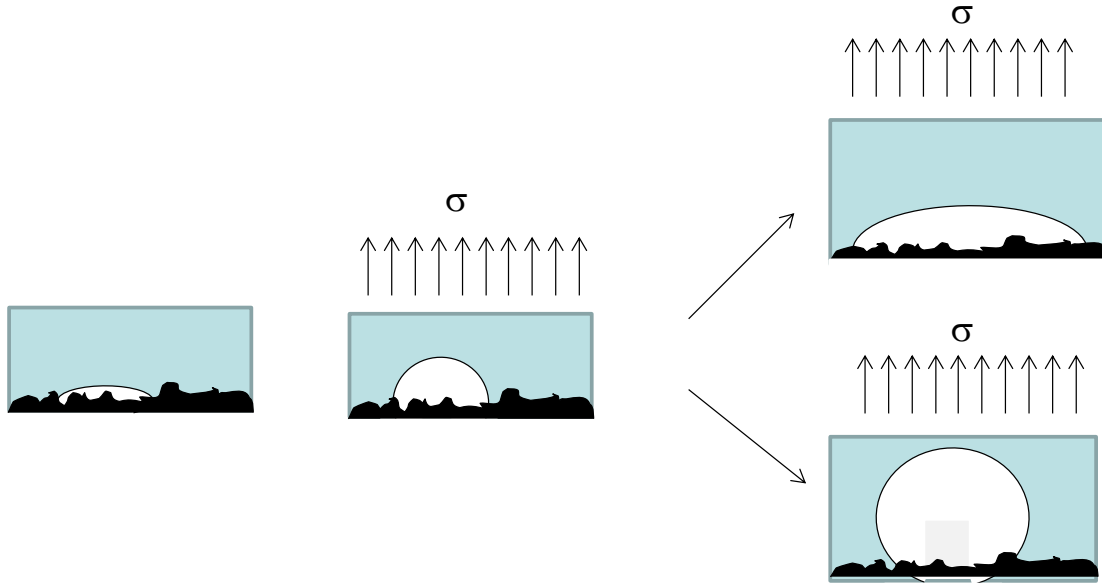
Figure 18: Schematic of early stage of debonding. Cavities grow from defects to hemispheres locally and the macroscopic stress field becomes much flatter promoting the nucleation of cavities randomly distributed along the surface.

The two key mechanisms shown in Figure 18 have been identified experimentally as 1) a more interfacial mechanism where cavities grow as cracks, mainly along the interface, and 2) a bulk mechanism where cavities grow mainly grow in the direction parallel to the tensile direction, and form cigars(Creton et al., 2001, Deplace et al., 2009b).

We use here the beautiful experiments of Yamaguchi et al.(Yamaguchi et al., 2007) to illustrate this difference. Yamaguchi et al. used an instrumented probe tester with an optical prism, to image the shape of the cavities, not in projection as it is usually done, but from a 45° angle which provides a 3D viewing. They

compared the debonding mechanisms of three differently crosslinked acrylic PSA. As shown on Figure 19, the less crosslinked adhesive forms nearly spherical cavities and the initial triple line where the cavity nucleated is actually pinned to the interface. On the other hand, the more crosslinked adhesive forms disk-like cracks that do not grow significantly in the bulk and eventually coalesce at a relatively low level of deformation. Such difference in mechanism can also be obtained by changing the surface chemistry of the interface while keeping the same identical bulk adhesive(Creton et al., 2001, Schach et al., 2007).
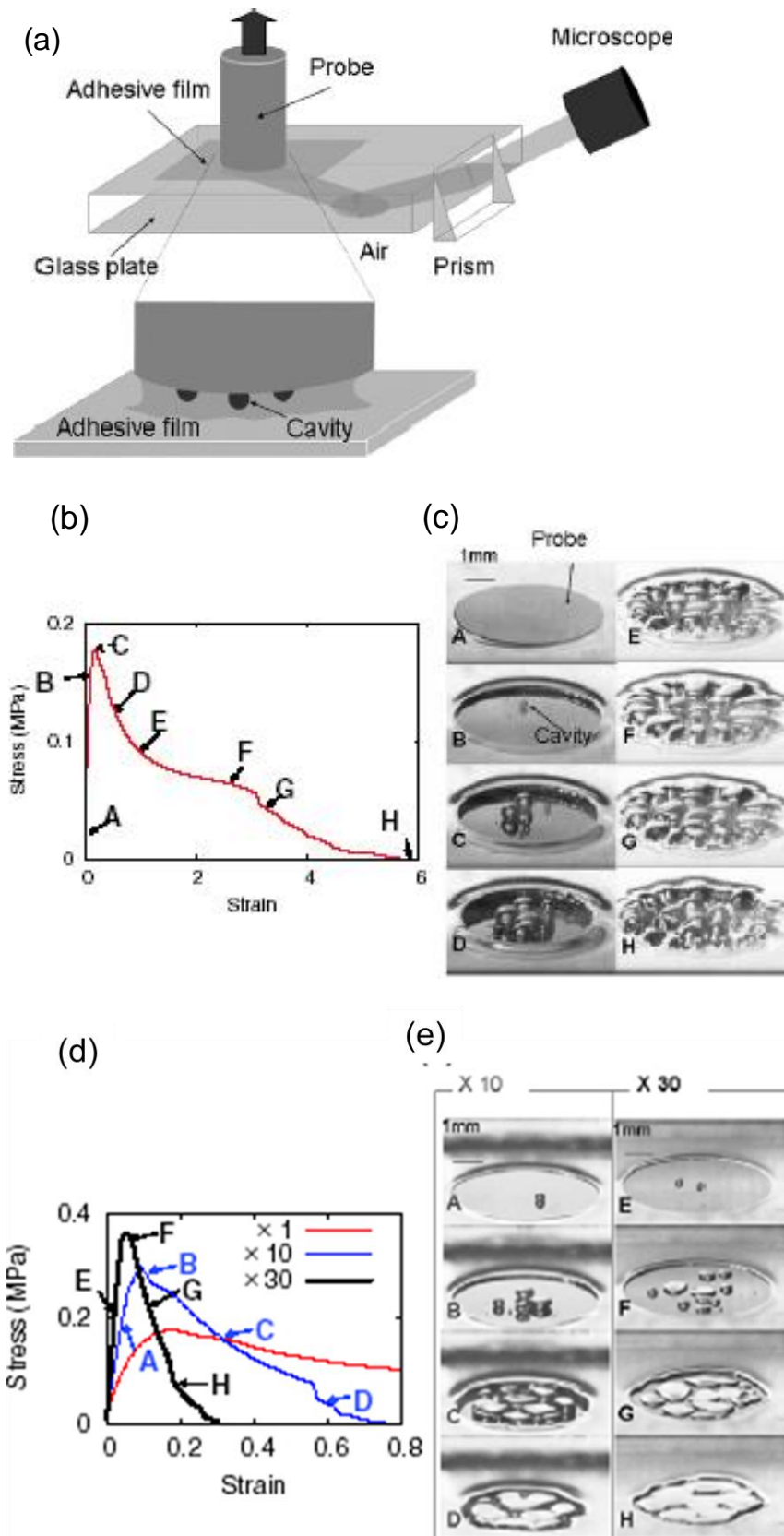
Figure 19: a) Setup used by Yamaguchi et al. to observe cavities at a 45° angle. b) Stress-strain curve of the less crosslinked adhesive and c) sequential images (A-H) corresponding to the position on this stress-strain curve. d) Stress-strain curves of all three adhesives. X10 and X30 correspond to ten and thirty times more crosslinker. e) snapshots of the cavities corresponding to positions on the blue (x10, images A-D)) and red (x30,images E-H) curves. Reprinted from (Yamaguchi et al., 2007).

The transition between bulk growth and interfacial growth of defects is important since this early bifurcation in mechanism leads to vastly different levels of dissipated energy during debonding. If the cavities grow in the bulk, the walls between cavities stretch in the tensile direction, eventually forming bridging fibrils when the walls break and, as shown in Figure 19, do not coalesce. On the other hand, the interfacial propagation mechanism leads to

the coalescence of the individual cracks nucleated on different defects at the interface, with little deformation of the bulk adhesive.

The transition between interfacial and bulk mechanism can actually be predicted quite well from linear arguments and a detailed derivation was first proposed by Crosby et al.(Crosby et al., 2000) for elastic materials and extended by Deplace et al.(Deplace et al., 2009b) and Nase et al.(Nase et al., 2008) for viscoelastic adhesives.

(a)
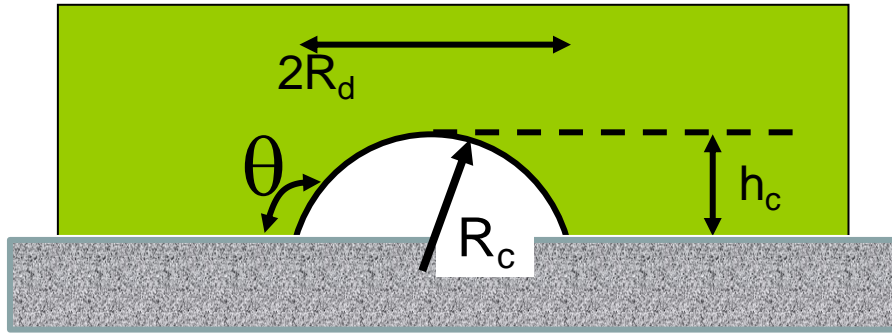
(b)
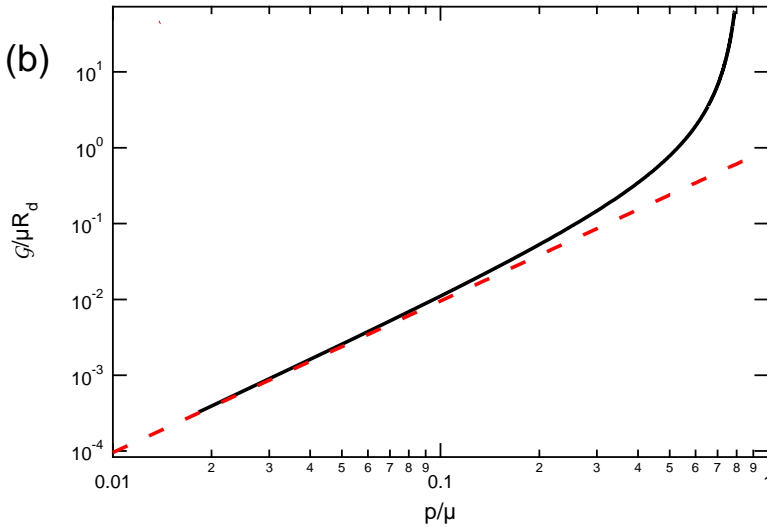
Figure 20: a) Schematic of a single penny-shaped crack at the interface between a hard surface and the soft material as described in the main text. b) Normalized energy release rate for a penny-shaped crack growing in the bulk as a function of normalized hydrostatic tensile pressure p. The full line is the prediction for a neo-Hookean material while the dashed line is the linear elastic prediction given by equation 28. Data from (Shull and Creton, 2004).

Following Hui, Shull and coworkers(Lin and Hui, 2004, Shull and Creton, 2004) it is useful to analyze the growth of a single defect as shown on Figure 20. If we consider the response of an initial penny-shaped interfacial crack ($h_c/R_d \ll 1$) to an increasing hydrostatic tension p representative of the stress state near the center

of a very confined layer. For $p/E \ll 1$, we recover the crack driving force from standard linear elasticity theory (Lawn, 1993):

$$\mathcal{G} = \frac{3R_d E}{2\pi}\left(\frac{p}{E}\right)^2 \qquad \textbf{28}$$

As p/E increases, several things happen. The crack begins to inflate in the vertical direction, and the value of h_c in Figure 20 increases. The energy release rate also increases in agreement with equation 28, which remains valid for values of p/E less than about 0.4(Lin and Hui, 2004).

However, linear elasticity is not valid to describe the deformation of an adhesive at large strains and yet understanding the effect of such complexity on the mechanism is essential. The easiest approximation to our problem of expansion of a crack at the interface is the related (but much simpler) problem of the expansion of a cavity in the bulk of a rubber. If we assume an initial spherical cavity of radius R_0 expanding in a neo-Hookean material of Young's modulus E and use finite strain mechanics, the relation between the applied pressure and the radial stretch is given by (Green and Zerna, 1954, Gent and Lindley, 1959):

$$p = \frac{1}{6}E\left(5 - \frac{4}{\lambda} - \frac{1}{\lambda^4}\right) \qquad \mathbf{29}$$

It is immediately apparent that this equation does not have a solution for $p > 5/6\ E$. When the hydrostatic traction p approaches the elastic modulus of the material, the cavity should expand indefinitely. This surprising result is analogous to the well-known rubber balloon inflation instability and it is due to the combination of the non linear behavior of the material and the spherical geometry. In real experiments of cavitation in the bulk, the hydrostatic traction applied around the cavity relaxes as the cavity expands (Dollhofer et al., 2004, Chiche et al., 2005a, Chikina and Gay, 2000). Moreover, the material is typically not neo-hookean and may have a limiting value of the stretch λ where it stiffens and eventually fractures (Gent and Wang, 1991, Lin and Hui, 2004), so that its bulk fracture energy Γ also matters (Cristiano et al., 2010) as discussed in more detail section 6.4. For small cavities and/or soft rubbers, such as adhesives, the surface tension of the expanding cavity may also play a role (Dollhofer et al., 2004, Muralidharan et al., 2005). Nevertheless, equation 29 predicts a significant expansion of a cavity if the hydrostatic tension exceeds the Young modulus. Experimentally, cavities appear in soft confined materials, at stresses of the order of 3 times the Young's modulus (Lakrout et al., 1999, Lindner et al., 2006, Chiche et al., 2005a), which is not out of line with this simple prediction.

How is this connected to our problem of small crack (R_d, $h_c << h$) expansion at the interface ? Several scenarios can occur and in the following we have assumed that Γ is a rate independent purely interfacial property (a proper interfacial fracture energy) and that the elastic modulus E is an elastic (rate independent) constant. We also have ignored the details of the large strain properties of the adhesive, limiting the finite strain response to a neo-Hookean behavior.

As discussed above, for $\Gamma/E < R_d$, the initial defects at the interface will propagate following equation 28 as p/E increases, and will eventually coalesce causing the complete detachment of the adhesive from the surface. This regime is commonly encountered when well crosslinked rubbers are debonded from solid surfaces (Nase et al., 2008, Nase et al., 2010) or when soft adhesives are debonded from silicone release liners (Josse et al., 2004). For $R_d < \Gamma/E < h$ the crack will grow first in the bulk but will not propagate along the interface until $p/E \sim 1$. This a direct consequence of the non-linear instability, since, as p approaches 5/6 E, the energy release rate of the interfacial crack $\mathcal{G}$ increases nonlinearly to a much higher value that is determined by the large-strain response of the soft material. The specific value of p/E corresponding to this nonlinear increase depends on the details of the strain energy function that is used to describe the material and can be simulated (Lin and Hui, 2004). The example in Figure 20 is for a neo-Hookean material. This large increase in $\mathcal{G}$ corresponds to an increase from a value that is below Γ to a value that is above Γ, and the small cracks will grow in an unstable and rapid fashion at the interface and in the bulk until the stress relaxes. This non linear increase in $\mathcal{G}$ leads to a criterion for interfacial cavitation that is coupled to the elastic modulus of the material, and that is insensitive to Γ (Creton et al., 2001). This situation is typically observed for general purpose PSA (Chiche et al., 2000, Lindner et al., 2004). Finally for $\Gamma/E > h$ any cavity at the interface prefers to grow in the bulk and interfacial propagation is excluded. This regime is observed for some high strength PSA (Brown et al., 2002, Creton et al., 2009), but it is typically the situation encountered for soft adhesives developing strong chemical bonds (as opposed to Van der Waals bonds) with the surface.

In summary the transition between interfacial and bulk deformation can be approximately predicted by:

$$\frac{\Gamma}{Eh} = 1 \qquad \textbf{30}$$

i.e for $\Gamma > Eh$ the initial defects will mainly expand in the bulk of the adhesive layer.

Viscoelasticity will modify in many important ways the behavior of our model soft elastic adhesive. First of all, the fact that the small strain modulus of the material is frequency and temperature dependent, means that the temperature of the test and the probe velocity during debonding will clearly influence the results. In particular, the peak stress measured in a probe test (see

$$\sigma_N = \frac{F}{A_{\max}}$$

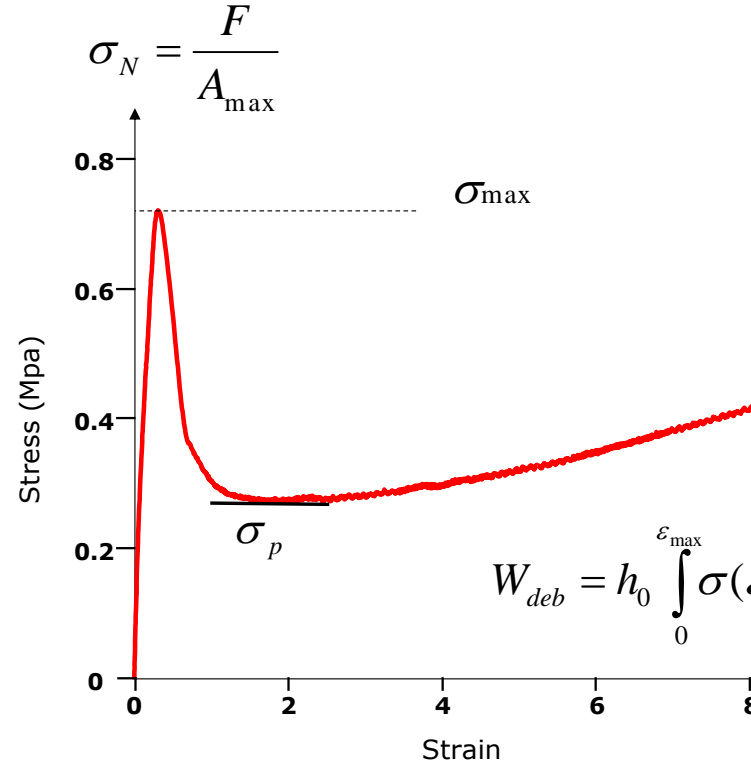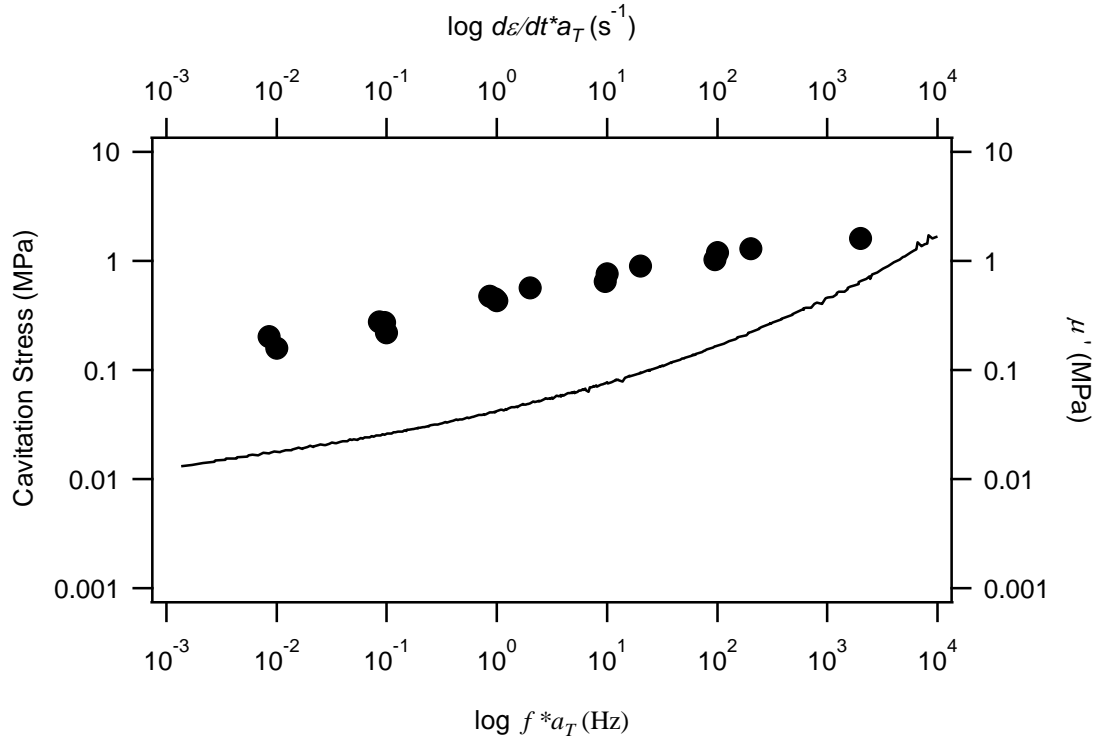$$W_{deb} = h_0 \int\limits_0^{\varepsilon_{\max}} \sigma($$

Figure 5), related to the expansion of cavities, can be plotted as a master curve (using the T-t equivalence) and is markedly dependent on the reduced strain rate (Lakrout et al., 1999) with a dependency that will typically parallel that of the modulus as shown on Figure 21.

Note that this rate dependence of the peak stress in the probe test justifies the rate dependence of the debonding stress used by Kaelble in his model described in section 5.2.

Then the dependence of the interfacial fracture energy Γ on crack velocity (we are speaking now of the microscopic cavity as a penny-shaped crack) and on the linear viscoelastic properties of the soft material $\mu'(\omega)$ and $\mu''(\omega)$, has been extensively studied for nearly elastic rubbers (de Gennes, 1996, Saulnier et al., 2004, Barthel and Fretigny, 2009, Baney et al., 2001). The key idea of these models is that the presence of a crack, even propagating at a constant speed, introduces a singularity at the crack tip where strain amplitudes and strain rates are very inhomogeneous. This spatial heterogeneity in strain rates means that the rate at which energy is dissipated depends on the viscoelastic properties of the adhesive and will vary spatially. For a classical rubbery adhesive, the value of $\mu''(\omega)$ and tan $\delta\,(\omega)$ increase with decreasing temperature or increasing applied angular frequency ω, leading to a predicted increase of Γ with crack velocity. We stress the fact that all of these models treat the viscoelastic dissipation as a perturbation of the LEFM crack tip stress singularity and thus lead to an intrinsic separability between an interfacial fracture energy Γ (v) and the bulk response of the adhesive that can be considered as elastic or viscoelastic in an independent manner. Although quantitative comparisons with experiments suggest that large strain effects cannot be ignored (Gent, 1996a, Barthel and Fretigny, 2009), we will leave this discussion to the fracture section and assume, as many authors, that the interfacial fracture energy Γ (v) can be empirically given by (Maugis and Barquins, 1978b):

$$\Gamma(v) = \Gamma_0(1 + \phi(a_T v)) \qquad \textbf{31}$$

where $\phi(a_T v)$ is a velocity dependent dissipative factor and Γ_0 is the threshold adhesion energy for vanishing crack velocities. If only van der Waals forces are present at the interface, Γ_0 reduces to the thermodynamic Dupré work of adhesion w.

If we now replace E by $3\mu'(\omega)$ and Γ by equation 31 in equation 30, and we assume that we are in the viscoelastic regime, i.e. $\phi(a_T v) \gg 1$, we can rewrite the transition condition as:

$$\frac{\Gamma_0 \phi(a_T v)}{3\mu'(\omega)h} = 1 \qquad \textbf{32}$$

Experimentally, equation 32 can be tested in two different ways. If Γ_0 is fixed, the transition between bulk deformation and interfacial crack propagation is controlled by the viscoelastic properties of the soft adhesive, and if the adhesive is fixed, changing the substrate leads to a change in Γ_0 which in turn affects the transition in mechanism.

It is generally found experimentally (Maugis and Barquins, 1978b) that the term $\phi(a_T v)$ has the same frequency dependence as $tan\delta(\omega)$ so that based on equation 32 if one plots $\Gamma_0 tan\delta(\omega)$ as a function of $\mu'(\omega)h$ for different materials and substrates, the materials where interfacial debonding mechanisms are observed will appear in different regions of the plot that those who deform in the bulk. This has been tested experimentally for a series of silicone adhesives with different values of $\mu'(\omega)$, h_0 and $tan\delta(\omega)$. The results are shown on Figure 22. It is clear that bulk deformation occurs for low values of $\mu'h_0$ (soft layers) and high values of $\Gamma_0 tan \delta$ (dissipative layers). The separation between the two regimes is quite abrupt for this system.
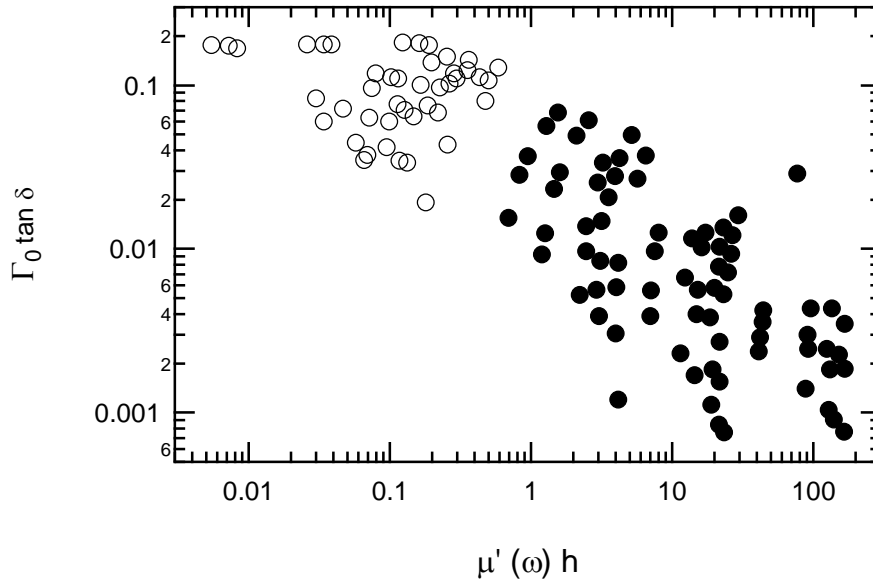
Figure 22: Open symbols represent bulk deformation and black solid symbols interfacial crack propagation. Experiments right at the transition can show both mechanisms due to fluctuations in the sample preparation. Data from (Nase et al., 2008).

5.3.2 Case I: Interfacial crack propagation

Up until this point we have focused the discussion on the energy dissipated by the deformation of the adhesive and not on the nature and strength of the interfacial interactions between the adhesive and the surface that have been bundled into a threshold adhesion energy of Γ_0. For the reversible separation between the two surfaces $\Gamma_0 = w$. Of course for deformable and viscoelastic adhesives this situation is completely hypothetical and separation from the surface always entails significant energy dissipation, both locally near the crack tip and globally in the whole sample. The question is then whether there is a direct relation between w and $\Gamma(v)$. Early papers on adhesion of PSA (Andrews and Kinloch, 1973a, Andrews and Kinloch, 1973b, Andrews and Kinloch, 1974, Gent and Schultz, 1972) argued that the measured $\Gamma(v)$ was directly proportional to an interfacial term without proving that this interfacial term was w. Then systematic experiments studying the adhesion of nearly elastic crosslinked rubbers on glass, supported the validity of equation 31 with $\Gamma_0 = w$ (Maugis and Barquins, 1978b). For general polymer interfaces the identification of Γ_0 with w is not correct and Γ_0 can be significantly larger than w due to extraction of interdiffused chains(Brown,

1993, Creton et al., 1994, Schach et al., 2007, Raphaël and de Gennes, 1992, Léger et al., 1999)or chain extension before fracture due to stronger bonds like covalent(Ahagon and Gent, 1975a, Ahagon and Gent, 1975b), hydrogen bonding or dipolar interactions(Ahn and Shull, 1998a, Ahn and Shull, 1998b).

Another very important insight came from the elegant experiments of Zhang Newby et al. (Zhang Newby et al., 1995) who clearly demonstrated that the influence of the interface on the dissipation $\Gamma(v)$ is not only due to the value of Γ_0 but can be critically affected by the ability of surfaces to slide relative to each other before failure. They prepared three substrates functionalized with fluorinated silanes, hydrogenated silanes and PDMS and peeled the same adhesive from those model surfaces. What they found was that the peel force at an identical peel rate did not scale at all with w (which is a well-defined property here). The mechanism proposed was that in the absence of slippage the deformation field at the crack front is significantly modified as shown on Figure 23. This change in crack front shape increases significantly the peel force due to additional shearing in the adhesive layer as demonstrated experimentally(Zhang Newby and Chaudhury, 1997, Amouroux et al., 2001) and theoretically(Krishnan and Hui, 2009).

40
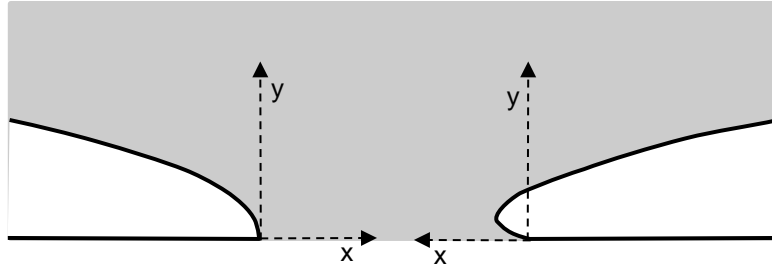
Figure 23: Sketch of the crack front configuration during the interfacial debonding of a soft viscoelastic adhesive and a rigid substrate in the case of low resistance to sliding (left) and high resistance to sliding (right).

Therefore, a low resistance to friction of the surface is one of the strategies to have a so-called release surface. Such a low resistance to friction can be obtained of course with liquid surfaces, which act as lubricant layers (Yao et al., 2013, Lafuma and Quéré, 2011). However, such liquid layers would need reservoirs to maintain the non-sticky character over repeated contacts. A more stable solution from the engineering point of view is to use crosslinked polymers with a very low glass transition temperature and the most commonly used material is silicone rubber (Kinning and Schneider, 2002), i.e. PDMS based polymers. However, any other polymer material with a low T_g will also provide a low resistance to friction provided that the adhesive and the surface are strongly immiscible with each other.

While interfacial slippage reduces adhesion, polymer chain interdiffusion across the interface

increases the level of interfacial interactions (more van der Waals bonds) or creates topological interactions called entanglements which in both cases increase Γ_0. This correlation between the formation of interfacial entanglements and adhesion has been clearly demonstrated for uncrosslinked high molecular weight polymer melts by Schach et al. with a series of probe tack experiments coupled with neutron reflectivity measurements of the width of the interface a_i (Schach et al., 2007). A weak immiscibility (measured by the interaction parameter χ) causes a higher level of chain interpenetration at the interface(Jones and Richards, 1999) and increases significantly the value of the work of debonding W_{deb} as shown in Figure 24.
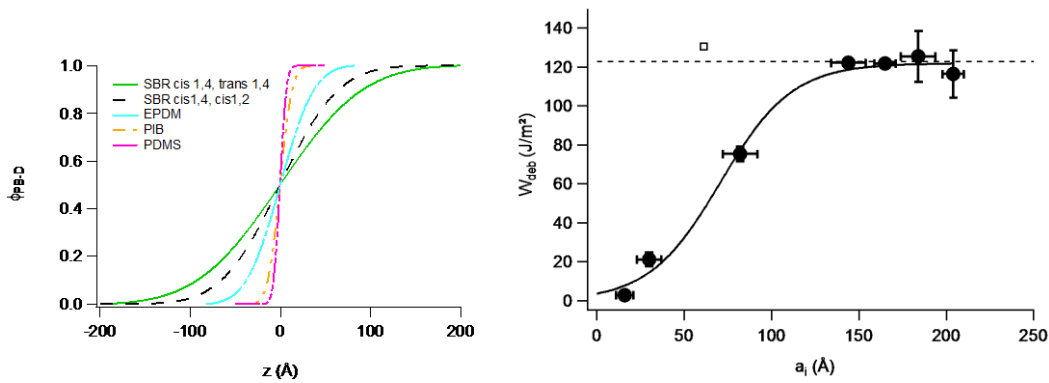
Figure 24: a) Concentration profile at the interface between deuterated polybutadiene and different polymers. B) Work of debonding W_{deb} measured by probe tack as a function of interfacial width a_i. Data from (Schach et al., 2007).

Since in this series of experiments, a thick (200 μm) identical layer of polybutadiene, is debonded from thin (100 nm) layers of different polymers, one can infer from these results that the changes in degree of interpenetration at the interface (Figure 24a) result mainly in changes in Γ_0 which then affect the energy dissipated by

the polybutadiene layer during the complex debonding process. Note that the horizontal line in Figure 24b represents the energy of fracture of the polybutadiene thick layer. As the interfacial width a_i increases from 1 to 15 nm, the failure mechanism changes from interfacial propagation of cracks (Figure 23 left) to crack

blunting and bulk deformation (Figure 23 right)

which we will now discuss.

5.3.3 Case II: From bulk deformation to fibril debonding

In some cases bulk deformation becomes dominant over crack front propagation. As shown in Figure 12, if the adhesion is significant, the debonding of the soft layer involves the nucleation and growth in the bulk of the adhesive of a large population of initially spherical cavities nucleating and then growing into structures elongated in the tensile direction. An example of this population of cavities for a

typical probe tack experiment is shown on Figure 25. The cavities appear relatively evenly spaced and of a typical size that is of the order of the thickness of the film(Chikina and Gay, 2000, Chiche et al., 2005a) but depends on the viscoelastic properties of the adhesive(Peykova et al., 2012, Lakrout et al., 1999) and on the roughness of the probe(Chiche et al., 2005a).
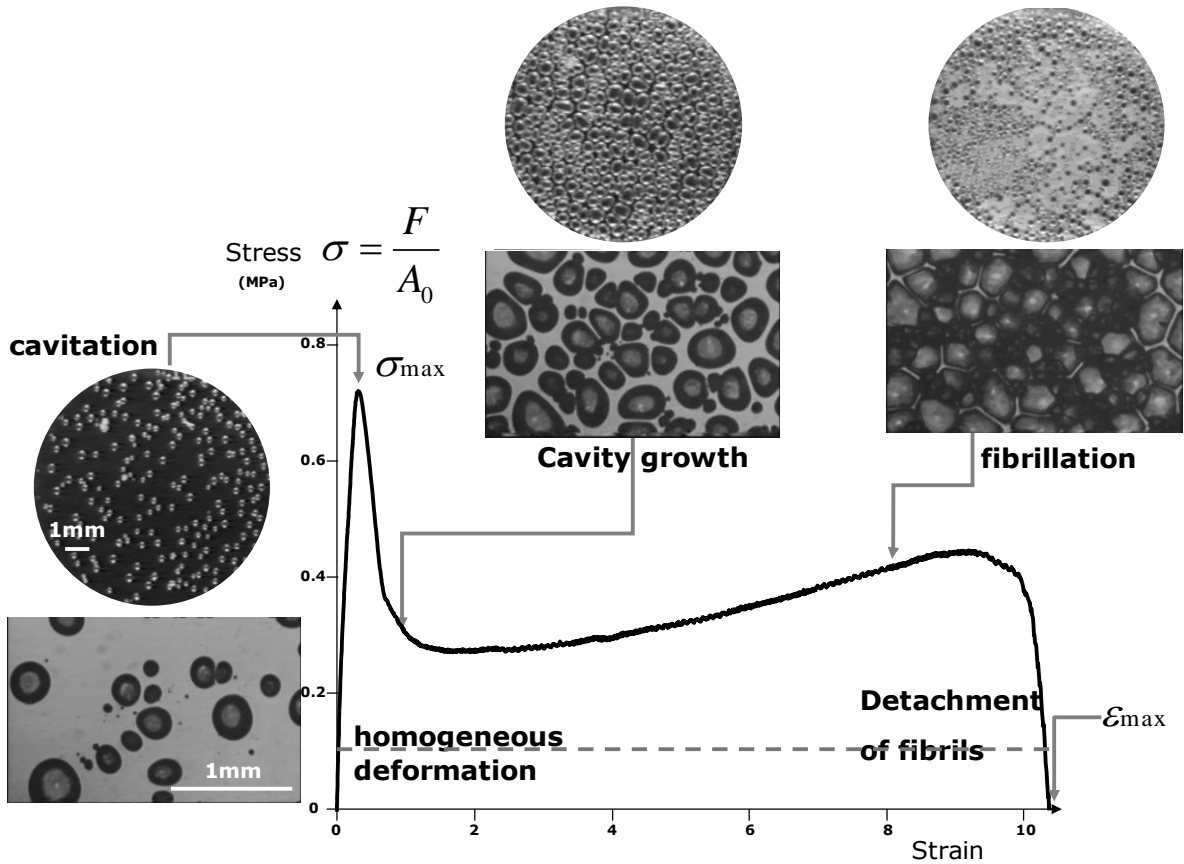
Figure 25: Images of the debonding process in a probe test. The arrows correspond to the point where each picture was taken.

The growth of the cavities and in particular the progressive change in shape of the cavities from a sphere to a cylinder with increasing displacement of the probe is a rather complex 3D process where energy is dissipated throughout the adhesive mass. Scaling approaches or simplified approaches have been developed by physicists to describe at least the features of the debonding process in a probe test, where the local loading conditions are better controlled. Gay and coworkers were first to propose a scaling and physically based model of the role of cavitation at the interface (Gay and Leibler.L., 1999, Chikina and Gay, 2000) on

tackiness. The transition from individual growth of cavities to the collective growth of the foam structure is the most difficult part of the process to model. The rheological properties of the material are complex, the boundary conditions with the adhering surface are not easy to define so that to our knowledge no fully fledged simulations have yet been published reproducing the full complexity of the debonding mechanism of a PSA layer. However, some studies using computational fluid mechanics have simulated the growth of cavities in the bulk of the viscoelastic layer (no interface) and provide some insight on the important role

played by elasticity in the deformed adhesive(Papaioannou et al., 2014, Yamaguchi and Doi, 2006).

From an experimental point of view, a recent study(Tanguy et al., 2014) focused on the measurement of the true tensile stress experienced by the material in the walls between cavities by monitoring, in real time, the projected area of the cavities and of the walls as a function of average layer stretch $\lambda = h/h_0$, and showed that three typical situations can arise as shown in Figure 26 . If the material is very elastic (Bg1110), the average stress on ligaments between cavities keeps increasing with minor bulk deformation (Figure 26c). This builds up stress concentration at the edge of the cavities, which propagate as cracks along the interface

until complete debonding as discussed in previous sections. If the material is insufficiently elastic (A650), the average true stress remains stable with strain, but the average stretch of the filament diverges (upward curvature in Figure 26b) and will lead to the unstable shrinking of the ligament up to failure. Finally for an optimized viscoelasticity (A1570), the fibril cross section stabilizes due to strain hardening, the true stress only slightly increases with stretch and the fibril stretch increases at the same rate as the nominal stretch (downward curvature in Figure 26b) and a stable fibril extends until strain hardening will detach it from the surface.
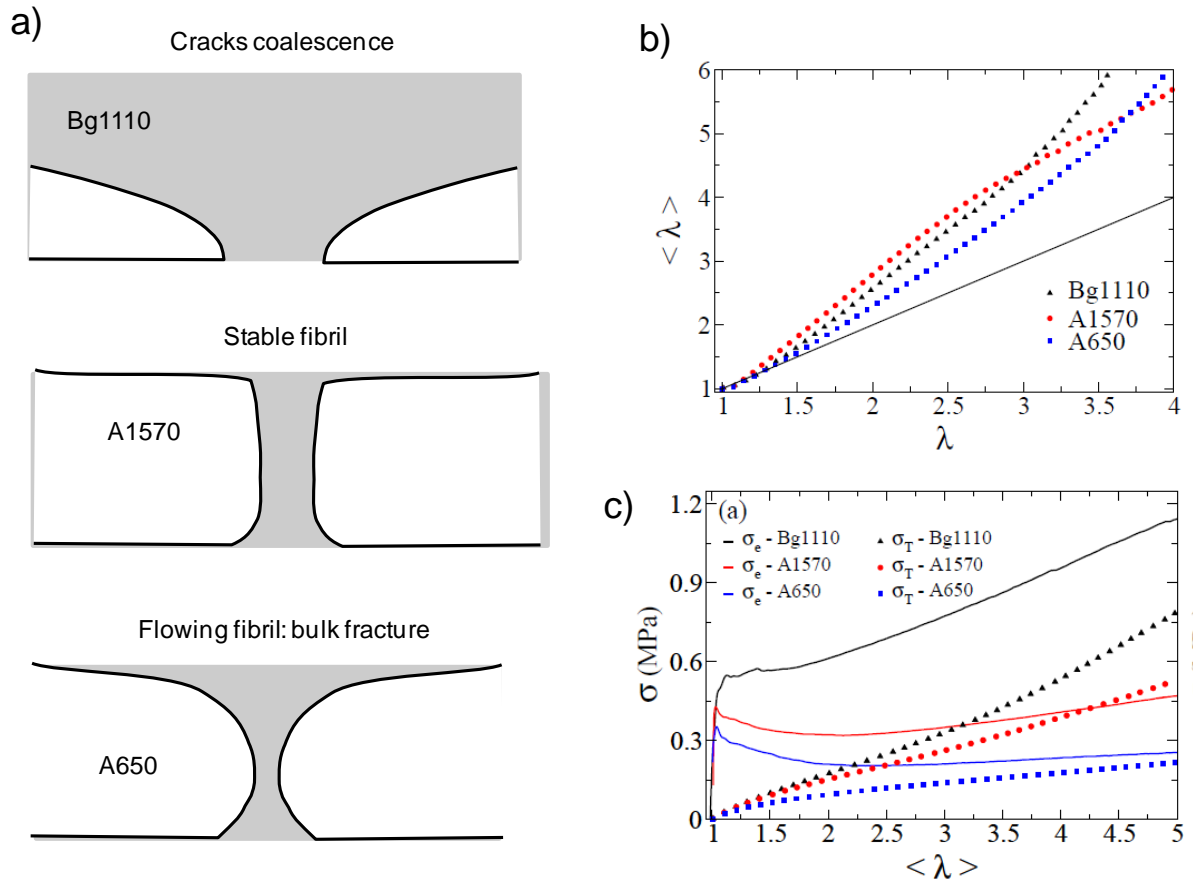
Figure 26: Left: Schematic of the three limiting cases of bulk deformation during debonding. Right top: Average stretch in the region between cavities as a function of nominal stretch of the adhesive layer in the tensile direction. Bottom right: lines represent the average stress in the region between cavities and markers show the tensile stress-strain curve of the adhesive material at comparable strain rates. Bg1110 is the more elastic material, A1570 the optimized one and A650 the more fluid one. Reprinted from (Tanguy et al., 2014).

Although the linear viscoelastic properties predict reasonably well the transition between

interfacial crack propagation and bulk deformation, they are clearly not able to predict

whether the final failure will occur by a fracture of the extended fibrils, or by a detachment of these fibrils from the surface. This is an essential difference for application properties since a flow or fracture of the fibrils in large strain leads to residues on the probe while a detachment leads to a clean surface. In both cases, to predict or understand these differences it is essential to characterize and understand the non-linear elastic behavior all the way to the failure

process. An example of the relevance of extensional properties for the interpretation of tack curves is shown on Figure 27. The comparison of the uniaxial tensile curves of Figure 27a and the probe tack curves of Figure 27b on the same adhesives show that the nominal stress level in the region where fibrils (or walls between cavities) extend, is controlled by the extensional properties of the adhesive itself.
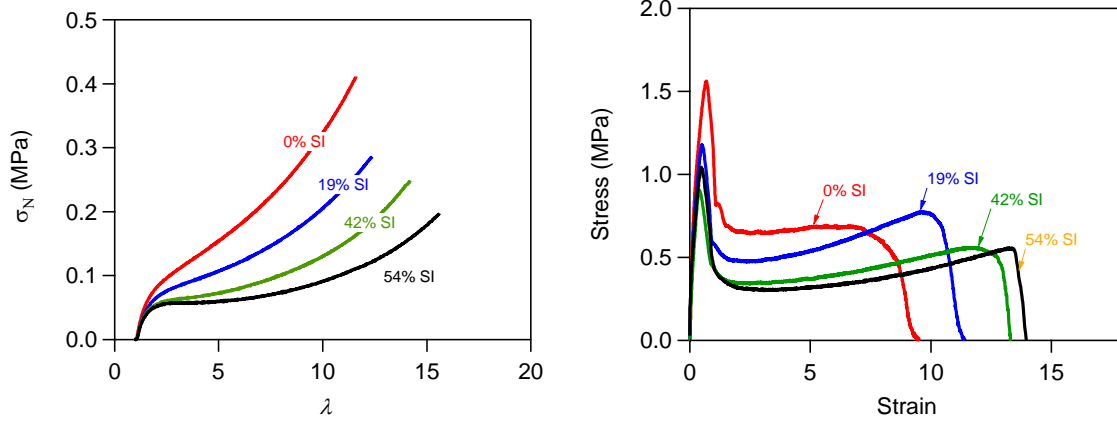
Figure 27: a) Tensile tests of four different adhesives with nearly identical linear viscoelastic properties, but very different large strain properties. b) Probe tack tests carried out at similar strain rates with 100 μm thick films of the same adhesive series. Data from (Creton et al., 2005). 0, 19, 42 and 54 % SI correspond to the composition of the block copolymer blend used in the adhesive(see (Roos and Creton, 2005).

This characterization of the material properties in uniaxial extension and its connection with the material structure was discussed in section 4 for generic elastic entangled and crosslinked networks. It is useful to extend this analysis to the specific case of PSA's.

The experimental output of a uniaxial tensile test of a PSA is typically a stress vs. stretch curve that resembles that of Figure 11a, with a pronounced softening and a stiffening at high strain. Although this nominal stress vs. stretch curve is informative by itself, the reduced Mooney stress $f*$ plotted as a function of $1/\lambda$ such as in Figure 11b provides more information on the structure of the adhesive. First of all the position of the minimum in reduced stress is clearly representative of the onset point of the stiffening due to finite chain extensibility. Two material parameters can be defined from $f*(\lambda)$: a reduced modulus at the minimum of $f*$, which we will call C_{hard} and a value of stretch at the onset of strain stiffening defined as λ_{hard}. As discussed in section 4, the initial shear modulus of the material μ is due to permanent crosslinks and entanglements. As discussed in section 4, the contribution of entanglements to the stress can either decrease with time due to flow, as in a

polymer melt (Doi and Edwards, 1986), or decrease with stretch because of chain orientation, in an entangled and crosslinked rubber (Rubinstein and Panyukov, 2002). Both mechanisms are active, but the first relaxation mechanism is irreversible and leads to viscoelastic dissipation, while the second mechanism is reversible and leads to non-linear elasticity. Some soft adhesives such as the acrylic networks rely mainly on the first mechanism to obtain the necessary strain softening (Deplace et al., 2009c), while some others like those based on block copolymers rely mainly on the second mechanism (Roos and Creton, 2005).

If the tensile test is performed very slowly so that all relaxation mechanisms have occurred over the time scale of the experiments, we expect μ_x to be related to the C_{hard} of Figure 11b by:

$$\mu_x \approx C_{hard} \qquad \textbf{33}$$

And for a homogeneously crosslinked adhesive, we expect λ_{hard} to be related to the finite extensibility of the crosslinked chains by:

$$\lambda_{hard} \approx \left(\frac{\rho RT}{C_{hard}}\right)^{1/2} \qquad \textbf{34}$$

where ρ is the density of the polymer. However, experiments are rarely carried out infinitely slowly and the measured $C_{hard}(\dot{\lambda})$ and $\lambda_{hard}(\dot{\lambda})$ are usually characteristic of a given stretch rate (Degrandi-Contraires et al., 2013, Bellamine et al., 2011). The third parameter that can be extracted from the Mooney representation of the reduced stress is $C_{soft}(\dot{\lambda})$, characteristic of the softening process due to viscoelastic relaxation and/or presence of entanglements. Although in past studies several definitions have been used for $C_{soft}(\dot{\lambda})$, we feel at this stage that the best way to define it is simply by subtracting $C_{hard}(\dot{\lambda})$, from the initial elastic modulus:

$$C_{soft} \approx \mu - C_{hard} \qquad \textbf{35}$$

These values of $\boldsymbol{C_{hard}}(\dot{\lambda})$, $\boldsymbol{C_{soft}}(\dot{\lambda})$ and $\boldsymbol{\lambda_{hard}}(\dot{\lambda})$ are the signature of the large strain behavior of the PSA and have a profound effect on the debonding mechanisms as illustrated in Figure 29 which can be summarized as follows: If $\boldsymbol{C_{hard}}(\dot{\lambda}) \sim 0$ or cannot be defined, the polymer is a fluid and fibrils, if they form, will shrink and break before detaching from the surface. On the other hand, for a typical lightly crosslinked PSA $\boldsymbol{C_{hard}}(\dot{\lambda}) \sim$ 10-30 kPa over the usual stretch rates relevant for adhesive tests and this is sufficient to cause detachment of the fibrils. Given that the initial moduli of the PSAs are generally in the range 30-100 kPa, it is easy to see that the proportion of the modulus due to permanent crosslinks is low, usually less than 30%. The effect of the crosslinking on the tack measurements is illustrated by the example of Figure 28. Two PSAs made from an identical blend of acrylic monomers have been first polymerized, then either left uncrosslinked, or lightly crosslinked. Figure 28a and b show the linear viscoelastic properties of the polymers in the range of frequencies relevant for tack tests and only small differences can be seen. On the other hand, Figure 28d and e show the large strain properties of the same adhesives in uniaxial extension. Although the initial small strain modulus appears indeed identical the curves then significantly diverge. Finally, Figure 28c shows the results of a tack test carried out on the same adhesives. While the lightly crosslinked adhesive shows a marked plateau at constant nominal stress, typical of PSAs, and an adhesive detachment from the steel substrate, the uncrosslinked material forms filaments that can flow and eventually break before being able to detach. Clearly the strain hardening, which is not necessarily predicted by the linear properties, plays a crucial role in the mechanisms of fibril detachment. It should be noted that this important effect of a light level of crosslinking can be used to design optimized PSAs with a heterogeneous structure. While linear properties are sensitive to the number of elastic chains per unit volume, the strain hardening process is sensitive to the details of how the chains are connected together and percolate to form a continuous network. This issue is particularly important when adhesive films are prepared from the drying of individual latex particles creating a spatially inhomogeneous structure (Bellamine et al., 2011, Degrandi-Contraires et al., 2011, Degrandi-Contraires et al., 2013, Deplace et al., 2009a, Deplace et al., 2009c, Foster et al., 2009).
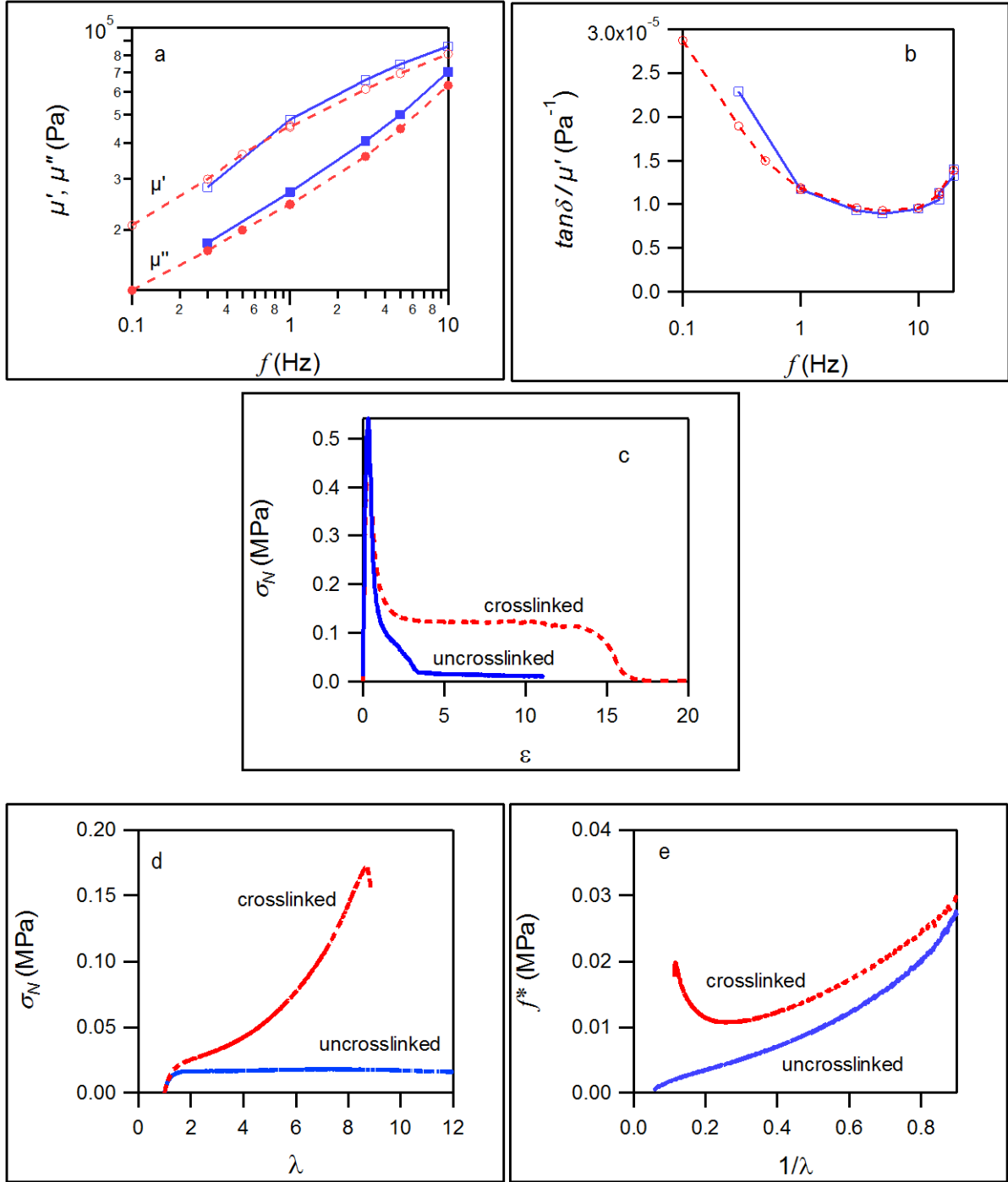
Figure 28: Effect of crosslinking of an acrylic PSA. Solid red line: uncrosslinked material, dashed blue line: crosslinked material. (a) Linear rheology. evolution of the elastic μ' (empty symbols) and dissipative μ'' (filled symbols) moduli as a function of the frequency. (b) Evolution of the ratio $tan~\delta/\mu'$; (c) Stress-strain tack curves. Tack experiments were performed at 10 μm/s on stainless steel; (d) Tensile test: Nominal stress σ_N vs. strain tensile curves. (e) Tensile tests: f^* vs. $1/\lambda$ of the same tensile results. Data from (Deplace et al., 2009b).

The parameters extracted from the uniaxial tension test that we have defined can also be used to build a more refined "application window" of PSAs based on their balance of properties. An example of map as a function of C_{hard} and C_{soft} is given in Figure 29. The region on the left side corresponds to more elastic materials than what is necessary for PSA. Typically such materials relax the stress moderately and are too elastic to blunt the cracks as in Figure 23b and fail by interfacial crack propagation. At the bottom of the graph lie fluids which can be highly sticky, but are not able to detach from the surface without residues.

The Dahlquist criterion, which specifies that PSA should not have a shear modulus at 1 Hz above 0.1 MPa, is plotted as a diagonal line and limits the overall modulus C_{hard} + C_{soft}. Within the PSA regime one can distinguish different applications of PSA requiring a different balance of properties. Removable PSA are typically soft and weakly adherent, requiring a more elastic character. Labels need to stick on many surfaces and often should not be detachable without damage, while double-sided structural tapes need to use the highest modulus permitted by the Dahlquist criterion.
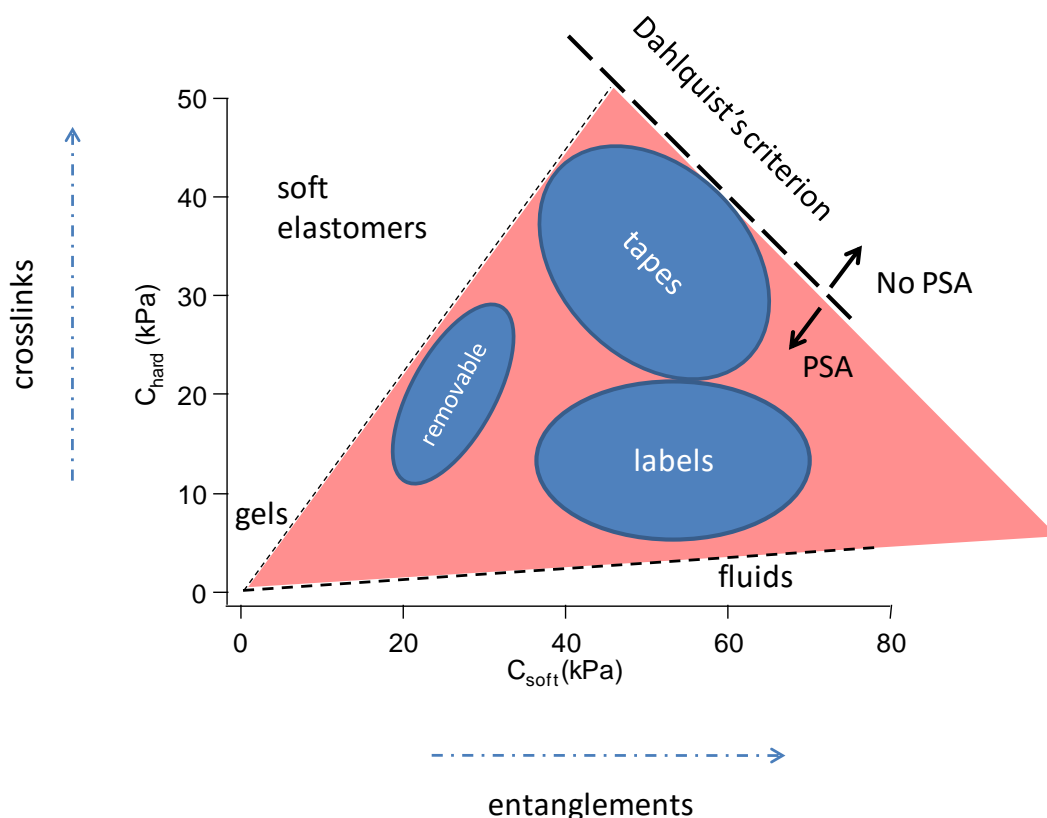
Figure 29: Application map of PSA as a function of the two large strain parameters C_{hard} and C_{soft} representing the crosslink and entanglement densities respectively at the relevant strain rate.

5.4 MATERIALS USED FOR PRESSURE-SENSITIVE-ADHESIVES

This last section on adhesives will address more specifically the materials effect. While a detailed review of the chemistry of PSAs is outside the scope of this review, some general features of the materials can be discussed. In particular, we will address how to obtain the nonlinear viscoelastic properties needed for spontaneous adhesion from polymer design and give some examples.

From the point of view of an adhesive technologist, adhesives can be classified into three categories: 1) reactive soft adhesives, which are applied in the liquid state and become a tough rubber once chemically cured, 2) so-called "hot-melt" adhesives, which are applied at higher temperatures in the liquid state and then solidify during cooling, generally involving crystallization and 3) pressure-sensitive adhesives (PSA), which adhere by simple mechanical contact without any need of chemical or physical change of state. The properties of the first two categories depend heavily on the details of the chemistry used and on the formulation (for the hot melts in particular) and are reviewed in many specialized technology oriented textbooks (Chaudhury and Pocius, 2002, Pocius, 2002). On the other hand, pressure-sensitive-adhesives contain relatively few additives and their adhesive behavior is dominated by the rheological properties of the polymer, which is the main component of the adhesive. As a result, it is possible to understand

the properties of PSA from polymer physics considerations and this is the focus of this section.

We have seen that polymers used in PSA must have four important properties, according to Dahlquist's criterion, which roughly speaking control their spontaneous bonding behavior and the energy dissipated during debonding. The first is a glass transition temperature well below the usage temperature: PSA rely on rubber elasticity for their properties and this can only occur when polymer chains are mobile. The second is a low shear modulus (10-100 kPa) when tested at a characteristic frequency of 1 Hz. This condition implies that the strain energy necessary to conform to even rough surfaces at deformation rates of the order of 1 s^{-1} should be of the order of the gain in surface energy when forming an interface and has been discussed in section 5.1. The third one is an elastic character at low frequency or long times, which prevents

or slows down creep. These three necessary conditions guarantee spontaneous adhesion and clean removal from most surfaces. Yet to achieve large energy dissipation upon debonding and become a useful adhesive in the practical sense, a fourth condition must be met, the material must have a significant degree of viscoelasticity in small and large strain. This fine adjustment of the viscoelastic properties while satisfying the first three conditions is at the core of the know-how of PSA manufacturers.

Such a combination of requirements on the macroscopic properties can in principle be obtained from any polymer with a low glass transition temperature, by adjusting its molecular weight, and crosslinking density, but in practice only a few families of polymers are used to manufacture PSA. Table I lists some families of PSA with some selected experimental references focusing on those families of adhesives.

Family	Type of Polymer	Tg adjustement	Non-linear rheology adjustment	Applications	References
Acrylic	Poly n-butyl acrylate, Poly (2-ethylhexyl acrylate)	comonomers	Chemical crosslinking	UV and oxidation resistant, all purpose	(Gower and Shanks, 2004b, Tobing et al., 2001, Lindner et al., 2006, Lakrout et al., 2001)
Natural Rubber	Natural rubber	Tackifying resin	Strain induced crystallization, chemical crosslinking	Cheap, high Strength	(Aubrey and Sherriff, 1980, Sherriff et al., 1973)
A-B-A Block Copolymers	Styrene-isoprene-styrene	Tackifying resin	Physical crosslinking by polystyrene domains	High Strength, Does not work above 70°C	(Nakajima, 1992, Gibert et al., 1999, Creton et al., 2005, Daoulas et al., 2004)
Silicones	Polydimethylsiloxane, polyvinylsiloxane	MQ resin	Chemical crosslinking	High and low T resistance, biocompatible, low adhesion	(Lin et al., 2007)
Polyisobutylene	Polyisobutylene + butyl rubber	Tackifying resin	Chemical crosslinking	Biocompatibility, good UV, oxidation resistance	(Krenceski and Johnson, 1989)

Table 1: Families of PSA with typical monomers used in the polymer and selected references

It is worthwhile now to translate the physical and rheological properties that are required to display adhesion into polymer chain architecture. Since the modulus must be below 0.1 MPa at 1 Hz, it is clear that glassy and semi-crystalline polymers cannot be the main component to make a PSA. However, classically crosslinked rubbers cannot be used either, since they typically reach elastic shear moduli μ of several hundreds of kPA and up to several MPa

with a level of viscoelasticity insufficient to relax the stress singularity at the edge of a growing cavity and blunt the crack (see equation 32 and Figure 29). As a result, while rubbers have some level of adhesion on solid surfaces (like a tire on the road), they always debond by interfacial crack propagation without forming fibrils. The optimum level of crosslinking is a crucial parameter to optimize for all families of PSA(Gower and Shanks, 2004a, Deplace et al.,

2009a, Zosel, 1991) and depends markedly on the application but is typically just above the point of percolation of the network (the gel point) so that the polymer is highly stretchable but cannot flow(Jensen et al., 2009).

Zosel, pointed out also in a seminal paper that a low entanglement density was a necessary condition to reach good adhesive properties(Zosel, 1985). This is understandable since entanglements are temporary crosslinks and a shear modulus μ at room temperature of 0.1 MPa corresponds to an average molecular weight between entanglements of roughly 25000 g/mole(Rubinstein and Colby, 2003). The earliest PSA were made with a blend of natural rubber and a low molecular weight resin with a T_g above room temperature(Butler, 1989, Aubrey and Sherriff, 1980, Sherriff et al., 1973). In this case the cohesion comes from the high molecular weight of the natural rubber and its physical crosslink structure. The role of the resin is to lower the plateau modulus by diluting the entanglement network and to increase the T_g of the blend an hence the viscoelastic dissipation at the strain rates relevant for debonding. The second very common family of PSA is that of acrylic polymers(Satas, 1989, Dale et al., 1989, Gower and Shanks, 2004a, Lindner et al., 2006). They are usually copolymers containing a combination of monomers used to adjust both T_g and entanglement density ν_e (although not independently). Because of their bulky side chains, acrylate monomers have sufficiently low entanglement densities to function as PSA without any additives. However, the adjustment of the rheological properties has to occur by synthesizing copolymers with different monomer compositions rather than by simply mixing ingredients, which makes them less attractive as model systems for physicists. In PSA based on acrylate monomers, a polar group, typically acrylic acid, is usually added to provide

better interactions with the surface, and to introduce physical crosslinks (in addition to entanglements) increasing the elongational viscosity and stabilizing the fibrillar structure once it is formed. A third widespread family that has been highly studied by polymer physicists is the styrene-isoprene-styrene (SIS) block copolymer family (Daoulas et al., 2004, Marin and Derail, 2006, Creton et al., 2009). PSA based on SIS copolymers are physically crosslinked by spherical polystyrene domains. A typical formulation would have about 40wt% of a combination of triblock and diblock copolymers and 60wt% of low molecular weight additives miscible with the polyisoprene (PI) domain only, which reduce the plateau modulus and adjust the glass transition temperature as described above(Nakajima, 1992, Gibert et al., 1999).

Finally, two more specialty families deserve to be mentioned. Silicone PSA(Sobieski and Tangney, 1989, Lin et al., 2007, Lin et al., 2009) do exist and are based on similar criteria as acrylics, i.e. a combination of monomers to adjust T_g and entanglement network. However, silicone PSA also use the so-called MQ resin, denser silica-like nanoparticles that are incorporated to increase dissipative processes during deformation. The other specialty family is that of hydrophilic PSA(Roos et al., 2002, Feldstein et al., 2006) and hydrocolloid PSA(Ferrari et al., 1995). Both are used for medical applications and should stick on wet or at least humid surfaces (skin or mucosa). They are usually composed of a significant proportion of very hydrophilic monomers, but controlling the change in properties occurring with variable water content is still a significant challenge so that applications only typically work for a limited time period. This is clearly the area in greatest need of a better understanding.

6. FRACTURE OF SOFT POLYMER NETWORKS

In the previous sections we focused on adhesion problems, i.e. situations where typically a thin layer of soft adhesive is sandwiched between two stiffer layers and is being detached from one of these layers. While this detachment process is clearly a fracture process, there are some specific aspects that are worthwhile pointing out now to distinguish it from the more general problem of fracture:

1) the locus of failure is at or near the interface. This situation is inherently asymmetric around the crack plane and interfacial interactions and bulk interactions are generally not the same;
2) the soft deformable adhesive film is almost always confined so that hydrostatic stresses play a key role in the fracture mechanisms;
3) soft adhesives are often very viscoelastic and highly deformable. Not only the SSY condition is never fulfilled, but dissipative zones are always

extending over the complete layer thickness. In other words, a value of the adherence energy can only be viewed as an apparent fracture energy Γ_{app} , i.e. as the property of a structure and not of a material or an interface.

The fracture problems that we will now address will be different from the above. Bonds broken during crack propagation will generally be the same that insure bulk cohesion, hydrostatic stresses will only play a role near the crack tip and Γ will be understood as a material property if the sample is large enough to satisfy the SSY condition (see introduction). Furthermore, and because we are now investigating bulk properties, the type of materials where fracture occurs by crack propagation are predominantly elastic, i.e. $\mu'(\omega) \gg \mu''(\omega)$ and are well crosslinked, i.e. $\mu_x \geq \mu_e$. Nevertheless, there is a clear analogy between the mechanisms of adherence and the mechanisms of fracture in the bulk and it is our goal to point out to the reader the similarities between the two cases. From a historical point of view, fracture of soft elastic materials cannot be dissociated from fracture of rubbers. Several researchers in the late 1950s and early 1960s, used Griffith's energy balance approach of fracture mechanics to treat and understand quite a wide range of failure phenomena in elastomers (Rivlin and Thomas, 1953, Thomas, 1955, Greensmith, 1960, Andrews, 1961, Gent et al., 1965, Lake and Thomas, 1967). Circumventing the difficulty of finite strains and of the nonlinearity of the material properties in calculating stress fields, they showed experimentally that the energy necessary to propagate a crack in the bulk Γ, either called "critical strain energy release rate"

$\mathcal{G}_c$ or "tearing energy" T in the original papers, was a characteristic of the rubber itself and was independent of the geometry of the test piece. Two important insights that dominate the modern vision of polymer networks fracture today were established during that period. First, Greensmith et al.(Greensmith et al., 1960) determined that the tear energies were highly dependent on crack propagation rate and temperature, varying from around 0.1 kJ/m² at very low rates (or elevated temperatures), to 100 kJ/m² for rapid growth (or lower temperatures). These variations paralleled qualitatively the variation of linear viscoelastic properties observed with rate and temperature. This led to the conclusion that the rate dependence of the fracture energy can be attributed to viscoelastic energy dissipation in the bulk. Then Lake and coworkers(Lake and Lindley, 1965) determined that even in the absence of viscoelastic dissipation (high temperature, slow crack velocity) the threshold value of Γ was still three orders of magnitude larger than the Dupré work of adhesion w.

We will now first address the physics underlying these two seminal results before discussing more recent developments concerning the role of large strains in the fracture propagation mechanisms, with a special focus on the physics of the crack tip blunting effect and the growth of internal defects towards cavities and fibrils. Analogies will thus be established between fracture of soft materials and the mechanisms of debonding of soft adhesives, focusing on scale separation of the different dissipation mechanisms.

6.1 THRESHOLD FRACTURE ENERGY

As mentioned above Lake and coworkers (Lake and Lindley, 1964, Lake and Lindley, 1965, Lake and Thomas, 1967) showed that in the absence of viscoelastic dissipation (at high temperature far from the T_g of the rubber or with oil-swollen rubbers), a minimum amount of mechanical energy Γ_0 of about 50-100 J/m² was required for a crack to propagate, for a broad range of elastomers differing widely in other strength properties. Lake and Thomas (Lake and Thomas, 1967) predicted from simple molecular arguments a threshold value of Γ_0 of the order of 20 J/m², scaling with $v_x^{-1/2}$ value where v_x is the density of crosslinks. They proposed that this rate independent dissipation process was due to the fact that when any of the main chain bonds breaks, the total bond energy of each bond of the

stretched chain is irreversibly lost. Therefore the minimum energy necessary to break the chain is proportional to the length of that chain, i.e. to the number of C-C bonds comprising that chain N_x. Assuming that only the chains crossing the plane of the crack will break, Γ_0 is then given by:

$$\Gamma_0 = N_x U_b \Sigma \qquad \textbf{36}$$

where Σ is the areal density of chains crossing the interface and U_b is the bond energy of a C-C bond (350 kJ/mol). For a homogeneously crosslinked network, Σ and v_x are not independent and one can write:

$$\Sigma \approx v_x a N_x^{1/2} \qquad \textbf{37}$$

where a is the size of the monomer. Substituting

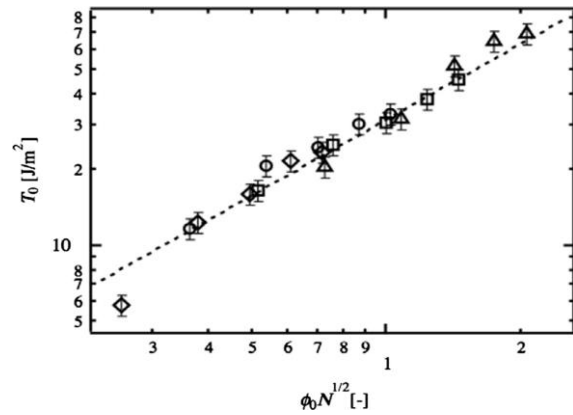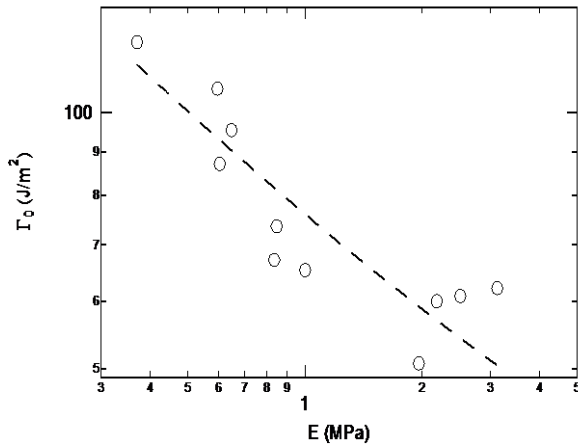equation 37 into equation 36, Γ_0 can then be rewritten as:

$$\Gamma_0 \approx N_x U_b \nu_x a N_x^{1/2} \approx U_b \nu_x a N_x^{3/2} \approx \frac{U_b a \rho}{M_0} N_x^{1/2} \qquad\qquad \mathbf{38}$$

where ρ is the monomer density and M_0 is the molar mass of the monomer.

This equation is valid for both elastomers and swollen gels since the difference between the two cases is mainly contained in ρ, which for elastomers is a bulk unswollen density ρ_0 of the order of 10^3 kg/m³ and for gels it is simply $\rho = \rho_0 \phi_p$ where ϕ_p is the polymer volume fraction.

If the chains in the network are Gaussian, the elastic modulus is $E = 3\nu_x k_B T$, so that Equation 38 can be rewritten as:

$$\Gamma_0 \approx U_b a \left(\frac{\rho}{M_0}\right)^{3/2} (3k_B T)^{1/2} E^{-1/2} \qquad \mathbf{39}$$

In other words, the threshold fracture energy Γ_0 is predicted to scale with the inverse square root of the elastic modulus, a classic yet not very intuitive result. It should be noted however that this simple model ignores any imperfections or heterogeneities in the network as well as the presence of entanglements.

This prediction can then be tested with model systems. Experimental evidence of the Lake and Thomas prediction are shown on Figure 30 and show that for both rubbers and hydrogels the key idea behind the Lake and Thomas model seems to be correct (cf equations 39 and 38).

Figure 30: a) Threshold fracture energy Γ_0, vs. Young's modulus E for elastomers (data from (Bhowmick et al., 1983)) and b) threshold fracture energy (original symbol T_0) of a series of model hydrogels based on the tetra-PEG segments. ϕ_0 is the monomer concentration in the gel and N is the number of monomers in each chain. Reprinted from (Sakai, 2013)

A key point beyond scaling is however the quantitative agreement. A more general version of Equation 36 can be written as (Akagi et al., 2013):

$$\mathbf{\Gamma_0 \approx N_x U_b \nu_x L} \qquad\qquad \mathbf{40}$$

While N_x and ν_x are physically well defined quantities that can be obtained (within a factor of 2) from bulk elasticity experiments and U_b cannot be too different from the bond energy of a C-C bond, the distance L over which energy is

irreversibly dissipated upon fracture, can only be estimated from fracture experiments. In unfilled rubbers threshold fracture energies are of the order of 50-100 J/m² (Gent and Tobias, 1982, Ahagon and Gent, 1975b, Bhowmick et al., 1983, Bhowmick, 1988). For $\mu_x \sim 0.5$ MPa and $M_0 = 100$ Dalton, we have a prediction of $\Gamma_0 \sim 25$ J/m², in very good agreement with the experimental values, suggesting that the original insight of Lake and Thomas was basically correct and L is of the order of the mesh size of the molecular network.

6.2 FRACTURE OF RUBBER AT FINITE CRACK PROPAGATION VELOCITY

In the previous section we have seen that at propagation threshold conditions, i.e. slow fracture very far from the glass transition temperature, the fracture of at least simple network rubbers can be well understood with simple molecular arguments. However, this ceases to be the case as the temperature decreases and becomes closer to the glass transition temperature of the rubber, or the rate at which the networks are broken increases. In this case Γ depends both on the rate and temperature at which the experiments are carried out and on the architecture of the crosslinked network in a fully analogous way to the adhesive case, so that the empirical equation 31 relating Γ and crack velocity remains valid. Several examples of measurements of $\Gamma(v)$ for typical networks as a function of rate and temperature are given in Figure 31 and show that the fracture energy increases very significantly with the crack propagation velocity. The functional form of $\Gamma(v)$ is generally similar to that found for adhesion, i.e. a threshold value Γ_0 and a power-law dependence at higher crack velocities, i.e. $\phi(a_T v) \sim v^n$. The value of the exponent n has been reported to vary between 0.1 and 1 depending on the material and examples reported in Figure 31 include two rubbers and two crosslinked gels(Gent et al., 1994, Cristiano et al., 2011, Tanaka et al., 2005, Baumberger et al., 2006a).

Since the force to break a highly energetic covalent bond does not increase that significantly with deformation rate, it is obvious that the measured increase in fracture energy with rate is due to a change in how the energy is transferred from the loading point to the fracture point. This is the realm of solid mechanics and it is important to focus now on larger length scales than the molecular scale. An interesting result shown in Figure 31 is the possibility to construct a master curve from fracture data measured at different temperatures by using velocity shifts of the horizontal axis. This result was interpreted early on as proof of the viscoelastic nature of the dissipative processes involved at the crack tip (Ahagon and Gent, 1975b, Plazek et al., 1988, Plazek et al., 1983, Bhowmick, 1986, Gent et al., 1994) in an analogous way to what has been discussed for adhesives in section 5. Based on this insight many researchers in physics and mechanics have sought to account quantitatively for the dissipation of energy during fracture by using linear viscoelastic properties of the materials. Although a detailed review of these models is beyond the scope of this paper, it is worthwhile to mention the pioneering efforts of Knauss (Mueller and Knauss, 1971), Schapery (Schapery, 1975b, Schapery, 1975a, Schapery, 1975c) and Christensen (Christensen and Wu, 1981), who calculate the stress fields ahead of a propagating crack assuming infinitesimal strains and linear viscoelasticity and introducing a cohesive zone to remove the singularity. And more recently, the scaling approach of de Gennes (de Gennes, 1997, de Gennes and Troian, 1990, de Gennes, 1988), which estimates the energy dissipation of a crack propagating in a viscoelastic medium as a function of propagation velocity, and the contribution of Persson who extended the model to a more general linear viscoelastic rheology (Persson et al., 2005, Persson and Brener, 2005). Despite making sound scaling predictions these models and their variations (Saulnier et al., 2004, Barthel and Fretigny, 2009) always significantly underpredict the actual dissipation measured at the crack tip during fracture at a set velocity. The reason is evident when one looks at the frequencies involved. Typically a well crosslinked rubber is used about 40-50°C above its glass transition temperature mainly to avoid viscoelastic losses and heating during normal use. At that temperature the ratio of the dissipative vs. storage component of the 1 Hz modulus is well below 0.1. As pointed out by Gent in his landmark paper (Gent, 1996a), when comparing the master curves of the fracture energy and that of the elastic modulus (taking the glass transition temperature as a common reference), the strong increase in the fracture energy occurs between V = 10^{-20} and 10^{-8} m/s, while the increase in dissipation due to linear viscoelasticity occurs between ω = 10^{-4} and 10^2 rad/s. Following a simple dimensional argument, if a crack moves at a velocity V and we assume that the dissipation occurs over a characteristic length scale L_0, the characteristic dissipation frequency should be $\omega = V/L_0$. However the dissipation ranges observed by Gent imply that the size of the dissipative zone at the crack tip would be of the order of $L_0 \sim 10^{-12}$ m, which is below atomic dimensions. Hence, the simple linear viscoelastic calculation, which assumes that dissipation depends on frequency alone and not on strain amplitude, must be incorrect.

What is missing in this picture is the role played by large strain elasticity and localized damage in controlling the size of the dissipative zone and the nature of dissipation.
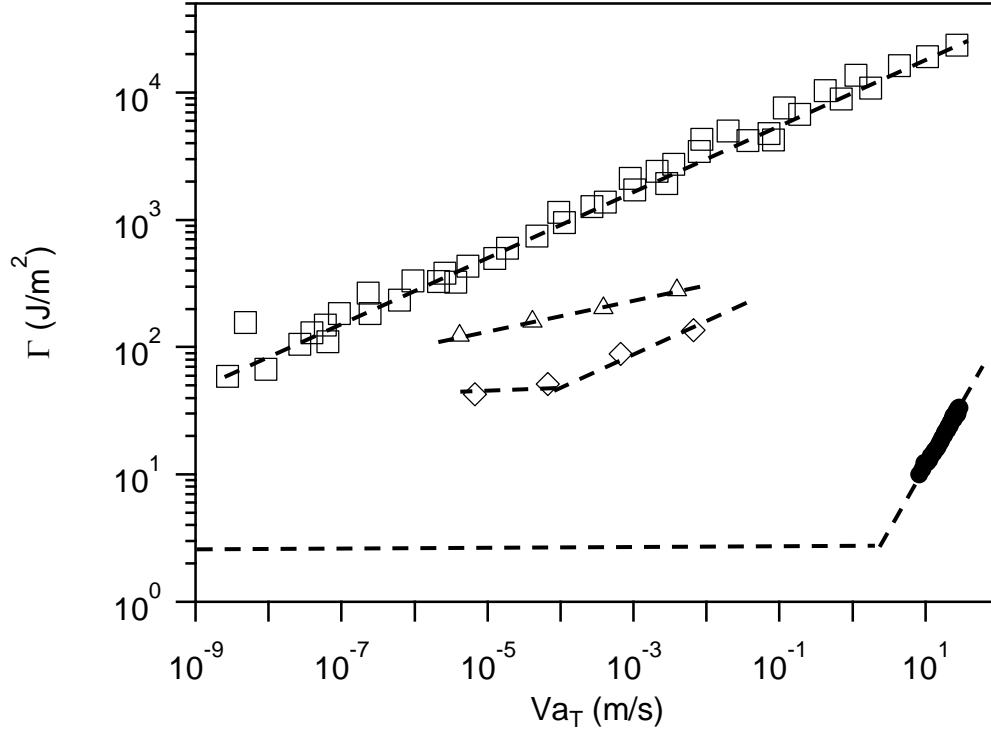
Figure 31: a) Fracture energy Γ as a function of propagation velocity or reduced propagation velocity for different materials. □) Master curve at 25°C for a styrene-butadiene rubber (T_g = -25°C) tested with the trouser tear geometry. Data from (Gent et al., 1994). ◊) Polyurethane rubber (T_g = -55°C) at 25°C tested with the single edge notch geometry. Data from (Cristiano et al., 2011). △) Double network hydrogel at 25°C. Data from (Tanaka et al., 2005). ●) Gelatin gel (5 wt% polymer) at room temperature in the pure shear geometry. Data from (Baumberger et al., 2006a). Horizontal lines are values of Γ_0 when reported.

6.3 CRACK TIP ANALYSIS: CRACK BLUNTING, LARGE STRAIN EFFECTS

For many years large strain elasticity was completely absent from the physical picture of the crack tip and the few papers being published on the subject (Stephenson, 1982, Knowles and Sternberg, 1973, Knowles and Sternberg, 1974, Geubelle and Knauss, 1994) did not permeate beyond the mechanics community. The development of other types of soft materials, such as gels, which are very relevant for life sciences, have since then fostered a renewed interest in the solid mechanics and the physics community in a better understanding of the fracture mechanics of soft materials.

As discussed in the introduction, the important quantity to assess is the elasto-adhesive length $\ell_{EA} = \Gamma/E$. Based on the experimental results of Figure 30 and Figure 31, the elasto-adhesive length for tough rubbers (E ~1 MPa) ranges between 50 μm and 1 cm, and for gels (E ~ 5-50 kPa) it ranges between 200 μm and 1 cm, but can reach values larger than 10 cm for the tough gels described in section 7. Below this length scale the crack tip strains are larger than 100%

and the material response and properties are well into its non linear regime.

This argument has been first proposed by Hui et al. in their seminal paper (Hui et al., 2003), based on the following approximate treatment, which considers the change of crack tip radius with increasing loading on a slit-like crack in a soft material. In each step of the loading the crack is treated as a plane stress elliptical crack of half length c and half height b in a uniformly stressed infinite plane. The radius of curvature at the crack tip ρ is:

$$\rho = \frac{b^2}{c} \qquad\qquad \textbf{41}$$

And the tensile stress at the crack tip is :

$$\sigma_{max} = \frac{2\sigma c}{b} = 2\sigma\sqrt{\frac{c}{\rho}} \qquad\qquad \textbf{42}$$

The question is now to determine, for such a crack, the increase in σ_{max} as a function of the applied remote stress σ. For small strain

elasticity, the relation between local stress and remote stress is fixed by LEFM and an increase in remote stress σ will always lead to an increase in local stress σ_{max} until the crack propagates as discussed in the introduction. However, if finite strains are allowed and ρ can change with increasing loading, σ_{max} progressively ceases to increases with σ and tends toward $2E$ as the remote stress σ approaches the modulus E. This situation is called elastic blunting by Hui et al.

The assumptions in (Hui et al., 2003) are very stringent and do not consider other failure mechanisms than crack propagation nor the effect of strain stiffening on the crack tip stresses, but the general message should be that for materials where the cohesive strength exceeds the elastic modulus, a large highly stretched region of size of the order of Γ/E exists near the crack tip during crack propagation.

Yet most real soft materials cannot deform to infinite strains with the same modulus and experience strain stiffening at large strains or damage micromechanisms at the molecular level, which modify the stress field. Hence, the tip of a blunted crack usually contains a highly stretched region very elongated in the tensile direction and rather narrow in the crack propagation direction. Such a highly stretched region at the tip of the crack has been simulated (Long et al., 2011) and can be directly visualized nowadays by digital image correlation (Mzabi et al., 2011, Kwon et al., 2011). As shown on Figure 32 for the tip of a crack in a filled styrene-butadiene rubber, the measured strain field directly ahead of the crack tip is not singular in both directions, but has been measured to decrease roughly as $x^{-0.4}$ in front of the crack tip and is nearly constant in the transverse direction over a height approaching 50-100 μm very close to the tip.
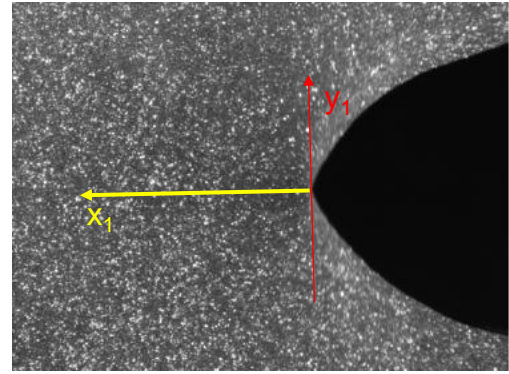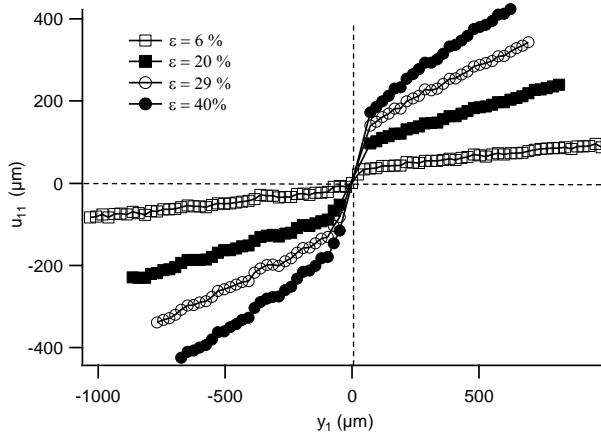
Figure 32: Displacement at the crack tip as measured by DIC in filled elastomers. u_{11} is the displacement of a point along the red line as a function of its position. The crack tip is at the origin. There is clearly a localized highly stretched region while outside of this zone u_{11} is linear with position and corresponds to the macroscopic strain applied to the pure shear sample. Data from (Mzabi, 2010).

The presence of this highly stretched region in a blunt crack was simulated by Hui and coworkers (Long et al., 2011, Krishnan et al., 2008) who also suggested that such a crack should propagate by the nucleation of smaller cracks in the highly strained zone. Mzabi et al.(Mzabi et al., 2011) proposed the following model, inspired by Brown's models for crack growth in a craze in glassy polymers(Brown, 1991) and for the fracture of double network gels(Brown, 2007), which bridge macroscopic loading and local growth of a small micro crack of length c_l in the center of this highly strained zone. According to the deformation field observed at the crack tip by Mzabi et al., the strained zone can be approximately described as a homogeneously

strained initially square zone of undeformed height H_0. We can then define an approximate local energy release rate g_{local} using the analogy of this local loading with the pure shear test(Mzabi et al., 2011):

$$g_{local} = WH_0 \qquad \textbf{43}$$

where W is the local strain energy density, that can be approximated by:

$$W = \int_0^{\varepsilon_{max}} \sigma d\varepsilon \qquad \textbf{44}$$

54

where ε_{max} is defined as the strain at the closest point to the crack tip that can be measured ~ 15 μm, and the integral is carried out over the unloading curve in uniaxial tension. We now illustrate how this concept of g_{local} can be used with an example of analysis of crack propagation in a series of elastomers in cyclic fatigue. A classic test for engineering rubbers is the resistance to crack propagation in cyclic fatigue (Mars and Fatemi, 2004). A sinusoidal tensile load is applied to a prenotched sample in the pure shear geometry (Figure 7). Since in the pure shear geometry the applied energy release rate is independent of crack length, this geometry applies a macroscopic energy release rate varying from 0 to G_{max}.

Typically the results are presented in terms of dc/dn, i.e. the differential increase in length of

the crack dc per cycle as a function of applied G_{max}. Changes in formulation parameters like adding nanofillers or changing the crosslink density by a factor of two, can change the crack velocity by up to two orders of magnitude (Mzabi et al., 2011). Yet if the strain field ahead of accommodated cracks (after 50000 cycles) is characterized by DIC, it is possible to extract from the measurement an approximate value of ε_{max} and H_0 and then to estimate from equation 43 a value of g_{local} for each crack tip measurement. Figure 33 shows the value of dc/dn as a function of $G=G_{max}$ and as a function of g_{local} for three different materials. While the data plotted as a function of the applied macroscopic G_{max} are very scattered, they collapse on a single master curve when plotted as a function of g_{local}.
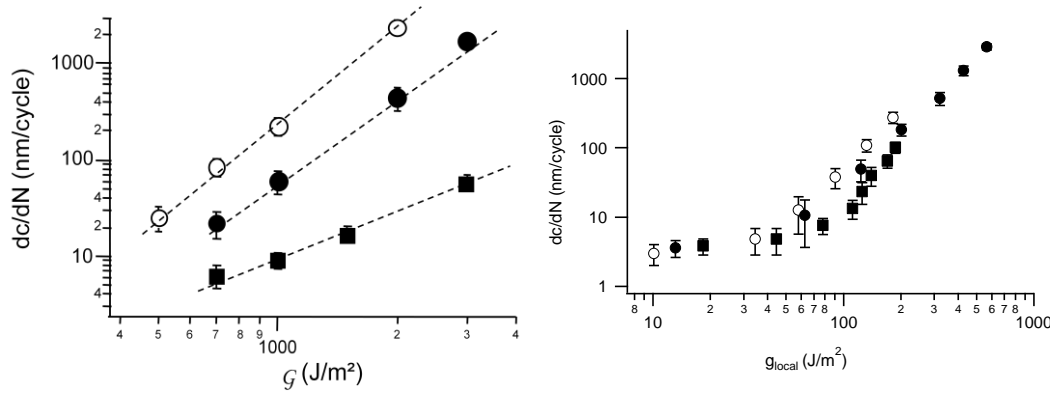
Figure 33: a) Plot of *dc/dn* as a function of applied macroscopic energy release rate G_{max} for a series of filled and unfilled rubbers and b) Plot of the same dc/dn as a function of g_{local}. ○ unfilled SBR rubber, ■ 20 vol% carbon black, low crosslinking density; ● 20 vol% carbon black, low crosslinking density. Data from (Mzabi et al., 2011).

Although this result has been obtained for a single system, it implies that the actual failure of covalent bonds at the crack tip may be controlled by the energy released locally (in a small region close to the crack tip) and that tough soft materials are actually able to shield crack tip bonds by dissipating energy over a larger volume further away from the tip.

The measured g_{local} of equation 43 quantifies approximately the elastic energy seen by the micro crack in the highly oriented zone of size ~ 15 μm right in front of the tip of the crack. Moreover, observations made by SEM and optical microscopy of the crack front show the local development of a fibrillar structure(see Figure 34)(Mzabi, 2010, Beurrot et al., 2010). The connection between g_{local} and the local stress σ_f at the point where molecular fracture occurs (ranging between the inter-crosslink distance

~5nm and the fibril size ~1 μm) can be done in three steps as proposed by Hui et al for glassy polymers presenting an analogous crazing structure(Hui et al., 1992a). First a local stress intensity factor k_{local} associated to g_{local} by:

$$k_{local} = \sqrt{E_{eff} g_{local}} \qquad \mathbf{45}$$

can be defined, where E_{eff} is now an effective unloading modulus of the material. The local stress field in this oriented zone can then be related to k_{local} by:

$$\sigma(x) = \frac{k_{local}}{\sqrt{2\pi x}} \qquad \mathbf{46}$$

And finally the fracture propagation criterion can be set at the molecular scale by equating the characteristic stress estimated with equation 46 at a distance l_{fib} over which continuum mechanics breaks down with the critical stress to break the covalent bonds of the rubber σ_f giving:

$$\sigma_f = \frac{\sqrt{E_{eff} g_{local}}}{\sqrt{2\pi l_{fib}}} \qquad \textbf{47}$$

relating effectively g_{local} with the molecular fracture stress (controlling crack propagation) through a fibril diameter length scale l_{fib}, which in principle could be measured experimentally.
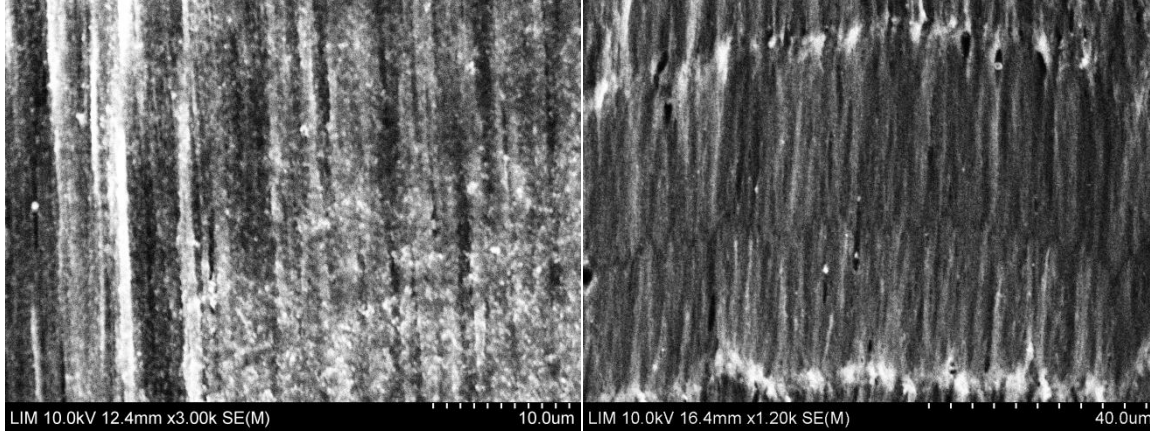
Figure 34: SEM image of the crack front showing the fibrillar structure. Images from (Mzabi, 2010).

This concept of local mechanics, and in particular damage and dissipation near the crack tip is a focus of current research interest both in fracture of gels (Baumberger and Ronsin, 2010, Seitz et al., 2009, Baumberger et al., 2006b) and in fracture of rubbers (Mzabi et al., 2011, Rublon et al., 2013, Brüning et al., 2013, Trabelsi et al., 2002, Zhang et al., 2015). Finding adapted and quantitative micromechanical models for the crack tip, accounting for both the non-linear elasticity, anisotropy (as induced by crystallization or polymer orientation for example) and damage, is clearly an important future challenge.

6.4 FRACTURE BY CAVITATION

Until now we have considered fracture in uniaxial tension. However, when incompressible soft materials are loaded under a nearly hydrostatic tensile stress, failure generally occurs by the formation of cavities. This phenomenon often called cavitation in the literature is of great practical interest since soft materials are often loaded in confined geometries for example in coatings or adhesives (see section 5.3). Furthermore, a dilatant stress of considerable magnitude is set up near hard fillers (Cho et al., 1987, Cho and Gent, 1988) and at the tip of a sharp crack (Gent, 1990) so that cavities of various sizes often appear in front of cracks (Hui et al., 2003).

Yet, the details of the cavity nucleation and growth are still incompletely understood and a reliable cavitation criterion based on materials properties is still lacking. A variety of models have been proposed to describe the expansion of a pre-existing cavity as a function of the elastic properties of the material, its surface tension or its fracture energy (Ball, 1982, Biwa, 2006, CHANG and PAN, 2001, Dollhofer et al., 2004, Fond, 2001, Ganghoffer and Schultz, 1995, Horgan and Polignone, 1995, Hou and Abeyaratne, 1992, Lopez-Pamies, 2009, Polignone and Horgan, 1993, Volokh, 2007). However, experimental studies in well controlled conditions have been much less available to the theoretical community. The earliest documented evidence of the cavitation process is rather old (Yerzley, 1939, Busse, 1938) and experiments were carried out with commercial rubbers (neoprene and natural rubber) using a relatively confined geometry called "poker-chip". The rubber disks were glued to a cylindrical sample holder and stretched in the thickness direction. Both studies observed that the stress-strain curve obtained in that

geometry showed a marked and irreversible softening above a well-defined value of stress and noted that the fracture surfaces after failure contained the evidence of what they called "internal cracks" or macroscopic cavities.

Some years later Gent and Lindley (Gent and Lindley, 1959) used the same "poker-chip" geometry on natural rubber formulations to carry out their widely known systematic investigation. They prepared vulcanized rubber disks of identical diameter and different thicknesses varying therefore the aspect ratio (i.e. the level of confinement). They found that the critical stress (defined as the apparent yield point in the stress-strain curve) decreased as the test-piece thickness was increased from very small values, becoming substantially constant for moderately thick samples as shown on Figure 35.
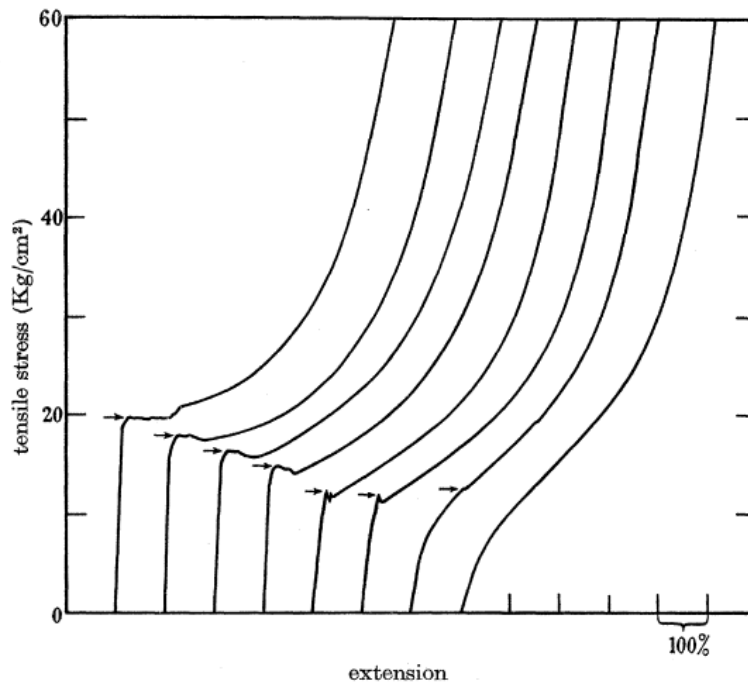
Figure 35: Experimentally determined load-extension relations for bonded rubber cylinders of vulcanizate D. Test-piece dimensions: diameter, 2 cm; thickness (from left to right), 0.056, 0.086, 0.145, 0.183, 0.32, 0.365, 0.565, 0.98 cm. Data shifted horizontally. Reprinted from (Gent and Lindley, 1959).

Post mortem observations showed that a series of small internal cracks were formed in the thin disks (uniformly distributed across the section), and only one or two large cracks were formed in the centre in moderately thick disks. This result has been since completed by real-time X-ray tomography observations showing that the cavities actually appear progressively and toward the center of the sample first(Bayraktar et al., 2008a). The switch from multiple growth of small cavities to single growth of a large cavity as the ratio between diameter and thickness of the sample decreases has also been recently predicted by finite element simulations(Lefèvre et al., 2015). Interestingly the fact that the yield stress increases with degree of confinement is counterintuitive and contrary to cavity expansion simulation results(Lefèvre et al., 2015) and suggests that there is more than the expansion of a cavity in the observed damage mechanism.

Maybe the most important observation of Gent and Lindley's seminal work is however that (for a fixed geometry) the apparent yield point in the stress-strain curves of the poker-chip samples is a reproducible material constant proportional to the elastic modulus. This certainly brought Gent and Lindley to name this internal cracking process a cavitation process and to model it as a simple deformation process (i.e. independent of initial cavity size) rather than as a fracture process. They used the elastic theory of cavity inflation developed by Green and Zerna (Green and Zerna, 1954) for neo-Hookean behaviour to justify that the apparent yield point in the stress-strain curve appeared when the local hydrostatic pressure reached a critical value of $5E/6$ (where E is the small strain Young's modulus of the rubber). This criterion of critical pressure proportional to the modulus was also confirmed by the studies of Cho and Gent (Cho and Gent, 1988) using layers of transparent silicone rubber bonded to two steel balls or to two parallel steel cylinders. Optical observations

showed the presence of large cavities in the rubber layers concomitantly with the occurrence of the apparent yield stress. Note that this connection between the modulus of the material and the apparent yield stress due to cavity formation was also made for much softer thin confined layers of adhesives (see Figure 21 and Figure 25) where fracture of the material and large deformation coexist(Lakrout et al., 1999, Brown and Creton, 2002, Chiche et al., 2005a).

Coming back to elastomers, for thinner layers (layer thickness less than 5% of sphere diameter) two interesting effects were observed. 1) In a continuous tensile test the critical stress increased markedly above the elastic modulus. 2) If on the other hand the load was kept constant just below the critical value, cavities progressively appeared over time. These two results seem to indicate that the material is in a metastable state when the applied stress exceeds the small strain elastic modulus. These early results showed a strong correlation between the critical stress (described as the apparent yield point) and the elastic modulus of

the rubber, while post-mortem observations and common sense point to a fracture process, which should introduce the idea of defect size and should not be necessarily proportional to the modulus.

This apparent discrepancy has been pointed out theoretically (Gent and Wang, 1991, Lin and Hui, 2004) and recently re-examined experimentally. Using a series of unfilled and fully transparent model polyurethanes synthesized directly in a disc-like confined sample holder, Cristiano et al.(Cristiano et al., 2010) studied the effect of network architecture and temperature on the onset of cavitation. Combining experiments and simulation, they found that while the modulus of their network increased with temperature (as expected for any unfilled rubber), the critical hydrostatic stress P_c to observe cavitation decreased markedly with temperature (Figure 36a) in clear contradiction with earlier results from Gent and Lindley(Gent and Lindley, 1959) and models based on cavity expansion by deformation alone(Lefèvre et al., 2015, Lopez-Pamies et al., 2011, Hou and Abeyaratne, 1992).
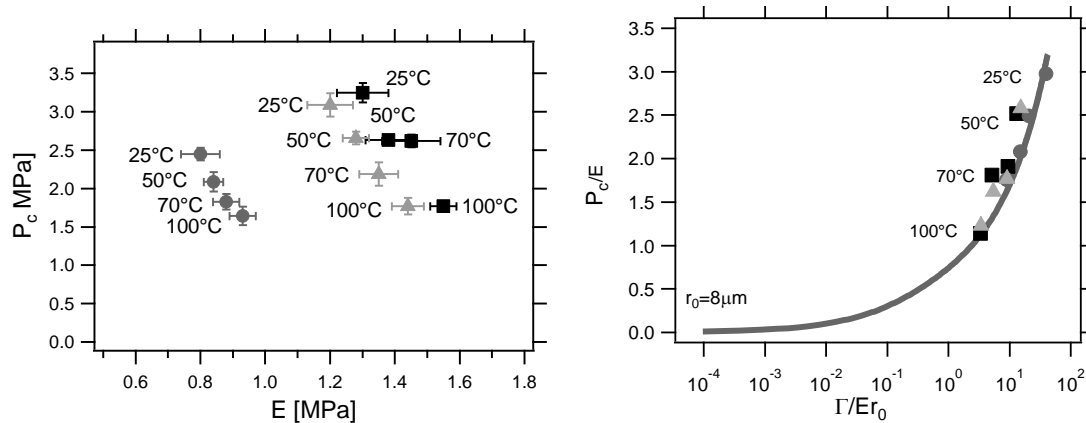
Figure 36 a) Cavitation strength P_c as a function of the Young's modulus E for three different materials and different temperatures. b) Same data replotted to show the dependence of the cavitation strength P_c on both the elastic modulus E and the fracture energy Γ in dimensionless form. The dashed line is the prediction of the model with r_0 = 8 μm. Data from (Cristiano et al., 2010).

They also presented an improved model taking into account the importance of the fracture energy Γ measured in mode I (double edge notch geometry) on the onset of cavitation. Using a penny-shape precursor crack in an infinite medium as an idealized geometry and a nonlinear constitutive model with exponential hardening as in (Seitz et al., 2009) they were able to predict the relation between the pressure P and energy release rate $\mathcal{G}$ as a function of initial crack size. This non-linear elastic model

was able to properly fit the dependence of the pressure P_c at the onset of cavitation on both the Young's modulus and the fracture energy Γ by using a constant value of the initial crack radius r_0 = 8μm (Figure 36b). The elasto-adhesive length Γ/E, (which varied between 25 and 320 μm depending on the temperature and material) is here much larger than the initial crack radius implying that nonlinear elasticity must be used to calculate $\mathcal{G}$. This result will be even more relevant for cavitation in adhesives (section 5.3)

where the modulus is typically one to two orders of magnitude lower. Interestingly, the model suggests that resistance to fracture by cavitation P_c can be improved by increasing both the mode I fracture toughness Γ of the material and its degree of strain hardening which effectively

reduces the applied $\mathcal{G}$ at a fixed stress level. This combination of stiffening at low λ and high value of Γ is precisely what has recently been discovered in double network gels and elastomers(Nakajima et al., 2013b, Ducrot et al., 2014) and will be discussed in section 7.2.

6.4 *CONCLUSIONS AND SOME REMARKS ON DAMAGE MECHANISMS*

We have seen in this section that the fracture of soft materials is inherently a multi-scale process with at least three important length scales. At the molecular level the bonds break and some energy dissipation occurs by the Lake-Thomas mechanism. If only this molecular mechanism is active (as in Figure 30) the fracture process is called threshold fracture. However, in the general case two other important dissipative mechanisms are active and couple to the failure of chemical bonds. Far from the crack tip the viscoelastic nature of the soft material can dissipate energy if the applied strain rate near the crack tip is in the range of strain rates where the material is dissipative. Then locally, very close to the crack tip, but over a region of the order of 50-100 μm, the material is highly deformed and generally experiences some concomitant damage such as cavitation (section 6.3) and stringing or some diffuse bond breakage.

For natural rubber, which is able to strain crystallize, it has been known for quite a while that the crystallization ahead of a propagating crack has a significant toughening effect (Huneau, 2011, Thomas and Whittle, 1970). While modern X-ray techniques have allowed to map the crystallizing region and to investigate dynamic effects(Beurrot-Borgarino et al., 2013, Candau et al., 2014, Trabelsi et al., 2002), a full micromechanical model is still lacking to connect the extent of strain-induced crystallization and the measured value of the fracture energy Γ.

For filled rubbers the questions becomes more complex due to the inherently heterogeneous structure of the material and the local confinement introduced by the presence of nanofillers. For example it has been shown that nanocavities can appear above a true stress of the order of 25 MPa even in uniaxial extension (Zhang et al., 2013, Zhang et al., 2012). The presence of such nanocavities has also recently been detected directly in front of the crack tip(Zhang et al., 2015).

7. NEW TRENDS

In this section, we will present and briefly discuss some new trends in adhesion and fracture of soft materials. Rather than listing the very large literature reporting novel soft materials with ever exciting new properties we will focus on three new concepts, which in our opinion deserve attention and couple polymer physics and mechanics. The first one is the use of labile bonds in solid materials, i.e. bonds that can

be broken and reformed leading to self-healing properties and viscoelastic properties without permanent damage. The second concept is that of interpenetrated networks, also called double networks, where having cocontinuous networks in the material leads to tremendous increases in toughness. Finally the third concept is that of

biomimetism for reversible adhesion. The investigation of the reversible adhesion of insects, lizards and other small animals has led to a wealth of new science inspired by the adhesive features occurring in nature.

7.1 *LABILE BONDS IN ADHESION AND FRACTURE OF SOFT MATERIALS*

It is common to distinguish solids and liquids by their macroscopic mechanical behavior. Solids resist creep and cannot deform indefinitely without permanent damage (fracture). On the other hand liquids have the ability to flow and

change shape without any permanent damage, but cannot maintain static loads for long times. Liquids only contain weak intermolecular bonds that can readily exchange, while classic soft solids, in addition to these weak bonds, contain a network of connected strong bonds that never spontaneously break and give the solid character. In between these two extremes it is possible to make materials containing also

stronger bonds than the typical van der Waals bonds of liquids, but still able to be dynamic (break and reform). Materials containing such bonds of intermediate energy can self-assemble and form so-called supramolecular structures(Aida et al., 2012, Sijbesma et al., 1997, Lange et al., 1999, Narita et al., 2013, Cordier et al., 2008) or in the case of filled systems can form dynamically the bonds between filler and polymer(Carlsson et al., 2010, Lin et al., 2010, Rose et al., 2013, Haraguchi et al., 2011).

The role of these non permanent bonds on adhesion and fracture has been the focus of much attention in the materials science community in particular because of their self-healing properties. It is an engineer's dream to design a material that can repair itself after it has been fractured and this would of course be particularly desirable for long–term performance where for example fatigue cracks can propagate slowly over time and eventually cause the catastrophic failure of the material. If mechanisms existed whereby the crack, opened by the mechanical stress, could self-heal and reform the same chemical bonds across the crack faces, the lifespan of the mechanical part would be greatly increased. Of course this self-healing property requires some molecular mobility, which is a natural property of liquids. Therefore any self-healing material must possess simultaneously the properties of solids and liquids. For a homogeneous material the diffusion coefficient D and the viscosity η are closely coupled by the Stokes-Einstein relation:

$$D\eta = \frac{k_B T}{6\pi r_H} \qquad \textbf{48}$$

where r_H is the hydrodynamic radius of the diffusing particle. Equation 48 basically states that it is very difficult to have molecular diffusion (required for healing of cracks) without flow (which is generally undesirable in solids).

Any viable strategy for self-healing must therefore break this paradox. Cordier et al. developed a new elastomer made from oligomers connected by multiple hydrogen bonds (Cordier et al., 2008). These oligomers are dynamic, but there is always a large number of closed bonds so that the material behaves as a solid and displays rubber elasticity while remaining completely soluble and processable like a thermoplastic. Most interesting are its self-healing properties. When the material is cut, it can be reassembled and can retrieve its original strength, as long as the surfaces are freshly cut (Maes et al., 2012). Tack experiments have been carried out between plates and the increase in adhesion energy with time is represented in Figure 37.
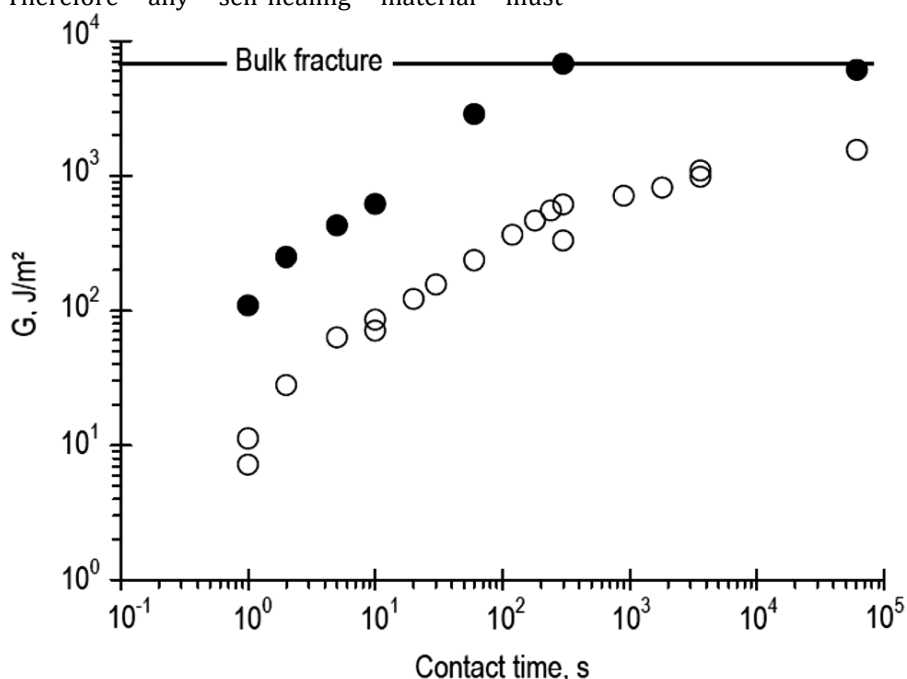
Figure 37: Fracture energy of healed supramolecular rubber as a function of contact time. Open circles represent melt pressed surfaces, while the filled circles represent freshly broken fracture surfaces. Bulk fracture is only achieved for these freshly broken surfaces (Maes et al., 2012).

The claimed healing mechanism here is not interdiffusion of chains (although it must occur), but rather the reformation of supramolecular bonds across the interface until the density of bonds reaches its equilibrium bulk value after a few minutes. While such healing behavior is commonly observed with polymer melts (Jud et al., 1981, Schach and Creton, 2008), which flow at long times, the supramolecular elastomers of Cordier et al. deform like crosslinked rubbers showing significant strain hardening as shown on Figure 38.
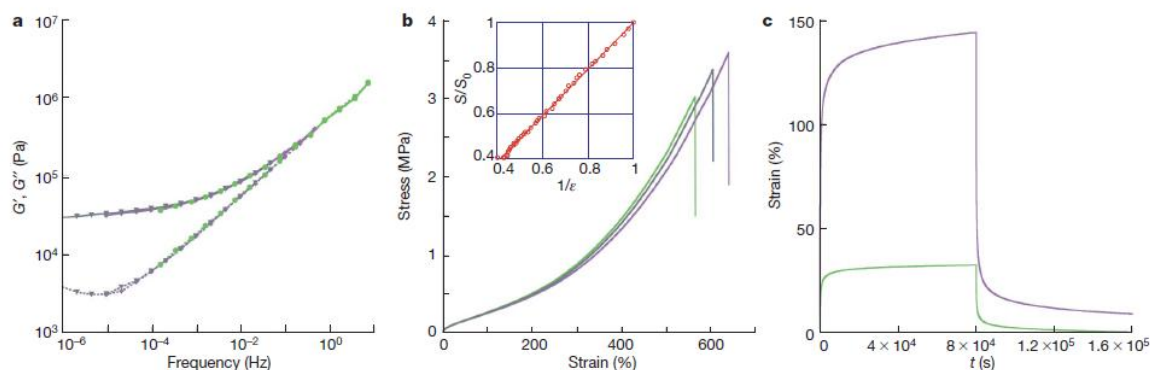
Figure 38: **a,** Frequency dependence of the storage (top, μ') and loss (bottom, μ'') moduli of the supramolecular elastomer obtained by classical time–temperature superposition shifts (note that G' and G" are used for the storage moduli in the original figure). The reference temperature is 50 °C and measurements were performed at 50 °C (green circles), 70 °C (purple diamonds) and 90 °C (black triangles). **b,** Stress–strain curve of supramolecular rubber. Data for three samples are shown. The inset shows that the cross-section area varies as the inverse of the tensile deformation confirming incompressibility. **c,** Creep–recovery experiment of the same elastomer for an applied stress of 5,000 Pa (green) and 20,000 Pa (purple). Figure reprinted from (Cordier et al., 2008).

A second example is the use of labile bonds in combination with permanent bonds (Narita et al., 2013, Carlsson et al., 2010, Rose et al., 2013, Haraguchi and Song, 2007, Miquelard-Garnier et al., 2009, Tuncaboylu et al., 2013, Long et al., 2014, Sun et al., 2012, Kean et al., 2014). In this case the solid character and resistance to creep is provided by the covalent bonds, which are generally rather dilute, and the viscoelastic dissipation, which is necessary to resist fracture, is provided by the labile bonds. A particularly interesting example of this toughening mechanism is the case of nanocomposite hydrogels (Lin et al., 2011, Carlsson et al., 2010, Lin et al., 2010), where polymers can adsorb reversibly on nanoparticles and introduce dissipative mechanisms during deformation by breaking and reforming, while the permanent bonds make sure that the shape is maintained as the load is removed. This non permanent adsorption mechanism has also been recently used to obtain macroscopic adhesion between wet living tissues (Rose et al., 2014).

The effect of such labile bonds on fracture should be twofold. On the one hand the breakable bonds should favor stress redistribution between covalent bonds and reduce stress concentration, and on the other hand each stretched chain able to break will irreversibly dissipate the elastic energy stored in the chain due to the Lake-Thomas mechanism(Long et al., 2014) described in section 6.1. Both mechanisms should lead to increased fracture toughness and indeed this type of gel is usually more extensible and breaks at higher values of stress than an equivalent gel with covalent bonds only. Yet an important notion is that of the characteristic exchange time of the labile bonds. If the bonds can exchange much faster than the rate at which polymer chains are being stretched, they should be invisible, while if the strain rate is much faster than the inverse of the characteristic exchange time the labile bonds should act as permanent bonds. Systematic experiments with notched samples have only been reported in a limited number of cases and indeed an increase in the fracture energy Γ has been observed when labile and permanent bonds were present (Lin et al., 2010). However, experiments were carried out as a function of composition rather than as a function of strain rate. It is therefore still difficult to relate the characteristic exchange time of the labile bonds with the macroscopic fracture energy.

7.2 INTERPENETRATED NETWORKS FOR FRACTURE TOUGHNESS

A particularly difficult combination of properties to obtain simultaneously is a perfectly reversible elastic behavior (with no hysteresis) and mechanical toughness. This has been for many years a very important limiting factor for hydrogels for example.

Hydrogels are extremely important in processed food but also in biological tissues and biomedical

applications(Calvert, 2009, Peppas et al., 2000). From the materials point of view hydrogels are polymer networks highly swollen with water. At short times (or high strain rates) their mechanical behavior is dominated by rubber elasticity and they essentially behave as very soft rubbers. However, when immersed in water they can also exchange water with the surrounding medium in response to an applied stress(Cai and Suo, 2012, Hui and Muralidharan, 2005). This phenomenon, called poroelasticity, only occurs at long times for macroscopic gels. The characteristic time scale of the water exchange depends on the characteristic size of the system and is controlled by the so-called collective diffusion coefficient, which is typically in the range of 10^{-12} cm^2/s.

Because they are highly swollen in water (10% polymer is typical), chemically crosslinked hydrogels are usually very elastic (Sakai et al., 2010, Sakai, 2013) and while they can be extensible, they are typically not very tough when they are notched as discussed in section 6.1. One strategy to make these chemical gels tough is to introduce viscoelastic dissipative processes, for example by introducing labile bonds as discussed in the previous section. However, this method always leads to significant strain rate dependence of the mechanical behavior even after many loading cycles and often to irreversible residual deformation upon

unloading after the first cycle (Sun et al., 2012, Tuncaboylu et al., 2011, Tuncaboylu et al., 2013, Rose et al., 2013).

Jian Ping Gong and her group(Gong et al., 2003, Tanaka et al., 2005, Gong, 2010, Ahmed et al., 2014) have developed since 2003 a completely different toughening method, which does not rely on viscoelastic dissipation by monomer friction, but rather on irreversible dissipation(Webber et al., 2007) by the Lake-Thomas mechanism. The synthesis of interpenetrated networks is achieved by sequences of synthesis, swelling and polymerization(Gong, 2014). These interpenetrated composites are constituted of two elastic networks with different levels of prestretch and maximum extensibility. The principle is shown on Figure 39. In the gels developed by Gong, one of the networks is stiff and highly prestretched, while the other is very extensible and at its reference configuration. This combination of properties leads to a simultaneous high stiffness (due to the high stress necessary to break the first network) and high extensibility controlled by the second network. A micromechanical model for the toughening effects has been proposed by Brown(Brown, 2007) while Tanaka obtained similar qualitative predictions with a more macroscopic approach(Tanaka, 2007).
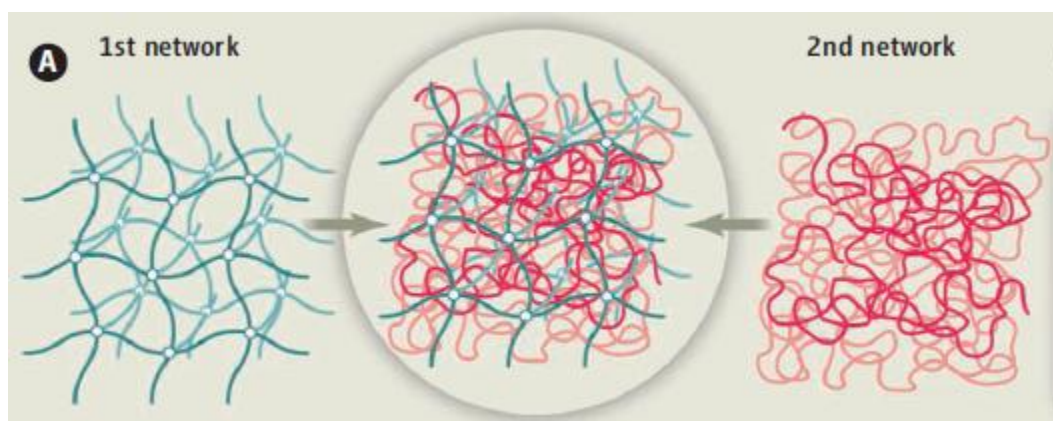
Figure 39: Schematic of the fabrication of a double network gel. The first network is initially synthesized in its Gaussian configuration. Then it is swollen in the second monomer. At this stage the first network is swollen isotropically, but the material is not tough. The second monomer is then polymerized and the interpenetrated networks are formed. Note that the second network chains are Gaussian. Reprinted from (Gong, 2014).

We describe here Brown's model. As the sample is deformed, the bonds of the first network break progressively and this occurs until the first network is fully broken into pieces. This internal breaking of bonds eventually leads to the "yielding" of the soft gel at a yield stress σ_y that is illustrated by the uniaxial step-cycle loading

tensile curves carried out as a function of λ shown in Figure 40 (Nakajima et al., 2013b). Brown hypothesizes that the crack only propagates in such a gel when the elastic energy per unit volume W_{2nd} stored in the second network (once the first is broken) times the deformed thickness of the yielded zone exceeds

the fracture energy of the second network alone Γ_2. This is equivalent to defining a local energy release rate in the yielded zone, in analogy with the modeling of the craze region in glassy polymers(Brown, 1991). This defines a value for the maximum thickness of the deformed yielded zone at the crack tip $\lambda_{max} H_0$, which has been observed experimentally for such gels(Yu et al., 2009). In the original model H_0 , i.e. the undeformed thickness of the yielded zone, is given by the following expression:

$$\Gamma \sim \sigma_y H_0 (\lambda_{max} - 1) \sim \frac{2\sigma_y \Gamma_2}{(\lambda_{max} - 1)E_2} \qquad \textbf{50}$$

$$H_0 \sim \frac{2\Gamma_2}{(\lambda_{max} - 1)^2 E_2} \qquad \textbf{49}$$

where λ_{max} is the limiting extensibility of the second network. Since the fracture of the first network into pieces occurs at nearly constant stress σ_y , the macroscopic fracture energy Γ of the gel is given by:
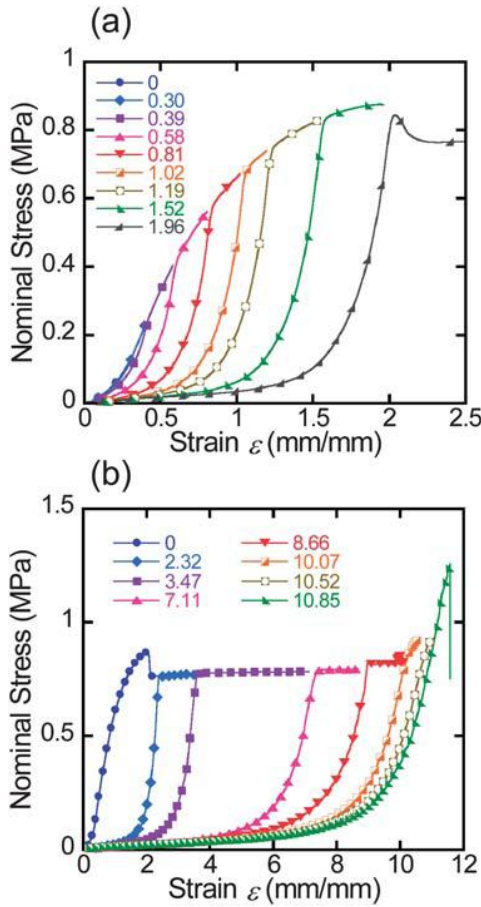
Figure 40: Tensile hysteresis loops of double network (DN) gels in (a) the pre-necking region and (b) the necking/hardening regions measured in a cyclic tensile test. The necking occurs at a well defined value of the stress. The symbol numbers denote the pre-experienced strain, ε_{max}, before measurement of each stress–strain curve. The tensile velocity was fixed at 100 mm min^{-1}. From (Nakajima et al., 2013b)

This model suggests that a large toughness can be obtained by combining a high yield stress (due to the breaking of the 1st network) and a low elastic modulus of the second network. This can generally obtained by a large contrast in crosslinking density between the two networks(Nakajima et al., 2013a, Nakajima et al., 2013b, Ahmed et al., 2014, Gong, 2010). However, the detailed effect of the crosslinking density on each parameter of equation 49 is difficult to check independently and more complete data sets would be needed to validate the model. The relevance of the toughening effect induced by the multiple network structure has been recently demonstrated to be more general by Ducrot et al. on fully hydrophobic (and unswollen) elastomers (Ducrot et al., 2014). Using interpenetrating networks of poly-methyl-acrylate and poly-ethylacrylate, they were able to increase the fracture energy of the original network from 50 J/m^2 to about 2-5 kJ/m^2 even if a necking was not obtained in uniaxial tension, since the sample rather broke before σ_Y could be reached.

The mechanism of bond breakage of the first network was elegantly demonstrated and mapped spatially and temporally during crack propagation by using chemoluminescent molecules, as shown in Figure 41.
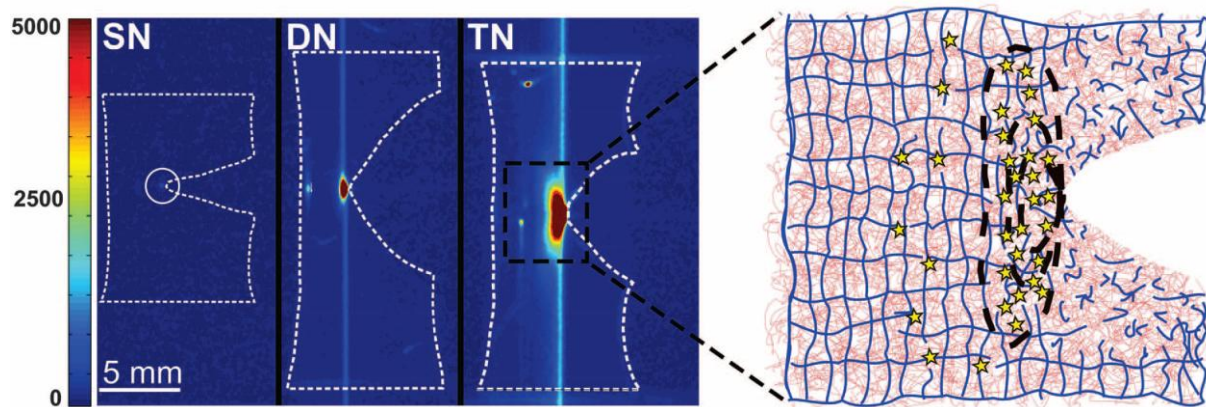
Figure 41: Intensity-colorized images of propagating cracks on notched samples containing a chemoluminescent cross-linker in the first network, showing the light emission due to the breakage of bonds in a single network (SN), double network (DN), and triple network (TN). The size and geometry of the sample are shown with a white dashed line. (Right) Schematic of the sacrificial bond-breaking mechanism in front of the crack tip for the multiple network; the first network is represented in blue, and the second and third networks are in red. From (Ducrot et al., 2014).

Interestingly the experiments of Ducrot et al. show that the breakdown of the first network chains occurs close to the crack tip well before the material yields macroscopically and causes a significant toughening. Moreover the size of the damage zone at the crack tip and the fracture toughness can be tuned by the respective volume fractions of the two or more networks.

7.3 BIOMIMETIC ADHESION OF SOFT MATERIALS

The third recent development in the field of soft adhesives is the so-called biomimetic approach to adhesion of soft materials through a controlled topography of the surface. This topic has been extensively reviewed by others(Meyers et al., 2008, del Campo and Arzt, 2008) so we will simply highlight some fundamental working principles. In 2000, Autumn et al. published a landmark paper on the adhesion mechanisms of gecko feet (Autumn et al., 2000). This paper demonstrated that the gecko can bond well and quickly release the contact on a variety of surfaces with the help of millions of 50-100 nm contact spatulae as shown on Figure 42. Each one of these spatulae can withstand strong forces in shear, but can be easily released if peeled off (Tian et al., 2006). For a more recent discussion of the adhesion of gecko's sophisticated feet see (Autumn et al., 2014) while for a discussion of adhesion and locomotion of insects see (Gorb, 2008, Zhou et al., 2014, Labonte and Federle, 2015).

| ZEISS | Field Of View 3.50 um | ——— 500.00 nm | Detector PrimaryETDetector | Image Size 1024x1024 |
| | Working Dist 7.2 mm | Acceleration V 35.0 kV | Blanker Current 0.3 pA | Mag (4x5 Polaroid) 32,440.88 X |
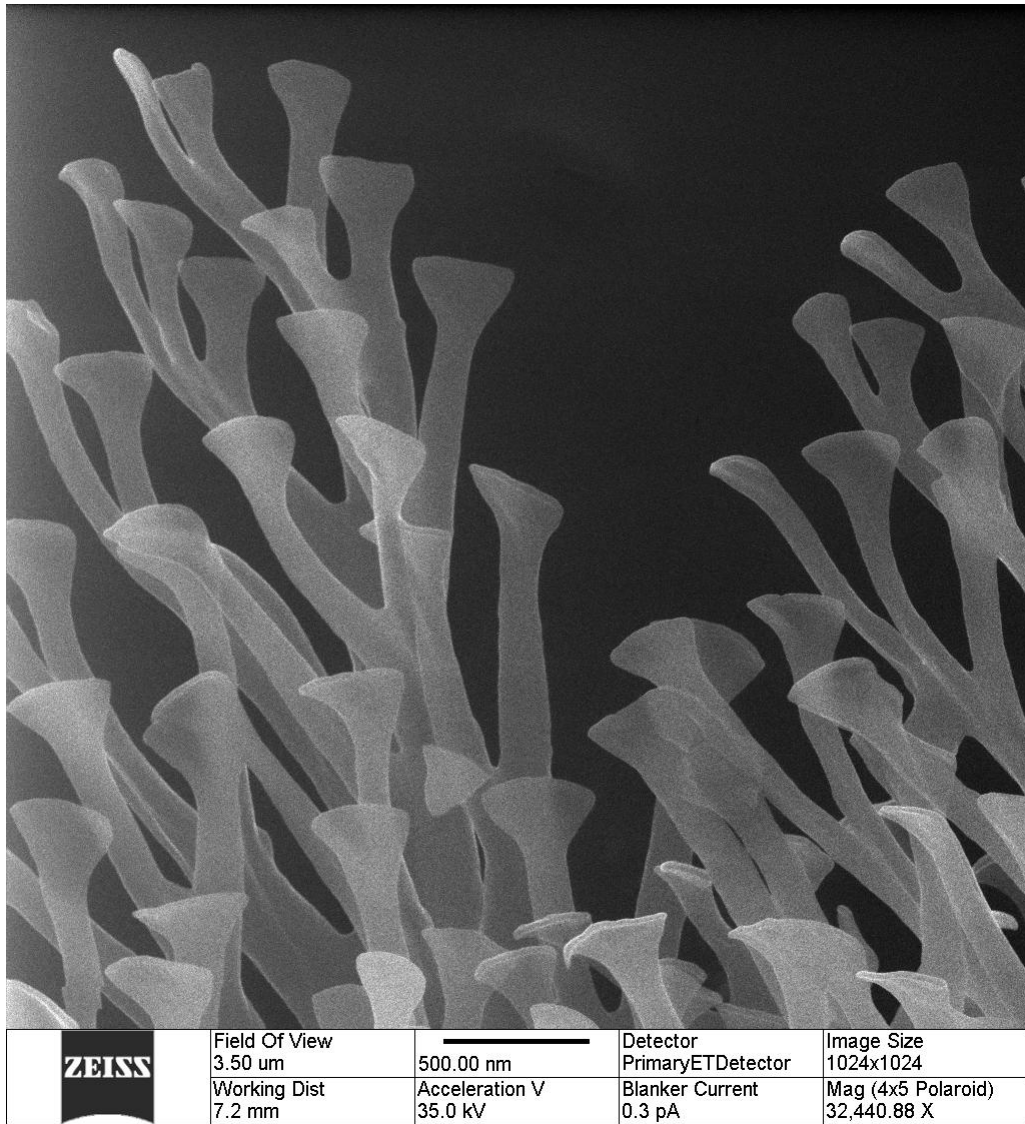
Figure 42: High resolution Helium-ion image of the adhesive spatula at the tip of gecko's feet(Autumn et al., 2014). Courtesy of K. Autumn (Lewis and Clark U.) and JJ Yang (Zeiss).

Although a direct copy of the structure of the gecko's feet appears impossible, several working principles have been used to design synthetic biomimetic reversible adhesives. The first important principle is the notion of contact splitting, i.e. replacing a large area of contact, which is sensitive to stress concentrations at the edges, with many small areas of contact, which are less sensitive to it (Spolenak et al., 2005a, Arzt et al., 2003, Hui et al., 2004, Glassmaker et al., 2004). This can be easily understood by using contact mechanics. The detachment force of a hemispherical contact is proportional to its radius R, while the density of hemispherical contacts per unit area scales with $1/R^2$. Hence, replacing a large contact with a great number of smaller ones leads to an enhancement of the detachment stress, which scales as the inverse of the radius R of the contacts. The efficiency of this strategy is illustrated in Figure 43 for the feet of different animal species.
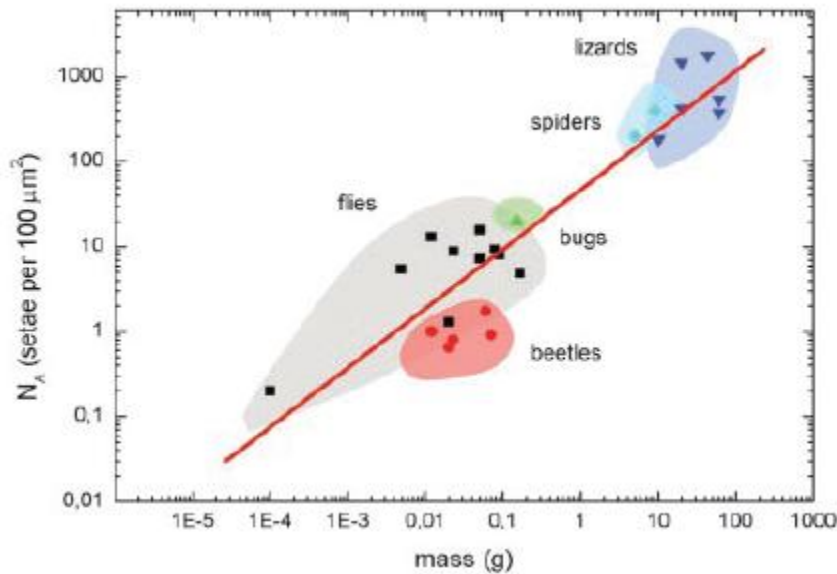
Figure 43: Dependence of the terminal element density (NA) of the attachment pads on the body mass (m) in hairy-pad systems of diverse animal groups. Figure taken from (Arzt et al., 2003).

Since the seminal paper of Arzt et al. (Arzt et al., 2003), highlighting design criteria, many new fibrillar surfaces have been developed to achieve reversible and relatively weak adhesion, in particular to create adhesive pads for the locomotion of robots on vertical walls or even on a ceiling (Geim et al., 2003, Yurdumakan et al., 2005). While the first generation of surfaces was composed of straight pillars, it was soon realized that such structures buckle and are not adapted to rough surfaces. Current improved versions use tilted soft pillars (Yang et al., 2012), which provide some compliance and adaptability to rough surfaces, or pillars with more complex shapes such as mushroom shapes (Spolenak et al., 2005b, Hossfeld et al., 2013), which suppresses the stress concentrations at the edges.

A very different strategy for removable attachment pads was proposed by Crosby and coworkers(King et al., 2014). The working principle of these pads does not rely on multicontacts, but rather on the combination of a very stiff yet flexible fabric core (which cannot easily store elastic energy under stretch but can bend), and the presence of a soft skin layer of elastomeric material (polyurethane in the original version) to provide some adhesion. This combination, which the authors call a "draping" adhesive, provides very high detachment forces when sheared while being easily removed by peeling and can be reattached many times without surface contamination. The high resistance to shear can be understood in analogy with the strong increase of the peeling force of PSA at vanishing angle discussed in section 5.2.

8. UNIFYING PICTURE

We have tried to cover in this review a broad picture of the current state of the art in adhesion and fracture of soft materials. Although the similarities between these two processes have often been pointed out, in particular by Gent in a landmark paper(Gent, 1996a), the connection was often only made between the molecular scale of the material properties and the macroscopic fracture toughness. We made a

specific effort to introduce, define and discuss the importance of intermediate length scales (100 nm- 100 μm) in these problems and to integrate the current understanding of the viscoelasticity and damage mechanisms in the material at the molecular level with the mechanics of soft materials at the micron scale such as cavitation, stringiness, fibril detachment, into a global view of fracture and adhesion that can be sketched in Figure 44, and applies to different length scales (macroscopic crack or debonding front, edge of a microscopic growing defect or cavity in the bulk or at the interface).
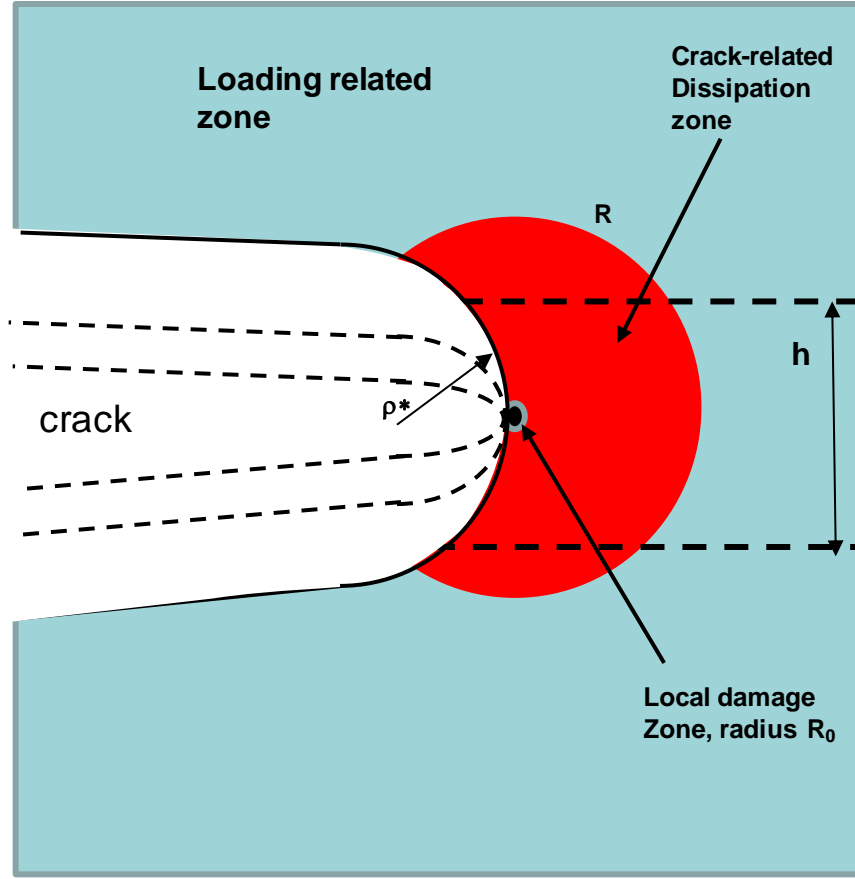
Figure 44: Schematic of a propagating crack in a soft material showing the radius of the dissipative zone R, the radius of the local damage zone R₀, the thickness of the sample *h* as well as several crack tip radii ⍴ that also represent the size of the large strain zone

A key point of this unified picture is the spatial separation between three different scales of dissipation. Far from the crack tip, there is a zone (in light blue) where the dissipation of the material is dominated by the far-field loading conditions. If the material is elastic, no dissipation occurs in that region. The zone of size R delimited in red is the zone where the dissipation of the material is dominated by the propagation of the crack. The dissipated energy in this region is generally called Γ. Finally, the black zone of size R_0 close to the tip is where local damage and molecular fracture generally occurs, inducing an energy dissipation named Γ_{local}. For the crack to propagate, the Griffith condition must be considered independently at the two scales R and R_0, resulting in the definition of two different energy release rates, named respectively G and g_{local}.

Based on this general picture, we can now discuss different situations to explain the separate role played by large strains and dissipative processes. The sizes R and R_0 of the two crack related dissipative regions need to be compared with two important geometric parameters, which are the crack length c and the smallest sample size h, as well as with the size of the region affected by large strain caused by the presence of the crack tip. This is represented by the radius of the opened propagating crack ρ^*, which corresponds to the elastoadhesive length $\ell_{EA} = \frac{\Gamma}{E}$, if R remains small related to the sample thickness h.

Let's first discuss the case of a long crack in a large medium. In the case of small-scale yielding discussed in the introduction (with both large strain and dissipation limited to a small region), the energy transfer is clearly established by LEFM concepts like G and K and fracture propagation is determined by the condition $G = \Gamma(v)$. If the dissipative region remains small (the red zone collapses into the black one), but the region where large strain is developed becomes large, i.e. if $R << \rho^*$, G can still be defined and evaluated through the method or Rivlin and Thomas or the J integral and $G = \Gamma_{local}$ is a proper propagation criterion. This is the case for both the threshold fracture of elastomers (section 6.1) and reversible adhesion of elastomers to solid surfaces (section 5.3.2).

When both large strain and energy dissipation occur over a large region, i.e. $R \sim \rho^*$, alternative strategies must be found. One way to approach the problem is to define a local energy release rate g_{local} applied to the black zone and then set the propagation criterion as $g_{local} = \Gamma_{local}$ (see section 6.3). Then the problem becomes to relate g_{local} to the energy release rate G applied to the red zone, which requires modeling the material response in the large strain region. The difference between the two representing the energy dissipated inside the red zone.

We remark that if the dissipation associated to the far-field loading is not negligible, the classical energy release rate G cannot be unambiguously defined. When the material response in this region can be considered linear viscoelastic, one convenient strategy to obtain an approximate value of G is to include the macroscopic relaxation of the material in the estimate of the elastic energy effectively releasable. In practice, this means using the elastic calculation for the sample and substituting the elastic modulus by $\mu'(t)$ or $\mu'(\omega)$ as discussed in section 5.3.2 and also used by Bhuyan et al.(Bhuyan et al., 2013). In the cases where large deformations are relevant over the whole sample, like in fracture of pure shear samples, another strategy to better estimate G or g_{local} is to consider the soft elastic solution, and then estimate the strain energy density $W(\lambda)$ at the point of crack propagation by using the *unloading* stress-strain curve rather than the loading curve (section 6.3).

The review shows that elasto-adhesive length, $\ell_{EA} = \Gamma/E$ plays a unifying role between fracture and adhesion. In the bulk fracture case, we can unambiguously define a macroscopic fracture energy $\Gamma(v)$ that is a material property and is independent of sample geometry for sufficiently large samples ($\Gamma(v)/E <$ sample size). In the adhesion case, large strain and dissipation generally affect the whole thickness of the sample and the debonding does not occur any longer by the propagation of a stress singularity. Therefore, the macroscopic dissipation can only be interpreted as an apparent fracture energy $\Gamma_{app}(v)$, which critically depends on sample geometry (in particular layer thickness h). We remark that although $\Gamma_{app}(v)$ is not a material property, the condition $\Gamma_{app}(v)/E > h$ is a sufficient condition to identify this regime, since $\Gamma_{app}(v)$ is generally smaller than $\Gamma(v)$.

So far we have discussed the extension of LEFM to the propagation of macroscopic fracture in a soft dissipative material. However, a propagating macroscopic peel front or a propagating crack are often preceded by the growth of micro cracks, cavities and highly oriented fibrils. This is particularly true during debonding of very soft adhesives, but also for fracture of tough soft materials. In this review we have shown that the global picture presented above of how elastic energy flows to the crack tip and is dissipated can also be applied at smaller scale, to the propagation of microfracture defects in the bulk or at the interface, which becomes part of the damage zone at the macroscale.

At the microscopic scale, Γ_{local} can be used to construct a local elasto-adhesive length Γ_{local}/E that should be compared with the size of defects R_d in order to determine if these defects will either grow as cracks ($\Gamma_{local}/E < R_d$) or expand as bulk cavities (section 5.3.1). However at the local scale, the material properties may be quite different in particular because of the orientation of polymer fibrils in the direction of the tensile opening stresses so that E should rather be substituted by an E_{local} in the estimation of the local elasto-adhesive length.

The same reasoning can be applied to the growth of cavities in the bulk of a soft material, which should be interpreted as the propagation of a blunted crack of length $R_d < \Gamma_{local}/E_{local}$ (section 6.4).

In both these cases the detailed study of the micromechanisms of fracture (section 5.3), which vary significantly depending on the large strain properties of the materials, provides crucial information, which can then be used as input for the macroscopic propagation of a peel front (section 5.2) or a crack.

This last point brings us now to summarize the main insights on materials properties and their characterization. Clearly both the strong adhesives and tough soft materials discussed in this review require the existence of important molecular dissipative mechanisms (see section 5 and 7), coexisting with a molecular percolating network preventing macroscopic flow. In order to predict the fracture toughness of soft materials or their adhesive properties it is essential to characterize the strain-rate dependence as well as the strain dependence of these dissipative mechanisms. Uniaxial tensile experiments carried out at different strain rates are highly complementary with classical frequency dependent linear viscoelastic measurements. For polymer based soft adhesives, we propose to represent the reduced stress f^* as a function of $1/\lambda$ (section 5.3.3) to

separate the small-strain shear modulus μ into a permanent (C_{hard}) and non-permanent (C_{soft}) component and we propose to use these large strain parameters to draw a properties map (Figure 29). Furthermore systematic cycles of loading and unloading at large strains are also essential to separate damage mechanisms from viscoelasticity for all the complex and dissipative soft materials treated in this review.

9. OPEN QUESTIONS AND CONCLUSION

To conclude the review we propose now a discussion of some open challenges that need to be addressed to understand better these rather complex processes.

Maybe the most important experimental challenge is that of collecting better experimental data at the scale of the process zone close to the crack tip, using newly available techniques. In experimental mechanics, techniques such as (1) digital image correlation to measure displacement fields(Hild et al., 2015), or (2) birefringence mapping to measure stresses or levels of local anisotropy, (3) or infrared observations to map temperatures changes and characterize dissipative processes, have significantly increased their spatial resolution and are better adapted to large strains, and thus hold great potential while having still been only sparsely used to characterize fracture of soft materials.

Wide angle X-ray scattering has been used in the past to characterize static strain induced crystallization(Trabelsi et al., 2002), but recently the wide availability of synchrotrons has made it possible to carry out time-resolved experiments with unprecedented spatial resolution(Zhang et al., 2015, Rublon et al., 2013, Brüning et al., 2013), which can map damaged regions around the crack tip. Local crystallization, but also nanocavitation (with small and ultra small angle X-ray scattering) can be characterized in this way. If the heterogeneities are larger (100 nm-100 μm), X-ray computed microtomography (micro-CT) is becoming increasingly available and the reconstruction algorithms provide excellent spatial resolution when sufficient contrast in density is present(Bayraktar et al., 2008b, Jago, 2012) .

At the more molecular scale mechanochemistry has proved to be a powerful technique to investigate molecular damage mechanisms in cracks. Mechanoluminescent molecules have been used to map individual bond breakage more quantitatively(Kean et al., 2014, Ducrot et al., 2014, Chen and Sijbesma, 2014), and

mechanophores are only starting to be used to map dissipative mechanisms in fracture problems(Zhang et al., 2014).

On the modeling side many important challenges remain both on the materials modeling side and on the mechanics modeling side.

When the dissipative zone at the crack tip is affected by multiple mesoscale damage mechanisms such as cavitation, fibrillation and local fractures, the mechanical properties of the damaged materials cannot be simply predicted from the constitutive law of the undamaged material. These mechanisms should either be treated in detail as an evolving structure or by a suitable homogeneization procedure that includes the details of the damage into an effective constitutive law. This is currently still rarely done for soft materials, but a combination of detailed characterization of large strain properties and creative modeling strategies should be the way to progress in this area.

A more philosophical question underlying all the discussed approaches is the level of separability between the energy dissipated in the bulk deformation (the blue zone of Figure 44) and an energy dissipation mechanism Γ (the red zone of Figure 44) that can be unambiguously related to the propagation of a crack, this concept is so far only empirically validated on a limited number of systems and a general framework is missing.

Somewhat related to the above is the correct criterion for the detachment from the surface or breakage in the bulk of a microscopic and highly strained fibril. At the molecular scale, fracture of a covalent bond should be stress related as demonstrated for example by AFM single molecule experiments(Merkel et al., 1999), fracture of single molecules in flow(Nguyen et al., 1997) or fracture of block copolymers at the interface between glassy polymers(Creton et al., 2002). However, when it comes to a micron scale soft viscoelastic fibril, should we consider a stress or an energy based criterion? In this case the difficulty lies in the combination of poorly defined geometry of the fibril and complex

material properties, which makes even estimating the local stress or a g_{local} very difficult.

As discussed above in addition to the mesoscopic damage mechanisms such as cavitation and microcracks, the material itself dissipates energy in a non-trivial way when deformed in large strain. The molecular origin of this dissipation is generally either molecular viscosity (nonlinear viscoelasticity) or damage through irreversible breakage of polymer chains (Lake-Thomas mechanism). More recently the use of reversible labile bonds (also referred to as sacrificial bonds), which are able to break under stress and reform and hence dissipate energy as discussed in section 7 also called sacrificial bonds have been introduced in soft materials(Sun et al., 2012, Grande et al., 2015). Although some level of permanent bonds is probably necessary to avoid creep, the optimum ratio of reversible to permanent bonds to maximize Γ is a subject of current study, as is the effect of the characteristic rate at which these sacrificial bonds can break and reform.

Although we limited our review to soft solids, which do not flow at long times, the distinction between soft viscoelastic solids and viscoelastic fluids can be subtle at short or intermediate times. Soft adhesives actually combine large strain non-linear elasticity with significant viscoelasticity and lie exactly at the interface between liquids (with which they share the deformability and strong strain rate dependent behavior) and soft elastic solids (with which they share the capability to store elastic energy and the finite deformability). Two modeling options are then possible: 1) keeping a clear reference configuration and introducing a time-dependent viscoelastic behavior into a non-linear elastic model or 2) modeling a fluid and introducing elasticity as a time-dependent additional stress tensor. Some recent efforts to combine both approaches(Glassmaker et al., 2008, Deplace et al., 2009a, Padding et al., 2012, Padding et al., 2011) are promising but the field is still in its infancy.

Overall we feel that after many years of relative stagnation, a strong interest in the mechanics of soft living and artificial tissues in biology and medicine combined with a push toward developing stronger and lighter structures in industry, has fueled an increasing number of materials science studies creating new materials with improved mechanical properties. Yet the understanding of how soft materials can combine strength and toughness with a low elastic modulus and a large reversible deformability remains incomplete and will be the key to develop new applications such as soft robots, artificial muscles or transparent ionically conducting materials. New experimental, analysis and modeling techniques powered by the progress in electronics and software can now give unprecedented time and space resolved information on the structure, dynamics and damage mechanisms in soft materials and we feel that there are outstanding opportunities for curious physicists to enter the field and make a significant contribution.

10. REFERENCES

AHAGON, A. & GENT, A. N. 1975a. Effect of interfacial bonding on the strength of adhesion. *Journal of Polymer Science, Polymer Physics Edition,* 13**,** 1285-1300.

AHAGON, A. & GENT, A. N. 1975b. Threshold fracture energies for elastomers. *Journal of Polymer Science, Polymer Physics Edition,* 13**,** 1903-1911.

AHMED, S., NAKAJIMA, T., KUROKAWA, T., ANAMUL HAQUE, M. & GONG, J. P. 2014. Brittle–ductile transition of double network hydrogels: Mechanical balance of two networks as the key factor. *Polymer,* 55**,** 914-923.

AHN, D. & SHULL, K. R. 1998a. Effects of methylation and neutralization of carboxylated poly(n-butyl acrylate)on the interfacial and bulk contributions to adhesion. *Langmuir,* 14**,** 3637-3645.

AHN, D. & SHULL, K. R. 1998b. Effects of substrate modification on the interfacial

adhesion of acrylic elastomers. *Langmuir,* 14**,** 3646-3654.

AIDA, T., MEIJER, E. W. & STUPP, S. I. 2012. Functional Supramolecular Polymers. *Science,* 335**,** 813-817.

AKAGI, Y., SAKURAI, H., GONG, J. P., CHUNG, U.-I. & SAKAI, T. 2013. Fracture energy of polymer gels with controlled network structures. *The Journal of Chemical Physics,* 139**,** 144905.

AMOUROUX, N., PETIT, J. & LÉGER, L. 2001. Role of interfacial resistance to shear stress and adhesive peel strength. *Langmuir,* 17**,** 6510-6517.

ANDREWS, E. H. 1961. Stresses at a crack in an elastomer. *Proceedings of the Physical Society, London,* 77**,** 483-498.

ANDREWS, E. H. & KINLOCH, A. J. 1973a. Mechanics of Adhesive Failure I. *Proceedings of the Royal Society of London, series A: Mathematical and Physical Sciences,* 332**,** 385-399.

ANDREWS, E. H. & KINLOCH, A. J. 1973b. Mechanics of Adhesive Failure II. *Proceedings of the Royal Society of London, series A: Mathematical and Physical Sciences,* 332**,** 401-414.

ANDREWS, E. H. & KINLOCH, A. J. 1974. Mechanics of elastomeric adhesion. *Journal of Polymer Science: Part C Polymer Symposia,* 46**,** 1-14.

ARZT, E., GORB, S. & SPOLENAK, R. 2003. From micro to nano contacts in biological attachment devices. *Proceedings of the National Academy of Sciences,* 100**,** 10603-10606.

AUBREY, D. W. & SHERRIFF, M. 1980. Peel Adhesion and Viscoelasticity of Rubber-Resin Blends. *Journal of Polymer Science, Polymer Chemistry Edition,* 18**,** 2597-2608.

AUTUMN, K., LIANG, Y. A., HSIEH, S. T., ZESCH, W., CHAN, W. P., KENNY, T. W., FEARING, R. & FULL, R. J. 2000. Adhesive force of a single gecko foot-hair. *Nature,* 405**,** 681-685.

AUTUMN, K., NIEWIAROWSKI, P. H. & PUTHOFF, J. B. 2014. Gecko Adhesion as a Model System for Integrative Biology, Interdisciplinary Science, and Bioinspired Engineering. *Annual Review of Ecology, Evolution, and Systematics,* 45**,** 445-470.

BALL, J. M. 1982. Discontinuous Equilibrium Solutions and Cavitation in Non-Linear Elasticity. *Philosophical Transactions of the Royal Society of London, series A: Mathematical, Physical and Engineering Sciences,* 306**,** 557-611.

BANEY, J. M., HUI, C.-H. & COHEN, C. 2001. Experimental Investigations of a stress

Intensity factor based description of the adhesion of viscoelastic materials. *Langmuir,* 17**,** 681-687.

BARQUINS, M. & MAUGIS, D. 1988. Stick-Slip and Peeling of Adhesive Tapes. *In:* ALLEN, K. W. (ed.) *Adhesion 12.* London: Elsevier.

BARTHEL, E. & FRETIGNY, C. 2009. Adhesive contact of elastomers: effective adhesion energy and creep function. *Journal of Physics D-Applied Physics,* 42**,** 195302.

BARTHEL, E. & HAIAT, G. 2002. Approximate model for the adhesive contact of viscoelastic spheres. *Langmuir,* 18**,** 9362-9370.

BAUMBERGER, T., CAROLI, C. & MARTINA, D. 2006a. Fracture of a biopolymer gel as a viscoplastic disentanglement process. *European Physical Journal E,* 21**,** 81-89.

BAUMBERGER, T., CAROLI, C. & MARTINA, D. 2006b. Solvent control of crack dynamics in a reversible hydrogel. *Nature Materials,* 5**,** 552-555.

BAUMBERGER, T. & RONSIN, O. 2010. A convective instability mechanism for quasistatic crack branching in a hydrogel. *The European Physical Journal E,* 31**,** 51-58.

BAYRAKTAR, E., BESSRI, K. & BATHIAS, C. 2008a. Deformation behaviour of elastomeric matrix composites under static loading conditions. *Engineering Fracture Mechanics,* 75**,** 2695-2706.

BAYRAKTAR, E., ISAC, N., BESSRI, K. & BATHIAS, C. 2008b. Damage mechanisms in natural (NR) and synthetic rubber (SBR): nucleation, growth and instability of the cavitation*. *Fatigue & Fracture of Engineering Materials & Structures,* 31**,** 184-196.

BELLAMINE, A., DEGRANDI, E., GERST, M., STARK, R., BEYERS, C. & CRETON, C. 2011. Design of Nanostructured Waterborne Adhesives with Improved Shear Resistance. *Macromolecular Materials and Engineering,* 296**,** 31-41.

BENYAHIA, L., VERDIER, C. & PIAU, J. M. 1997. The mechanisms of peeling of uncross-linked pressure sensitive adhesives. *Journal of Adhesion,* 62**,** 45-73.

BEURROT-BORGARINO, S., HUNEAU, B., VERRON, E. & RUBLON, P. 2013. Strain-induced crystallization of carbon black-filled natural rubber during fatigue measured by in situ synchrotron X-ray diffraction. *International Journal of Fatigue,* 47**,** 1-7.

BEURROT, S., HUNEAU, B. & VERRON, E. 2010. In situ SEM study of fatigue crack growth mechanism in carbon black-filled

natural rubber. *Journal of Applied Polymer Science,* 117**,** 1260-1269.

BHOWMICK, A. K. 1986. TEAR STRENGTH OF ELASTOMERS OVER A RANGE OF RATES, TEMPERATURES AND CROSS-LINKING - TEARING ENERGY-SPECTRA. *Journal of Materials Science,* 21, 3927-3932.

BHOWMICK, A. K. 1988. Threshold fracture of elastomers. *Journal of Macromolecular Science. Reviews in macromolecular Chemistry and Physics,* C28**,** 339-370.

BHOWMICK, A. K., GENT, A. N. & PULFORD, C. T. R. 1983. Tear Strength of elastomers under threshold conditions. *Rubber Chemistry and Technology,* 56**,** 226-232.

BHUYAN, S., TANGUY, F., MARTINA, D., LINDNER, A., CICCOTTI, M. & CRETON, C. 2013. Crack propagation at the interface between soft adhesives and model surfaces studied with a sticky wedge test. *Soft Matter,* 9**,** 6515-6524.

BIRD, R. B., ARMSTRONG, R. C. & HASSAGER, O. 1987. *Dynamics of Polymeric Liquids: Vol 1 Fluid Mechanics,* New York, Wiley.

BIWA, S. 2006. Cavitation in finite elasticity with surface energy effects. *International Journal of Non-Linear Mechanics,* 41**,** 1084-1094.

BOUCHAUD, E. & PAUN, F. 1999. Fracture and damage at a microstructural scale. *Computing in Science & Engineering,* 1**,** 32-38.

BRIGGS, L. J. 1950. Limiting negative pressure of water. *Journal of Applied Physics,* 21**,** 721-722.

BRIGGS, L. J. 1951. The limiting negative pressure of acetic acid,benzene,aniline,carbon tetrachloride, and chloroform. *Journal of Chemical Physics,* 19**,** 970-972.

BROWN, H. R. 1991. A Molecular Interpretation of the toughness of glassy polymers. *Macromolecules,* 24**,** 2752-2756.

BROWN, H. R. 1993. Effects of Chain pull-out on Adhesion of Elastomers. *Macromolecules,* 26**,** 1666-1670.

BROWN, H. R. 2007. A model of the fracture of double network gels. *Macromolecules,* 40**,** 3815-3818.

BROWN, K., HOOKER, J. C. & CRETON, C. 2002. Micromechanisms of tack of soft adhesives based on styrenic block copolymers. *Macromolecular Materials and Engineering,* 287**,** 163-179.

BROWN, K. R. & CRETON, C. 2002. Nucleation and Growth of cavities in soft viscoelastic layers under tensile stress. *European Physical journal E,* 9**,** 35-40.

BRÜNING, K., SCHNEIDER, K., ROTH, S. V. & HEINRICH, G. 2013. Strain-induced crystallization around a crack tip in natural rubber under dynamic load. *Polymer,* 54**,** 6200-6205.

BUSSE, W. F. 1938. Physics of rubber as related to the automobile. *Journal of Applied Physics,* 9**,** 438-451.

BUTLER, G. L. 1989. Natural Rubber Adhesives. *In:* SATAS, D. (ed.) *Handbook of Pressure Sensitive Adhesive Technology.* New York: Van Nostrand Reinhold.

CAI, S. & SUO, Z. 2012. Equations of state for ideal elastomeric gels. *EPL (Europhysics Letters),* 97**,** 34009.

CALVERT, P. 2009. Hydrogels for Soft Machines. *Advanced Materials,* 21**,** 743-756.

CANDAU, N., LAGHMACH, R., CHAZEAU, L., CHENAL, J. M., GAUTHIER, C., BIBEN, T. & MUNCH, E. 2014. Strain-Induced Crystallization of Natural Rubber and Cross-Link Densities Heterogeneities. *Macromolecules,* 47**,** 5815-5824.

CARLSSON, L., ROSE, S., HOURDET, D. & MARCELLAN, A. 2010. Nano-hybrid self-crosslinked PDMA/silica hydrogels. *Soft Matter,* 6**,** 3619-3631.

CHANG, W. J. & PAN, J. 2001. Cavitation instability in rubber with consideration of failure. *Journal of materials science,* 36**,** 1901-1909.

CHAUDHURY, M. K. & POCIUS, A. V. (eds.) 2002. *Surfaces, Chemistry and Applications,* Amsterdam: Elsevier.

CHEN, Y. & SIJBESMA, R. P. 2014. Dioxetanes as Mechanoluminescent Probes in Thermoplastic Elastomers. *Macromolecules,* 47**,** 3797-3805.

CHICHE, A., DOLLHOFER, J. & CRETON, C. 2005a. Cavity growth in soft adhesives. *European Physical Journal E,* 17**,** 389-401.

CHICHE, A., PAREIGE, P. & CRETON, C. 2000. Role of surface roughness in controlling the adhesion of a soft adhesive on a hard surface. *Comptes Rendus de l'Académie des Sciences de Paris, Série IV,* 1**,** 1197-1204.

CHICHE, A., ZHANG, W. H., STAFFORD, C. M. & KARIM, A. 2005b. A new design for high-throughput peel tests: statistical analysis and example. *Measurement Science & Technology,* 16**,** 183-190.

CHIKINA, I. & GAY, C. 2000. Cavitation in adhesives. *Physical Review Letters,* 85**,** 4546-4549.

CHO, K. & GENT, A. N. 1988. Cavitation in model elastomeric composites. *Journal of Materials Science,* 23**,** 141-144.

CHO, K., GENT, A. N. & LAM, P. S. 1987. Internal fracture in an elastomer containing a rigid inclusion. *Journal of Materials Science,* 22**,** 2899-2905.

CHRISTENSEN, R. M. & WU, E. M. 1981. A theory of crack growth in viscoelastic materials. *Engineering Fracture Mechanics,* 14**,** 215-225.

CICCOTTI, M., GIORGINI, B., VALLET, D. & BARQUINS, M. 2004. Complex dynamics in the peeling of an adhesive tape. *International Journal of Adhesion and Adhesives,* 24**,** 143-151.

CORDIER, P., TOURNILHAC, F., SOULIE-ZIAKOVIC, C. & LEIBLER, L. 2008. Self-healing and thermoreversible rubber from supramolecular assembly. *Nature,* 451**,** 977-980.

CRETON, C. 2003. Pressure-Sensitive-Adhesives: An Introductory Course. *MRS Bulletin,* 28**,** 434-439.

CRETON, C., BROWN, H. R. & SHULL, K. R. 1994. Molecular weight effects in chain pullout. *Macromolecules,* 27**,** 3174-3183.

CRETON, C. & FABRE, P. 2002. tack. *In:* DILLARD, D. A. & POCIUS, A. V. (eds.) *The Mechanics of Adhesion.* Amsterdam: Elsevier.

CRETON, C., HOOKER, J. C. & SHULL, K. R. 2001. Bulk and Interfacial Contributions to the Debonding Mechanisms of Soft Adhesives: Extension to Large Strains. *Langmuir,* 17**,** 4948-4954.

CRETON, C., HU, G. J., DEPLACE, F., MORGRET, L. & SHULL, K. R. 2009. Large-Strain Mechanical Behavior of Model Block Copolymer Adhesives. *Macromolecules,* 42**,** 7605-7615.

CRETON, C., KRAMER, E. J., BROWN, H. R. & HUI, C. Y. 2002. Adhesion and fracture of interfaces between immiscible polymers: from the molecular to the continuum scale. *Advances in Polymer Science,* 156**,** 53-136.

CRETON, C. & LAKROUT, H. 2000. Micromechanics of flat probe adhesion tests of soft viscoelastic polymer films. *Journal of Polymer Science: Part B: Polymer Physics,* 38**,** 965-979.

CRETON, C. & LEIBLER, L. 1996. How does tack depend on time of contact and contact pressure ? *Journal of Polymer Science: Part B: Polymer Physics,* 34**,** 545-554.

CRETON, C., ROOS, A. & CHICHE, A. 2005. Effect of the diblock content on the adhesive and deformation properties of PSAs based on styrenic block copolymers. *In:* POSSART, W. G. (ed.) *Adhesion: Current Research and Applications.* Weinheim: Wiley-VCH.

CRISTIANO, A., MARCELLAN, A., KEESTRA, B. J., STEEMAN, P. & CRETON, C. 2011. Fracture of Model Polyurethane Elastomeric Networks. *Journal of Polymer Science Part B-Polymer Physics,* 49**,** 355-367.

CRISTIANO, A., MARCELLAN, A., LONG, R., HUI, C. Y., STOLK, J. & CRETON, C. 2010. An experimental investigation of fracture by cavitation of model elastomeric networks. *Journal of Polymer Science Part B: Polymer Physics,* 48**,** 1409-1422.

CROSBY, A. J. & SHULL, K. R. 1999a. Adhesive failure analysis of pressure-sensitive adhesives. *Journal of Polymer Science: Part B: Polymer Physics,* 37**,** 3455-3472.

CROSBY, A. J. & SHULL, K. R. Debonding Mechanisms of Pressure-Sensitive-Adhesives. 22nd annual Meeting, 1999b Panama City. The Adhesion Society, 320-322.

CROSBY, A. J., SHULL, K. R., LAKROUT, H. & CRETON, C. 2000. Deformation modes of adhesively bonded elastic layers. *Journal of Applied Physics,* 88**,** 2956-2966.

DAHLQUIST, C. A. 1969. Pressure-Sensitive adhesives. *In:* PATRICK, R. L. (ed.) *Treatise on Adhesion and Adhesives.* New York: Dekker.

DALE, W. C., PASTER, M. D. & HAYNES, J. K. 1989. Mechanical Properties of Acrylic Pressure-sensitive Adhesives and their relationships to Industry Standard testing. *Journal of Adhesion,* 31**,** 1-20.

DAOULAS, K., THEODOROU, D. N., ROOS, A. & CRETON, C. 2004. Experimental and Self-Consistent Field Theoretical Study of Styrene Block Copolymer Self-Adhesive Materials. *Macromolecules,* 37**,** 5093-5109.

DE, D. & GENT, A. N. 1996. Tear strength of carbon-black-filled compounds. *Rubber Chemistry and Technology,* 69**,** 834-850.

DE GENNES, P. G. 1979. *Scaling concepts in polymer physics,* Ithaca, Cornell University Press.

DE GENNES, P. G. 1988. Fracture d'un adhésif faiblement réticulé. *Comptes Rendus de l'Académie des Sciences de Paris, Série II,* 307**,** 1949-1953.

DE GENNES, P. G. 1989. Weak adhesive junctions. *Journal de Physique,* 50**,** 2551-2562.

DE GENNES, P. G. 1996. Soft Adhesives. *Langmuir,* 12**,** 4497-4500.

DE GENNES, P. G. 1997. *Soft Interfaces,* Cambridge, Cambridge University Press.

DE GENNES, P. G. & TROIAN, S. M. 1990. Sur la fracture des adhésifs caoutchoutiques.

Comptes Rendus de l'Académie des Sciences de Paris, Série II, 311**,** 389-392.

DEGRANDI-CONTRAIRES, E., LOPEZ, A., REYES, Y., ASUA, J. M. & CRETON, C. 2013. High Shear Strength Waterborne Polyurethane/Acrylic Soft Adhesives. *Macromolecular Materials and Engineering,* 298**,** 612-623.

DEGRANDI-CONTRAIRES, E., UDAGAMA, R., BOURGEAT-LAMI, E., MCKENNA, T., OUZINEB, K. & CRETON, C. 2011. Mechanical Properties of Adhesive Films Obtained from PU-Acrylic Hybrid Particles. *Macromolecules,* 44**,** 2643-2652.

DEL CAMPO, A. & ARZT, E. 2008. Fabrication Approaches for Generating Complex Micro- and Nanopatterns on Polymeric Surfaces. *Chemical Reviews,* 108**,** 911-945.

DEPLACE, F., CARELLI, C., LANGENFELD, A., RABJOHNS, M. A., FOSTER, A. B., LOVELL, P. A. & CRETON, C. 2009a. Controlled Sparse and Percolating Cross-Linking in Waterborne Soft Adhesives. *ACS Applied Materials & Interfaces,* 1**,** 2021-2029.

DEPLACE, F., CARELLI, C., MARIOT, S., RETSOS, H., CHATEAUMINOIS, A., OUZINEB, K. & CRETON, C. 2009b. Fine tuning the adhesive properties of a soft waterborne adhesive from rheological measurements. *Journal of Adhesion,* 85**,** 18-54.

DEPLACE, F., RABJOHNS, M. A., YAMAGUCHI, T., FOSTER, A. B., CARELLI, C., LEI, C. H., OUZINEB, K., KEDDIE, J. L., LOVELL, P. A. & CRETON, C. 2009c. Bottom-up design of a soft-soft nanocomposite from polymer colloid particles. *Soft Matter,* 5**,** 1440-1447.

DERAIL, C., ALLAL, A., MARIN, G. & TORDJEMAN, P. 1997. Relationship between viscoelastic and peeling properties of model adhesives. Part 1. Cohesive fracture. *Journal of Adhesion,* 61**,** 123-157.

DERAIL, C., ALLAL, A., MARIN, G. & TORDJEMAN, P. 1998. Relationship between viscoelastic and peeling properties of model adhesives. Part 2. The interfacial fracture domains. *Journal of Adhesion,* 68**,** 203-228.

DERAIL, C., CAZENAVE, M. N., GIBERT, F. X., MARIN, G., KAPPES, N. & LECHAT, J. 2004. Rheological Properties of Hot-Melt Pressure-Sensitive Adhesive (HMPSAs) Based on Styrene-Isoprene Copolymers. Part 2: Innovative Molecular Design From

Predictive Formulation. *The Journal of Adhesion,* 80**,** 1131 - 1151.

DERUELLE, M., HERVET, H., JANDEAU, G. & LÉGER, L. 1998. Some remarks on JKR experiments. *Journal of Adhesion Science and Technology,* 12**,** 225-247.

DOI, M. & EDWARDS, S. F. 1986. *The theory of polymer dynamics,* Oxford, Oxford University Press.

DOLLHOFER, J., CHICHE, A., MURALIDHARAN, V., CRETON, C. & HUI, C. Y. 2004. Surface energy effects for cavity growth and nucleation in an incompressible neo-Hookean material - modeling and experiment. *International Journal of Solids and Structures,* 41**,** 6111-6127.

DUCROT, E., CHEN, Y., BULTERS, M., SIJBESMA, R. P. & CRETON, C. 2014. Toughening Elastomers with Sacrificial Bonds and Watching them Break. *Science,* 344**,** 186-189.

DUGDALE, D. S. 1960. Yielding of steel sheets containing slits. *Journal of Mechanics and Physics of Solids,* 8**,** 100-104.

EDWARDS, S. F. & VILGIS, T. A. 1988. The Tube Model-Theory of Rubber Elasticity. *Reports on Progress in Physics,* 51**,** 243-297.

ERB, R. A. & HANSON, R. S. 1960. The tensile strength and tacky behavior of polymeric liquids. *Transactions of the Society of Rheology,* 4**,** 91-116.

FELDSTEIN, M. M., KULICHIKHIN, V. G., KOTOMIN, S. V., BORODULINA, T. A., NOVIKOV, M. B., ROOS, A. & CRETON, C. 2006. Rheology of poly(N-vinyl pyrrolidone)-poly(ethylene glycol) adhesive blends under shear flow. *Journal of Applied Polymer Science,* 100**,** 522-537.

FERRARI, F., BERTONI, M., BONFERONI, M. C., ROSSI, S., CARAMELLA, C. & WARING, M. J. 1995. COMPARATIVE-EVALUATION OF HYDROCOLLOID DRESSINGS BY MEANS OF WATER-UPTAKE AND SWELLING FORCE MEASUREMENTS .2. *International Journal of Pharmaceutics,* 117**,** 49-55.

FOND, C. 2001. Cavitation criterion for rubber materials: a review of void-growth models. *Journal of Polymer Science: Part B: Polymer Physics,* 39**,** 2081-2096.

FOSTER, A. B., LOVELL, P. A. & RABJOHNS, M. A. 2009. Control of adhesive properties through structured particle design of water-borne pressure-sensitive adhesives. *Polymer,* 50**,** 1654-1670.

FULLER, K. N. G. & TABOR, D. 1975. The effect of surface roughness on the adhesion of elastic solids. *Proceedings of the Royal*

Society of London, series A: Mathematical and Physical Sciences, A345, 327-342.

GANGHOFFER, J. F. & GENT, A. N. 1995. Adhesion of a rigid punch to a thin elastic layer. *Journal of Adhesion,* 48, 75-84.

GANGHOFFER, J. F. & SCHULTZ, J. 1995. A new theoretical approach to cavitation in rubber. *Rubber Chemistry and Technology,* 68, 757-772.

GARDON, J. L. 1963a. Peel Adhesion. I. Some phenomenological aspects of the test. *Journal of Applied Polymer Science,* 7, 625-641.

GARDON, J. L. 1963b. Peel adhesion. II. A theoretical analysis. *Journal of Applied Polymer Science,* 7, 643-665.

GAY, C. 2002. Stickiness - Some fundamentals of adhesion. *Integrative and Comparative Biology,* 42, 1123-1126.

GAY, C. & LEIBLER.L. 1999. Theory of tackiness. *Physical Review Letters,* 82, 936-939.

GEIM, A. K., DUBONOS, S. V., GRIGORIEVA, I. V., NOVOSELOV, K. S., ZHUKOV, A. A. & SHAPOVAL, S. Y. 2003. Microfabricated adhesive mimicking gecko foot-hair. *Nature Materials,* 2, 461-463.

GENT, A. N. 1990. Cavitation in Rubber: A Cautionary Tale. *Rubber Chemistry and Technology,* 63, 49-53.

GENT, A. N. 1994. Compression of rubber blocks. *Rubber Chemistry and Technology,* 67, 549-558.

GENT, A. N. 1996a. Adhesion and strength of viscoelastic solids. Is there a relationship between adhesion and bulk properties? *Langmuir,* 12, 4492-4496.

GENT, A. N. 1996b. A New constitutive relation for rubber. *Rubber Chemistry and Technology,* 69, 59-61.

GENT, A. N. & KAANG, S. Y. 1987. Effect of peel angle upon peel force. *Journal of Adhesion,* 24, 173-181.

GENT, A. N., LAI, S. M., NAH, C. & WANG, C. 1994. Viscoelastic Effects in Cutting and Tearing Rubber. *Rubber Chemistry and Technology,* 67, 610-618.

GENT, A. N. & LINDLEY, P. B. 1959. Internal rupture of bonded rubber cylinders in tension. *Proceedings of the Royal Society of London, series A: Mathematical and Physical Sciences,* 249 A, 195-205.

GENT, A. N., LINDLEY, P. B. & THOMAS, A. G. 1965. CUT GROWTH AND FATIGUE OF RUBBERS. I. THE RELATIONSHIP BETWEEN CUT GROWTH AND FATIGUE. *Rubber Chemistry and Technology,* 38, 292-300.

GENT, A. N. & PETRICH, R. P. 1969. Adhesion of viscoelastic materials to rigid substrates. *Proceedings of the Royal Society of London, series A: Mathematical and Physical Sciences,* 310, 433-448.

GENT, A. N. & SCHULTZ, J. 1972. Effect of Wetting Liquids on the strength of adhesion of viscoelastic materials. *Journal of Adhesion,* 3, 281-294.

GENT, A. N. & TOBIAS, R. H. 1982. Threshold tear strength of elastomers. *Journal of Polymer Science: Polymer Physics Edition,* 20, 2051-2058.

GENT, A. N. & TOMPKINS, D. A. 1969. Nucleation and growth of gas bubbles in elastomers. *Journal of Applied Physics,* 40, 2520-2525.

GENT, A. N. & WANG, C. 1991. Fracture mechanics and cavitation in rubber-like solids. *Journal of Materials Science,* 26, 3392-3395.

GEUBELLE, P. & KNAUSS, W. 1994. Finite strains at the tip of a crack in a sheet of hyperelastic material: I. Homogeneous case. *Journal of Elasticity,* 35, 61-98.

GIBERT, F. X., ALLAL, A., MARIN, G. & DERAIL, C. 1999. Effect of the rheological properties of industrial hot-melt and pressure-sensitive adhesives on the peel behavior. *Journal of Adhesion Science and Technology,* 13, 1029-1044.

GIBERT, F. X., MARIN, G., DERAIL, C., ALLAL, A. & LECHAT, J. 2003. Rheological properties of hot melt pressure-sensitive adhesives based on styrene-isoprene copolymers. Part 1: A rheological model for SIS-SI formulations. *Journal of Adhesion,* 79, 825-852.

GIESEKUS, H. 1982. A simple constitutive equation for polymer fluids based on the concept of deformation-dependent tensorial mobility. *Journal of Non-Newtonian Fluid Mechanics,* 11, 69-109.

GLASSMAKER, N. J., HUI, C. Y., YAMAGUCHI, T. & CRETON, C. 2008. Detachment of stretched viscoelastic fibrils. *European Physical Journal E,* 25, 253-266.

GLASSMAKER, N. J., JAGOTA, A., HUI, C. Y. & KIM, J. 2004. Design of biomimetic fibrillar interfaces: 1. Making contact. *Journal of the Royal Society Interface,* 1, 23-33.

GONG, J. P. 2010. Why are double network hydrogels so tough? *Soft Matter,* 6, 2583-2590.

GONG, J. P. 2014. Materials both Tough and Soft. *Science,* 344, 161-162.

GONG, J. P., KATSUYAMA, Y., KUROKAWA, T. & OSADA, Y. 2003. Double-network

hydrogels with extremely high mechanical strength. *Advanced Materials,* 15**,** 1155-1158.

GORB, S. N. 2008. Biological attachment devices: exploring nature's diversity for biomimetics. *Philosophical Transactions of the Royal Society A: Mathematical, Physical and Engineering Sciences,* 366**,** 1557-1574.

GOWER, M. D. & SHANKS, R. A. 2004a. The effect of chain transfer agent level on adhesive performance and peel master-curves for acrylic pressure sensitive adhesives. *Macromolecular Chemistry and Physics,* 205**,** 2139-2150.

GOWER, M. D. & SHANKS, R. A. 2004b. The effect of varied monomer composition on adhesive performance and peeling master curves for acrylic pressure-sensitive adhesives. *Journal of Applied Polymer Science,* 93**,** 2909-2917.

GOWER, M. D. & SHANKS, R. A. 2005. Comparison of styrene with methyl methacrylate copolymers on the adhesive performance and peeling master curves of acrylate pressure sensitive adhesives. *Macromolecular Chemistry and Physics,* 206**,** 1015-1027.

GOWER, M. D. & SHANKS, R. A. 2006. Acrylic acid level and adhesive performance and peel master-curves of acrylic pressure-sensitive adhesives. *Journal of Polymer Science Part B-Polymer Physics,* 44**,** 1237-1252.

GRANDE, A. M., GARCIA, S. J. & VAN DER ZWAAG, S. 2015. On the interfacial healing of a supramolecular elastomer. *Polymer,* 56**,** 435-442.

GREEN, A. E. & ZERNA 1954. *Theoretical Elasticity,* Oxford, Oxford University press.

GREENSMITH, H. W. 1960. Rupture of rubber. VII. Effect of rate of extension in tensile tests. *Journal of Applied Polymer Science,* 3**,** 175-182.

GREENSMITH, H. W. 1963. Rupture of rubber. X. The change in stored energy on making a small cut in a test piece held in simple extension. *Journal of Applied Polymer Science,* 7**,** 993-1002.

GREENSMITH, H. W., MULLINS, L. & THOMAS, A. G. 1960. RUPTURE OF RUBBER. *Transactions of the Society of Rheology,* 4**,** 179-189.

GREENWOOD, J. A. & WILLIAMSON, J. B. P. 1966. Contact of nominally flat surfaces. *Proceedings of the Royal Society of London, series A: Mathematical and Physical Sciences,* A295**,** 300-319.

GRIFFITH, A. A. 1920. The Phenomena of Rupture and Flow in Solids. *Philosophical Transactions of the Royal Society of London, series A: Mathematical and Physical Sciences,* 221**,** 163-198.

HAIAT, G., PHAN HUY, M. C. & BARTHEL, E. 2002. The adhesive contact of viscoelastic spheres. *Journal of Mechanics and Physics of Solids,* 51**,** 69-99.

HAN, K., CICCOTTI, M. & ROUX, S. 2010. Measuring nanoscale stress intensity factors with an atomic force microscope. *EPL (Europhysics Letters),* 89**,** 66003.

HAQUE, M. A., KUROKAWA, T. & GONG, J. P. 2012. Anisotropic hydrogel based on bilayers: color, strength, toughness, and fatigue resistance. *Soft Matter,* 8**,** 8008-8016.

HARAGUCHI, K. & SONG, L. 2007. Microstructures Formed in Co-Cross-Linked Networks and Their Relationships to the Optical and Mechanical Properties of PNIPA/Clay Nanocomposite Gels. *Macromolecules,* 40**,** 5526-5536.

HARAGUCHI, K., UYAMA, K. & TANIMOTO, H. 2011. Self-healing in Nanocomposite Hydrogels. *Macromolecular Rapid Communications,* 32**,** 1253-1258.

HILD, F., BOUTERF, A. & ROUX, S. 2015. Damage measurements via DIC. *International Journal of Fracture,* 191**,** 77-105.

HORGAN, C. O. & POLIGNONE, D. A. 1995. Cavitation in nonlinearly elastic solids: A review. *Appl Mech Rev,* 48**,** 471-485.

HOSSFELD, C. K., SCHNEIDER, A. S., ARZT, E. & FRICK, C. P. 2013. Detachment Behavior of Mushroom-Shaped Fibrillar Adhesive Surfaces in Peel Testing. *Langmuir,* 29**,** 15394-15404.

HOU, H. S. & ABEYARATNE, R. 1992. Cavitation in Elastic and Elastic Plastic Solids. *Journal of the Mechanics and Physics of Solids,* 40**,** 571-592.

HUI, C.-Y. & MURALIDHARAN, V. 2005. Gel mechanics: A comparison of the theories of Biot and Tanaka, Hocker, and Benedek. *The Journal of Chemical Physics,* 123**,** 154905.

HUI, C. Y., GLASSMAKER, N. J., TANG, T. & JAGOTA, A. 2004. Design of biomimetic fibrillar interfaces: 2. Mechanics of enhanced adhesion. *Journal of the Royal Society Interface,* 1**,** 35-48.

HUI, C. Y., JAGOTA, A., BENNISON, S. J. & LONDONO, J. D. 2003. Crack blunting and the strength of soft elastic solids. *Proceedings of the Royal Society of London, series A: Mathematical and Physical Sciences,* 403**,** 1489-1516.

HUI, C. Y., LIN, Y. Y. & BANEY, J. M. 2000. The mechanics of tack: Viscoelastic contact on a rough surface. *Journal of Polymer Science: Part B: Polymer Physics,* 38**,** 1485-1495.

HUI, C. Y., RUINA, A., CRETON, C. & KRAMER, E. J. 1992a. Micromechanics of crack growth into a craze in a polymer glass. *Macromolecules,* 25**,** 3948-3955.

HUI, C. Y., XU, D. B. & KRAMER, E. J. 1992b. A Fracture Model for a weak interface in a viscoelastic material (small scale yielding analysis). *Journal of Applied Physics,* 72**,** 3294-3304.

HUNEAU, B. 2011. STRAIN-INDUCED CRYSTALLIZATION OF NATURAL RUBBER: A REVIEW OF X-RAY DIFFRACTION INVESTIGATIONS. *Rubber Chemistry and Technology,* 84**,** 425-452.

HYUN, K., WILHELM, M., KLEIN, C. O., CHO, K. S., NAM, J. G., AHN, K. H., LEE, S. J., EWOLDT, R. H. & MCKINLEY, G. H. 2011. A review of nonlinear oscillatory shear tests: Analysis and application of large amplitude oscillatory shear (LAOS). *Progress in Polymer Science,* 36**,** 1697-1753.

ITO, K., SHITAJIMA, K., KARYU, N., FUJII, S., NAKAMURA, Y. & URAHAMA, Y. 2014. Influence of the degree of crosslinking on the stringiness of crosslinked polyacrylic pressure-sensitive adhesives. *Journal of Applied Polymer Science,* 131**,** 40336.

JAGO, K. L. G. 2012. X-RAY COMPUTED MICROTOMOGRAPHY OF RUBBER. *Rubber Chemistry and Technology,* 85**,** 387-407.

JENSEN, M. K., BACH, A., HASSAGER, O. & SKOV, A. L. 2009. Linear rheology of cross-linked polypropylene oxide as a pressure sensitive adhesive. *International Journal of Adhesion and Adhesives,* 29**,** 687-693.

JONES, R. A. L. & RICHARDS, R. W. 1999. *Polymers at surfaces and interfaces,* Cambridge, Cambridge University Press.

JOSSE, G., SERGOT, P., DORGET, M. & CRETON, C. 2004. Measuring interfacial adhesion between a soft viscoelastic layer and a rigid surface using a probe method. *Journal of Adhesion,* 80**,** 87-118.

JUD, K., KAUSCH, H. H. & WILLIAMS, J. G. 1981. Fracture mechanics studies of crack healing and welding of polymers. *Journal of Materials Science,* 16**,** 204-210.

KAELBLE, D. H. 1959. Theory and Analysis of Peel Adhesion: Mechanisms and Mechanics. *Transactions of The Society of Rheology (1957-1977),* 3**,** 161-180.

KAELBLE, D. H. 1960. Theory and Analysis of Peel Adhesion: Bond Stresses and Distributions. *Transactions of the Society of Rheology,* 4**,** 45-73.

KAELBLE, D. H. 1964. Theory and analysis of peel adhesion: Rate-temperature dependence of viscoelastic interlayers. *Journal of Colloid Science,* 19**,** 413-424.

KAELBLE, D. H. 1965. Peel Adhesion: Micro-Fracture mechanics of interfacial unbonding of polymers. *Transactions of the Society of Rheology,* 9**,** 135-163.

KAELBLE, D. H. 1969. Peel Adhesion: influence of surface energies and adhesive rheology. *Journal of Adhesion,* 1**,** 102-123.

KAELBLE, D. H. 1971. Cavitation in viscoelastic media. *Transactions of the Society of Rheology,* 15**,** 275-296.

KAELBLE, D. H. 1992. Theory and Analysis of peel adhesion: adhesive thickness effects. *Journal of Adhesion,* 37**,** 205-214.

KAELBLE, D. H. & HO, C. L. 1974. Biaxial Bond Stress Analysis in Peeling. *Transactions of The Society of Rheology (1957-1977),* 18**,** 219-235.

KEAN, Z. S., HAWK, J. L., LIN, S., ZHAO, X., SIJBESMA, R. P. & CRAIG, S. L. 2014. Increasing the Maximum Achievable Strain of a Covalent Polymer Gel Through the Addition of Mechanically Invisible Cross-Links. *Advanced Materials,* 26**,** 6013-6018.

KING, D. R., BARTLETT, M. D., GILMAN, C. A., IRSCHICK, D. J. & CROSBY, A. J. 2014. Creating Gecko-Like Adhesives for "Real World" Surfaces. *Advanced Materials,* 26**,** 4345-4351.

KINNING, D. J. & SCHNEIDER, H. M. 2002. Release Coatings for Pressure Sensitive Adhesives. *In:* CHAUDHURY, M. & POCIUS, A. V. (eds.) *Surfaces, Chemistry and Applications.* 1st ed. Amsterdam: Elsevier.

KNOWLES, J. K. & STERNBERG, E. 1973. An asymptotic finite-deformation analysis of the elastostatic field near the tip of a crack. *Journal of Elasticity,* 3**,** 67-107.

KNOWLES, J. K. & STERNBERG, E. 1974. Finite-deformation analysis of the elastostatic field near the tip of a crack: Reconsideration and higher-order results. *Journal of Elasticity,* 4**,** 201-233.

KRENCESKI, M. A. & JOHNSON, J. F. 1989. Shear, Tack, and Peel of Polyisobutylene: Effect of Molecular Weight Distribution. *Polymer Engineering and Science,* 29**,** 36-43.

KRISHNAN, V. R. & HUI, C. Y. 2009. Finite strain stress fields near the tip of an interface crack between a soft incompressible elastic material and a rigid substrate. *European Physical Journal E,* 29**,** 61-72.

KRISHNAN, V. R., HUI, C. Y. & LONG, R. 2008. Finite Strain Crack Tip Fields in Soft Incompressible Elastic Solids. *Langmuir,* 24**,** 14245-14253.

KWON, H. J., ROGALSKY, A. D. & KIM, D. W. 2011. On the Measurement of Fracture Toughness of Soft Biogel. *Polymer Engineering and Science,* 51**,** 1078-1086.

LABONTE, D. & FEDERLE, W. 2015. Scaling and biomechanics of surface attachment in climbing animals. *Philosophical Transactions of the Royal Society B,* 370**,** 20140027.

LAFUMA, A. & QUÉRÉ, D. 2011. Slippery pre-suffused surfaces. *EPL (Europhysics Letters),* 96**,** 56001.

LAKE, G. J. & LINDLEY, P. B. 1964. Cut growth and fatigue of rubbers. II. Experiments on a noncrystallizing rubber. *Journal of Applied Polymer Science,* 8**,** 707-721.

LAKE, G. J. & LINDLEY, P. B. 1965. The mechanical fatigue limit for rubber. *Journal of Applied Polymer Science,* 9**,** 1233-1251.

LAKE, G. J. & THOMAS, A. G. 1967. The strength of highly elastic materials. *Proceedings of the Royal Society of London, series A: Mathematical and Physical Sciences,* A300**,** 108-119.

LAKROUT, H. 1998. *Micromécanismes de la pégosité des polymères fondus.* Université Paris 7.

LAKROUT, H., CRETON, C., AHN, D. & SHULL, K. R. 2001. Influence of molecular features on the tackiness of acrylic polymer melts. *Macromolecules,* 34**,** 7448-7458.

LAKROUT, H., SERGOT, P. & CRETON, C. 1999. Direct observation of cavitation and fibrillation in a probe tack experiment on model acrylic Pressure-Sensitive-Adhesives. *Journal of Adhesion,* 69**,** 307-359.

LANGE, R. F. M., VAN GURP, M. & MEIJER, E. W. 1999. Hydrogen-bonded supramolecular polymer networks. *Journal of Polymer Science Part a-Polymer Chemistry,* 37**,** 3657-3670.

LAWN, B. 1993. *Fracture of Brittle Solids,* Cambdridge, Cambridge University Press.

LEFÈVRE, V., RAVI-CHANDAR, K. & LOPEZ-PAMIES, O. 2015. Cavitation in rubber: an elastic instability or a fracture phenomenon? *International Journal of Fracture,* 192**,** 1-23.

LÉGER, L., RAPHAËL, E. & HERVET, H. 1999. Surface-anchored polymer chains: their role in adhesion and friction. *Advances in Polymer Science,* 138**,** 185-225.

LIN, S. B., DURFEE, L. D., EKELAND, R. A., MCVIE, J. & SCHALAU, G. K. 2007. Recent advances in silicone pressure-sensitive adhesives. *Journal of Adhesion Science and Technology,* 21**,** 605-623.

LIN, S. B., DURFEE, L. D., KNOTT, A. A. & SCHALAU, G. K. 2009. Silicone Pressure-Sensitive-Adhesive. *In:* BENEDEK, I. & FELDSTEIN, M. M. (eds.) *Technology of of Pressure-Sensitive Adhesives and Products.* Boca Raton: CRC.

LIN, W. C., FAN, W., MARCELLAN, A., HOURDET, D. & CRETON, C. 2010. Large Strain and Fracture Properties of Poly (dimethyl acrylamide)/silica Hybrid Hydrogels. *Macromolecules,* 43**,** 2554-2563.

LIN, W. C., MARCELLAN, A., HOURDET, D. & CRETON, C. 2011. Effect of polymer-particle interaction on the fracture toughness of silica filled hydrogels. *Soft Matter,* 7**,** 6578-6582.

LIN, Y. Y. & HUI, C. Y. 2004. Cavity growth from crack-like defects in soft materials. *International Journal of Fracture,* 126**,** 205-221.

LIN, Y. Y., HUI, C. Y. & BANEY, J. M. 1999. Viscoelastic contact, work of adhesion and the JKR technique. *J. Phys. D: Appl. Phys.,* 32**,** 2250-2260.

LINDNER, A., LESTRIEZ, B., MARIOT, S., BRUMMER, R., MAEVIS, T., LÜHMANN, B. & CRETON, C. 2006. Adhesive and rheological properties of lightly crosslinked model acrylic networks. *Journal of Adhesion,* 82**,** 267-310.

LINDNER, A., MAEVIS, T., BRUMMER, R., LÜHMANN, B. & CRETON, C. 2004. Subcritical Failure of Soft Acrylic Adhesives under Tensile Stress. *Langmuir,* 20**,** 9156-9169.

LONG, R., KRISHNAN, V. R. & HUI, C.-Y. 2011. Finite strain analysis of crack tip fields in incompressible hyperelastic solids loaded in plane stress. *Journal of the Mechanics and Physics of Solids,* 59**,** 672-695.

LONG, R., MAYUMI, K., CRETON, C., NARITA, T. & HUI, C.-Y. 2014. Time Dependent Behavior of a Dual Cross-Link Self-Healing Gel: Theory and Experiments. *Macromolecules,* 47**,** 7243-7250.

LOPEZ-PAMIES, O. 2009. Onset of Cavitation in Compressible, Isotropic, Hyperelastic Solids. *Journal of Elasticity,* 94**,** 115-145.

LOPEZ-PAMIES, O., IDIART, M. I. & NAKAMURA, T. 2011. Cavitation in elastomeric solids: I—A defect-growth theory. *Journal of the Mechanics and Physics of Solids,* 59**,** 1464-1487.

LORENZ, B., KRICK, B. A., MULAKALURI, N., SMOLYAKOVA, M., DIELUWEIT, S., SAWYER, W. G. & PERSSON, B. N. J. 2013. Adhesion: role of bulk viscoelasticity and surface roughness. *Journal of Physics: Condensed Matter,* 25**,** 225004.

LORENZ, B. & PERSSON, B. N. J. 2009. Interfacial separation between elastic solids with randomly rough surfaces: comparison of experiment with theory. *Journal of Physics: Condensed Matter,* 21**,** 015003.

MAES, F., MONTARNAL, D., CANTOURNET, S., TOURNILHAC, F., CORTE, L. & LEIBLER, L. 2012. Activation and deactivation of self-healing in supramolecular rubbers. *Soft Matter,* 8**,** 1681-1687.

MARIN, G. & DERAIL, C. 2006. Rheology and adherence of pressure-sensitive adhesives. *Journal of Adhesion,* 82**,** 469-485.

MARS, W. V. & FATEMI, A. 2004. Factors that affect the fatigue life of rubber: A literature survey. *Rubber Chemistry and Technology,* 77**,** 391-412.

MAUGIS, D. 1996. On the contact and adhesion of rough surfaces. *Journal of Adhesion Science and Technology,* 10**,** 161-175.

MAUGIS, D. & BARQUINS, M. 1978a. Adhérence d'une bille de verre sur un massif viscoélastique: étude du recollement. *Comptes Rendus de l'Académie des Sciences de Paris, Série II,* 287**,** 49-52.

MAUGIS, D. & BARQUINS, M. 1978b. Fracture Mechanics and the adherence of viscoelastic bodies. *Journal of Physics D: Applied Physics,* 11**,** 1989-2023.

MERKEL, R., NASSOY, P., LEUNG, A., RITCHIE, K. & EVANS, E. 1999. Energy landscapes of receptor-ligand bonds explored with dynamic force spectroscopy. *Nature,* 397**,** 50-53.

MEYERS, M. A., CHEN, P.-Y., LIN, A. Y.-M. & SEKI, Y. 2008. Biological materials: Structure and mechanical properties. *Progress in Materials Science,* 53**,** 1-206.

MIQUELARD-GARNIER, G., HOURDET, D. & CRETON, C. 2009. Large strain behaviour of new hydrophobically modified hydrogels. *Polymer,* 50**,** 481-490.

MUELLER, H. K. & KNAUSS, W. G. 1971. Crack Propagation in a Linearly Viscoelastic Strip. *Journal of Applied Mechanics,* 38**,** 483-488.

MÜNSTEDT, H. & LAUN, H. M. 1979. Elongational behaviour of a low-density polyethylene melt. II. Transient behaviour in constant stretching rate and tensile creep experiments. Comparison with shear data. Temperature dependence of the elongational properties. *Rheologica Acta,* 18**,** 492-504.

MURALIDHARAN, V., HUI, C. Y., DOLLHOFER, J., CRETON, C. & LIN, Y. Y. 2005. Machine Compliance and Hardening Effects on Cavity Growth in Soft Materials. *International Journal of Adhesion and Adhesives,* 26**,** 117-124.

MZABI, S. 2010. *Caractérisation et analyse des mécanismes de fracture en fatigue des élastomères chargés.* Université Pierre et Marie Curie.

MZABI, S., BERGHEZAN, D., ROUX, S., HILD, F. & CRETON, C. 2011. A critical local energy release rate criterion for fatigue fracture of elastomers. *Journal of Polymer Science: Polymer Physics,* 49**,** 1518-1524.

NAKAJIMA, N., BABROWICZ,R.,HARRELL,E.R. 1992. Rheology,Composition, and Peel Mechanism of block copolymer-tackifier-based pressure sensitive adhesives. *Journal of Applied Polymer Science,* 44**,** 1437-1456.

NAKAJIMA, T., FUKUDA, Y., KUROKAWA, T., SAKAI, T., CHUNG, U.-I. & GONG, J. P. 2013a. Synthesis and Fracture Process Analysis of Double Network Hydrogels with a Well-Defined First Network. *ACS Macro Letters,* 2**,** 518-521.

NAKAJIMA, T., KUROKAWA, T., AHMED, S., WU, W.-L. & GONG, J. P. 2013b. Characterization of internal fracture process of double network hydrogels under uniaxial elongation. *Soft Matter,* 9**,** 1955-1966.

NARITA, T., MAYUMI, K., DUCOURET, G. & HEBRAUD, P. 2013. Viscoelastic Properties of Poly(vinyl alcohol) Hydrogels Having Permanent and Transient Cross-Links Studied by Microrheology, Classical Rheometry, and Dynamic Light Scattering. *Macromolecules,* 46**,** 4174-4183.

NASE, J., CRETON, C., RAMOS, O., SONNENBERG, L., YAMAGUCHI, T. & LINDNER, A. 2010. Measurement of the receding contact angle at the interface between a viscoelastic material and a rigid surface. *Soft Matter,* 6**,** 2686-2691.

NASE, J., LINDNER, A. & CRETON, C. 2008. Pattern Formation During Deformation of a Confined Viscoelastic Layer: From a Viscous Liquid to a Soft Elastic Solid. *Physical Review Letters,* 101**,** 074503.

NGUYEN, T. Q., LIANG, Q. Z. & KAUSCH, H. H. 1997. Kinetics of ultrasonic and transient elongational flow degradation: a comparative study. *Polymer,* 38**,** 3783-3793.

NZIAKOU, Y. 2015. *Analyse multiéchelle des mécanismes d'endommagement de matériaux composites à morphologie complexe pour l'aéronautique* Université Pierre et Marie Curie.

PADDING, J. T., MOHITE, L. V., AUHL, D., BRIELS, W. J. & BAILLY, C. 2011. Mesoscale modeling of the rheology of pressure sensitive adhesives through inclusion of transient forces. *Soft Matter,* 7**,** 5036-5046.

PADDING, J. T., MOHITE, L. V., AUHL, D., SCHWEIZER, T., BRIELS, W. J. & BAILLY, C. 2012. Quantitative mesoscale modeling of the oscillatory and transient shear rheology and the extensional rheology of pressure sensitive adhesives. *Soft Matter,* 8**,** 7967-7981.

PAPAIOANNOU, J., GIANNOUSAKIS, A., DIMAKOPOULOS, Y. & TSAMOPOULOS, J. 2014. Bubble Deformation and Growth Inside Viscoelastic Filaments Undergoing Very Large Extensions. *Industrial & Engineering Chemistry Research,* 53**,** 7548-7569.

PASTEWKA, L. & ROBBINS, M. O. 2014. Contact between rough surfaces and a criterion for macroscopic adhesion. *Proceedings of the National Academy of Sciences,* 111**,** 3298-3303.

PEPPAS, N. A., BURES, P., LEOBANDUNG, W. & ICHIKAWA, H. 2000. Hydrogels in pharmaceutical formulations. *European Journal of Pharmaceutics and Biopharmaceutics,* 50**,** 27-46.

PERSSON, B. N. J. 2002. Adhesion between elastic bodies with randomly rough surfaces. *Physical Review Letters,* 89**,** 245502.

PERSSON, B. N. J., ALBOHR, O., CRETON, C. & PEVERI, V. 2004. Contact Area between a viscoelastic solid and a hard, randomly rough, substrate. *Journal of Chemical Physics,* 120**,** 8779-8793.

PERSSON, B. N. J., ALBOHR, O., HEINRICH, G. & UEBA, H. 2005. Crack propagation in rubber-like materials. *Journal of Physics-Condensed Matter,* 17**,** R1071-R1142.

PERSSON, B. N. J. & BRENER, E. A. 2005. Crack propagation in viscoelastic solids. *Physical Review E,* 71**,** 036123.

PERSSON, B. N. J., BUCHER, F. & CHIAIA, B. 2002. Elastic contact between randomly rough surfaces: Comparison of theory with numerical results. *Physical Review B,* 65**,** 184106-1/184106-7.

PERSSON, B. N. J. & TOSATTI, E. 2001. The Effect of Surface Roughness on the Adhesion of Elastic Solids. *Journal of Chemical Physics,* 115**,** 5597-5610.

PEYKOVA, Y., LEBEDEVA, O. V., DIETHERT, A., MÃ¼LLER-BUSCHBAUM, P. & WILLENBACHER, N. 2012. Adhesive properties of acrylate copolymers: Effect of the nature of the substrate and copolymer functionality. *International Journal of Adhesion and Adhesives,* 34**,** 107-116.

PHAN-THIEN, N. 1978. A Nonlinear Network Viscoelastic Model. *Journal of Rheology (1978-present),* 22**,** 259-283.

PLAZEK, D. J., CHOY, I. C., KELLEY, F. N., VONMEERWALL, E. & SU, L. J. 1983. VISCOELASTICITY AND TEARING ENERGY OF FLUORINATED HYDROCARBON ELASTOMERS. *Rubber Chemistry and Technology,* 56**,** 866-882.

PLAZEK, D. J., GU, G. F., STACER, R. G., SU, L. J., VONMEERWALL, E. D. & KELLEY, F. N. 1988. VISCOELASTIC DISSIPATION AND THE TEAR ENERGY OF URETHANE CROSS-LINKED POLYBUTADIENE ELASTOMERS. *Journal of Materials Science,* 23**,** 1289-1300.

POCIUS, A. V. 2002. *Adhesion and Adhesives Technology,* Munich, Hanser.

POIVET, S., NALLET, F., GAY, C. & FABRE, P. 2003. Cavitation-induced force transition in confined viscous liquids under traction. *Europhysics Letters,* 62**,** 244-250.

POLIGNONE, D. A. & HORGAN, C. O. 1993. Cavitation for incompressible anisotropic nonlinearly elastic spheres. *Journal of Elasticity,* 33**,** 27-65.

PSTC 2000. *Test methods for pressure sensitive adhesive tapes,* Oakbrook Terrace, USA, Pressure Sensitive Tape Council.

RAPHAËL, E. & DE GENNES, P. G. 1992. Rubber-Rubber Adhesion with connector molecules. *Journal of Physical Chemistry,* 96**,** 4002-4007.

RICE, J. R. 1968. A Path Independent Integral and the Approximate Analysis of Strain Concentration by Notches and Cracks. *Journal of Applied Mechanics,* 35**,** 379-386.

RIVLIN, R. S. & THOMAS, A. G. 1953. Rupture of rubber. I. Characteristic energy for tearing. *Journal of Polymer Science,* 10**,** 291-318.

ROOS, A. & CRETON, C. 2005. Nonlinear Elastic Properies of elastomeric block copolymers. *Macromolecules,* 38**,** 7807-7818.

ROOS, A., CRETON, C., NOVIKOV, M. B. & FELDSTEIN, M. M. 2002. Viscoelasticity and Tack of Poly(Vinyl Pyrrolidone)-Poly(ethylene glycol) blends. *Journal of Polymer Science: Part B: Polymer Physics,* 40**,** 2395-2409.

ROSE, S., DIZEUX, A., NARITA, T., HOURDET, D. & MARCELLAN, A. 2013. Time Dependence of Dissipative and Recovery Processes in Nanohybrid Hydrogels. *Macromolecules,* 46**,** 4095-4104.

ROSE, S., PREVOTEAU, A., ELZIERE, P., HOURDET, D., MARCELLAN, A. & LEIBLER, L. 2014. Nanoparticle solutions as adhesives for gels and biological tissues. *Nature,* 505**,** 382-385.

RUBINSTEIN, M. & COLBY, R. H. 2003. *Polymer Physics,* Oxford, Oxford University Press.

RUBINSTEIN, M. & PANYUKOV, S. 2002. Elasticity of polymer networks. *Macromolecules,* 35**,** 6670-6886.

RUBLON, P., HUNEAU, B., SAINTIER, N., BEURROT, S., LEYGUE, A., VERRON, E., MOCUTA, C., THIAUDIÈRE, D. & BERGHEZAN, D. 2013. In situ synchrotron wide-angle X-ray diffraction investigation of fatigue cracks in natural rubber. *Journal of Synchrotron Radiation,* 20**,** 105-109.

SAKAI, T. 2013. Gelation mechanism and mechanical properties of Tetra-PEG gel. *Reactive and Functional Polymers,* 73**,** 898-903.

SAKAI, T., AKAGI, Y., MATSUNAGA, T., KURAKAZU, M., CHUNG, U. & SHIBAYAMA, M. 2010. Highly Elastic and Deformable Hydrogel Formed from Tetra-arm Polymers. *Macromolecular Rapid Communications,* 31**,** 1954-1959.

SATAS, D. 1989. Acrylic Adhesives. *In:* SATAS, D. (ed.) *Handbook of pressure-sensitive-adhesives technology.* 2nd ed. New York: Van Nostrand Reinhold.

SAULNIER, F., ONDARCUHU, T., ARADIAN, A. & RAPHAEL, E. 2004. Adhesion between a viscoelastic material and a solid surface. *Macromolecules,* 37**,** 1067-1075.

SCHACH, R. & CRETON, C. 2008. Adhesion at interfaces between highly entangled polymer melts. *Journal of Rheology,* 52**,** 749-767.

SCHACH, R., TRAN, Y., MENELLE, A. & CRETON, C. 2007. Role of chain interpenetration in the adhesion between immiscible polymer melts. *Macromolecules,* 40**,** 6325-6332.

SCHAPERY, R. A. 1975a. Theory of Crack Initiation and Growth in Viscoelastic Media .1. Theoretical Development. *International Journal of Fracture,* 11**,** 141-159.

SCHAPERY, R. A. 1975b. Theory of Crack Initiation and Growth in Viscoelastic Media .2. Approximate Methods of Analysis. *International Journal of Fracture,* 11**,** 369-388.

SCHAPERY, R. A. 1975c. Theory of Crack Initiation and Growth in Viscoelastic Media .3. Analysis of Continuous Growth. *International Journal of Fracture,* 11**,** 549-562.

SEITZ, M. E., MARTINA, D., BAUMBERGER, T., KRISHNAN, V. R., HUI, C.-Y. & SHULL, K. R. 2009. Fracture and large strain behavior of self-assembled triblock copolymer gels. *Soft Matter,* 5**,** 447-456.

SENTMANAT, M., WANG, B. N. & MCKINLEY, G. H. 2005. Measuring the transient extensional rheology of polyethylene melts using the SER universal testing platform. *Journal Of Rheology,* 49**,** 585-606.

SHERRIFF, M., KNIBBS, R. W. & LANGLEY, P. G. 1973. Mechanism for the action of tackifying resins in pressure-sensitive adhesives. *Journal of Applied Polymer Science,* 17**,** 3423-3438.

SHULL, K. R. 2002. Contacts mechanics and the adhesion of soft solids. *Materials Science and Engineering R, reports,* 36**,** 1-45.

SHULL, K. R. 2006. Fracture and adhesion of elastomers and gels: Large strains at small length scales. *Journal of Polymer Science Part B-Polymer Physics,* 44**,** 3436-3439.

SHULL, K. R. & CRETON, C. 2004. Deformation Behavior of thin Compliant Layers under Tensile Loading Conditions. *Journal of Polymer Science: Part B: Polymer Physics,* 42**,** 4023-4043.

SIJBESMA, R. P., BEIJER, F. H., BRUNSVELD, L., FOLMER, B. J. B., HIRSCHBERG, J. H. K. K., LANGE, R. F. M., LOWE, J. K. L. & MEIJER, E. W. 1997. Reversible Polymers Formed from Self-Complementary Monomers Using Quadruple Hydrogen Bonding. *Science,* 278**,** 1601-1604.

SMITH, T. L. 1958. Dependence of the ultimate properties of a GR-S rubber on strain rate and temperature. *Journal of Polymer Science,* 32**,** 99-113.

SOBIESKI, L. A. & TANGNEY, T. J. 1989. Silicone Pressure Sensitive Adhesives. *In:* SATAS, D. (ed.) *Handbook of pressure sensitive adhesives.* 2nd ed. New York: Van Nostrand Reinhold.

SPOLENAK, R., GORB, S. & ARZT, E. 2005a. Adhesion design maps for bio-inspired attachment systems. *Acta Biomaterialia, 1,* 5-13.

SPOLENAK, R., GORB, S., GAO, H. & ARZT, E. 2005b. Effects of contact shape on the scaling of biological attachments. *Proceedings of the Royal Society A: Mathematical, Physical and Engineering Science, 461,* 305-319.

STEPHENSON, R. 1982. The equilibrium field near the tip of a crack for finite plane strain of incompressible elastic materials. *Journal of Elasticity, 12,* 65-99.

SUN, J.-Y., ZHAO, X., ILLEPERUMA, W. R. K., CHAUDHURI, O., OH, K. H., MOONEY, D. J., VLASSAK, J. J. & SUO, Z. 2012. Highly stretchable and tough hydrogels. *Nature, 489,* 133-136.

TANAKA, Y. 2007. A local damage model for anomalous high toughness of double-network gels. *Europhysics Letters, 78,* 56005.

TANAKA, Y., KUWABARA, R., NA, Y. H., KUROKAWA, T., GONG, J. P. & OSADA, Y. 2005. Determination of fracture energy of high strength double network hydrogels. *Journal of Physical Chemistry B, 109,* 11559-11562.

TANGUY, F., NICOLI, M., LINDNER, A. & CRETON, C. 2014. Quantitative analysis of the debonding structure of soft adhesives. *The European Physical Journal E, 37,* 1-12.

TEISSEIRE, J., NALLET, F., FABRE, P. & GAY, C. 2007. Understanding Cracking Versus Cavitation in Pressure-Sensitive Adhesives: The Role of Kinetics. *The Journal of Adhesion, 83,* 613 - 677.

THOMAS, A. G. 1955. Rupture of rubber.II. the strain concentration at an incision. *Journal of Polymer Science, 18,* 177-188.

THOMAS, A. G. & WHITTLE, J. M. 1970. Tensile Rupture of Rubber. *Rubber Chemistry and Technology, 43,* 222-228.

TIAN, Y., PESIKA, N., ZENG, H., ROSENBERG, K., ZHAO, B., MCGUIGGAN, P., AUTUMN, K. & ISRAELACHVILI, J. 2006. Adhesion and friction in gecko toe attachment and detachment. *Proceedings of the National Academy of Sciences, 103,* 19320-19325.

TOBING, S., KLEIN, A., SPERLINH, L.-H. & PETRASKO, B. 2001. Effect of network morphology on adhesive performance in emulsion blends of acrylic pressure sensitive adhesives. *Journal of applied polymer science, 81,* 2109-2117.

TRABELSI, S., ALBOUY, P.-A. & RAULT, J. 2002. Stress-Induced Crystallization around a Crack Tip in Natural Rubber. *Macromolecules, 35,* 10054-10061.

TRELOAR, L. R. G. 1958. *The physics of rubber elasticity* London, Oxford University Press.

TRELOAR, L. R. G. 1973. The elasticity and related properties of rubbers. *Reports on Progress in Physics, 36,* 755-826.

TUNCABOYLU, D. C., ARGUN, A., ALGI, M. P. & OKAY, O. 2013. Autonomic self-healing in covalently crosslinked hydrogels containing hydrophobic domains. *Polymer, 54,* 6381-6388.

TUNCABOYLU, D. C., SARI, M., OPPERMANN, W. & OKAY, O. 2011. Tough and Self-Healing Hydrogels Formed via Hydrophobic Interactions. *Macromolecules, 44,* 4997-5005.

URAHAMA, Y. 1989. Effect of Peel Load on Stringiness Phenomena and Peel Speed of Pressure-Sensitive Adhesive Tape. *Journal of Adhesion, 31,* 47-58.

VERDIER, C., PIAU, J. M. & BENYAHIA, L. 1998. Peeling of acrylic pressure-sensitive-adhesives: cross-linked versus uncross-linked adhesives. *Journal of Adhesion, 68,* 93-116.

VILLEY, R., CRETON, C., CORTET, P.-P., DALBE, M.-J., JET, T., SAINTYVES, B., SANTUCCI, S., VANEL, L., YARUSSO, D. J. & CICCOTTI, M. 2015. Rate-dependent elastic hysteresis during the peeling of pressure sensitive adhesives. *Soft Matter, 11,* 3480-3491.

VOLOKH, K. Y. 2007. Softening hyperelasticity for modeling material failure: Analysis of cavitation in hydrostatic tension. *International Journal of Solids and Structures, 44,* 5043-5055.

WANG, Y. Y., BOUKANY, P. Y., WANG, S. Q. & WANG, X. R. 2007. From elastic extension to elongational flow of entangled melts. *Physical Review Letters, 99,* 237801.

WEBBER, R. E., CRETON, C., BROWN, H. R. & GONG, J. P. 2007. Large Strain Hysteresis and Mullins effect of tough Double-Network Hydrogels. *Macromolecules, 40,* 2919-2927.

WILLIAMS, J. A. & KAUZLARICH, J. J. 2005. The influence of peel angle on the mechanics of peeling flexible adherends with arbitrary load–extension characteristics. *Tribology International, 38,* 951-958.

WILLIAMS, J. G. 1984. *Fracture Mechanics of Polymers,* Market Cross House, Cooper St, Chichester, West Sussex, PO 19, 1 EB, UK, Ellis Horwood Limited.

WILLIAMS, J. G. 1993. Root rotation and plastic work effects in the peel test. *Journal of Adhesion, 41*, 225-239.

WILLIAMS, M. L., LANDEL, R. F. & FERRY, J. D. 1955. The Temperature Dependence of Relaxation Mechanisms in Amorphous Polymers and Other Glass-forming Liquids. *Journal of the American Chemical Society, 77*, 3701-3707.

WILLIAMS, M. L. & SCHAPERY, R. A. 1965. Spherical flaw instability in hydrostatic tension. *International Journal of Fracture Mechanics, 1*, 64-71.

XU, D. B., HUI, C. Y. & KRAMER, E. J. 1992. Interface Fracture and viscoelastic deformation in finite size specimens. *Journal of Applied Physics, 72*, 3305-3316.

YAMAGUCHI, T. & DOI, M. 2006. Debonding dynamics of pressure-sensitive adhesives: 3D block model. *European Physical Journal E, 21*, 331-339.

YAMAGUCHI, T., KOIKE, K. & DOI, M. 2007. In situ observation of stereoscopic shapes of cavities in soft adhesives. *Europhysics Letters, 77*, 64002.

YAMAGUCHI, T., MORITA, H. & DOI, M. 2006. Modeling on debonding dynamics of pressure-sensitive-adhesives. *European Physical Journal E, 20*, 7-17.

YANG, S. Y., CARLSON, A., CHENG, H. Y., YU, Q. M., AHMED, N., WU, J., KIM, S., SITTI, M., FERREIRA, P. M., HUANG, Y. G. & ROGERS, J. A. 2012. Elastomer Surfaces with Directionally Dependent Adhesion Strength and Their Use in Transfer Printing with Continuous Roll-to-Roll Applications. *Advanced Materials, 24*, 2117-2122.

YAO, X., HU, Y., GRINTHAL, A., WONG, T.-S., MAHADEVAN, L. & AIZENBERG, J. 2013. Adaptive fluid-infused porous films with tunable transparency and wettability. *Nat Mater, 12*, 529-534.

YARUSSO, D. J. 1999. Quantifying the Relationship Between Peel and Rheology for Pressure Sensitive Adhesives. *The Journal of Adhesion, 70*, 299 - 320.

YERZLEY, F. L. 1939. Adhesion of neoprene to metal. *Industrial and Engineering Chemistry, 31*, 950-956.

YU, Q. M., TANAKA, Y., FURUKAWA, H., KUROKAWA, T. & GONG, J. P. 2009. Direct Observation of Damage Zone around Crack Tips in Double-Network Gels. *Macromolecules, 42*, 3852-3855.

YURDUMAKAN, B., RARAVIKAR, N. R., AJAYAN, P. M. & DHINOJWALA, A. 2005. Synthetic gecko foot-hairs from multiwalled carbon nanotubes. *Chemical Communications*, 3799-3801.

ZHANG, H., CHEN, Y. J., LIN, Y. J., FANG, X. L., XU, Y. Z., RUAN, Y. H. & WENG, W. G. 2014. Spiropyran as a Mechanochromic Probe in Dual Cross-Linked Elastomers. *Macromolecules, 47*, 6783-6790.

ZHANG, H., SCHOLZ, A. K., DE CREVOISIER, J., BERGHEZAN, D., NARAYANAN, T., KRAMER, E. J. & CRETON, C. 2015. Nanocavitation around a crack tip in a soft nanocomposite: A scanning microbeam small angle X-ray scattering study. *Journal of Polymer Science Part B: Polymer Physics, 53*, 422-429.

ZHANG, H., SCHOLZ, A. K., DE CREVOISIER, J., VION-LOISEL, F., BESNARD, G., HEXEMER, A., BROWN, H. R., KRAMER, E. J. & CRETON, C. 2012. Nanocavitation in Carbon Black Filled Styrene–Butadiene Rubber under Tension Detected by Real Time Small Angle X-ray Scattering. *Macromolecules, 45*, 1529-1543.

ZHANG, H., SCHOLZ, A. K., VION-LOISEL, F., MERCKEL, Y., BRIEU, M., BROWN, H., ROUX, S. P., KRAMER, E. J. & CRETON, C. 2013. Opening and Closing of Nanocavities under Cyclic Loading in a Soft Nanocomposite Probed by Real-Time Small-Angle X-ray Scattering. *Macromolecules, 46*, 901-913.

ZHANG NEWBY, B.-M., CHAUDHURY, M. K. & BROWN, H. R. 1995. Macroscopic evidence of the effect of interfacial slippage on adhesion. *Science, 269*, 1407-1409.

ZHANG NEWBY, B. M. & CHAUDHURY, M. K. 1997. Effect of Interfacial slippage on viscoelastic adhesion. *Langmuir, 13*, 1805-1809.

ZHOU, Y., ROBINSON, A., STEINER, U. & FEDERLE, W. 2014. Insect adhesion on rough surfaces: analysis of adhesive contact of smooth and hairy pads on transparent microstructured substrates. *Journal of the Royal Society Interface, 11*, 20140499.

ZOSEL, A. 1985. Adhesion and tack of polymers: influence of mechanical properties and surface tensions. *Colloid and Polymer Science, 263*, 541-553.

ZOSEL, A. 1989. Adhesive Failure and Deformation Behaviour of Polymers. *Journal of Adhesion, 30*, 135-149.

ZOSEL, A. 1991. Effect of Cross-Linking on tack and peel strength of polymers. *Journal of Adhesion,* 34**,** 201-209.

ZOSEL, A. 1992. Fracture energy and tack of pressure sensitive adhesives. *In:* SATAS, D. (ed.) *Advances in Pressure Sensitive Adhesive Technology.* Warwick, RI: Satas & Associates.

ZOSEL, A. 1997. The effect of bond formation on the tack of polymers. *Journal of Adhesion Science and Technology,* 11**,** 1447-1457.

ZOSEL, A. 1998. The effect of fibrillation on the tack of pressure-sensitive-adhesives. *International Journal of Adhesion and Adhesives,* 18**,** 265-271.

ZÜLLE, B., LINSTER, J. J., MEISSNER, J. & HÜRLIMANN, H. P. 1987. Deformation Hardening and thinning in both elongation and shear of a low density polyethylene melt. *Journal of Rheology,* 31**,** 583-598.